ANDRÉ KAZUO KUCHIISHI

# Mechanical behavior of cold recycled asphalt mixtures

São Paulo
2019

ANDRÉ KAZUO KUCHIISHI

# Mechanical behavior of cold recycled asphalt mixtures

Thesis presented to the *Escola Politécnica* of the *Universidade de São Paulo* to obtain the degree of Master of Science.

São Paulo
2019

ANDRÉ KAZUO KUCHIISHI

# Mechanical behavior of cold recycled asphalt mixtures

Thesis presented to the *Escola Politécnica* of the *Universidade de São Paulo* to obtain the degree of Master of Science.

Research Area:
Transportation Engineering

Advisor:
Prof. Kamilla Vasconcelos, PhD

São Paulo
2019

Este exemplar foi revisado e corrigido em relação à versão original, sob responsabilidade única do autor e com a anuência de seu orientador.

São Paulo, _____ de _____ de _____

Assinatura do autor: _____

Assinatura do orientador: _____

Catalogação-na-publicação

Kuchiishi, André Kazuo

Mechanical behavior of cold recycled asphalt mixtures / A. K. Kuchiishi -- versão corr. -- São Paulo, 2019.

190 p.

Dissertação (Mestrado) - Escola Politécnica da Universidade de São Paulo. Departamento de Engenharia de Transportes.

1.Mistura reciclada a frio 2.Rigidez 3.Viscoelasticidade 4.Sucção mátrica 5.Elasticidade não-linear I.Universidade de São Paulo. Escola Politécnica. Departamento de Engenharia de Transportes II.t.

To my parents, for their love and support.

## ACKNOWLEDGEMENTS

First, I would like to thank my parents Sayuri and Yudi for being so supportive during my entire life and for encouraging me to pursue my goals with integrity and respect. I owe you everything that I am and hope to be. A special thanks to my sister Emi that even without knowing helped me to overcome the difficult periods along these years. I would also like to thank Juliana for always believing in me and with whom I have been constantly sharing my moments of happiness and concern.

I would like to express my gratitude to my advisor, Professor Kamilla Vasconcelos, who I deeply admire as a Professor and human being, and who have helped me in many aspects of my professional and personal life. A would also like to acknowledge Professor Liedi Bernucci for her constant support, encouragement and for believing in my potential.

For the assistance with the enormous amount of material preparation, specimen compaction and laboratory tests execution, a special thanks to Vanderlei and Higor. I would also like to thank Lucas, Matheus, Iuri, João Paulo Carvalho and Vanderlei, who were fundamental during the construction of the experimental test sections and the functional and structural pavement monitoring.

For the extensive number of laboratory tests, material preparation procedures and computational simulations, I would like to thank the undergraduate student and future engineer Camila Christine.

I would also like to express my gratitude to all my friends and colleagues from Laboratory of Pavement Technology that have directly and indirectly contributed with this thesis: Diomária, Edson, Robson, Vanderlei, Erasmo, Higor, André, Camila, Fernanda Carvalho, Fernanda Gadler, Gabriel, Guilherme Castro, Guilherme Pereira, Ingrid, Iuri, Jean, João Paulo Carvalho, João Paulo Menses, José João, Laura, Leidy, Lucas, Manu, Márcia, Marina, Matheus, Paulo, Rafael, Rosângela, Talita, and Zila.

I would like to thank Frederico Guatimosim from Copavel Consultoria de Engenharia Ltda. for the availability to use the vibratory compaction hammer, the foaming machine

for specimen fabrication and the numerous discussions regarding cold recycling asphalt mixtures.

For the valuable discussions regarding suction pressure on unsaturated soils, I would also like to thank José Pires.

For assisting with the construction of the experimental test sections and with pavement monitoring, I would like to thank Guilherme and Alan from Centro de Desenvolvimento Tecnológico of Arteris.

A special thanks to Sérgio and Tiago with whom I had the first contact with the research field and that further motivated me continue in this path.

For the X-ray microcomputed tomography tests and analysis, I would also like to thank Olga Araújo and Professor Ricardo Lopes from the Laboratório de Instrumentação Nuclear at COPPE/UFRJ.

I also thank Filipe Franco for his availability in answering all my questions regarding the AEMC software simulations.

Finally, I would like to thank the Coordenação de Aperfeiçoamento de Pessoal de Nível Superior - Brasil (CAPES) and Agência Nacional de Transportes Terrestres (ANTT) for the financial support.

## RESUMO

A baixa proporção de vias pavimentadas no Brasil, a alta demanda pelo transporte rodoviário e a falta de investimentos em manutenções preventivas aceleram o surgimento de patologias no pavimento. Tais patologias comprometem a qualidade das rodovias, aumentando o consumo de combustível, a emissão de gases poluentes e os custos operacionais. Logo, as técnicas de reciclagem a frio podem ser vistas como uma alternativa vantajosa em termos de sustentabilidade e custo-benefício para a reabilitação de pavimentos. As misturas recicladas a frio (CRAMs, do inglês *cold recycled asphalt mixtures*), são compostas por material fresado (RAP, do inglês *reclaimed asphalt pavement*) estabilizado com emulsão asfáltica ou espuma de asfalto e fíler ativo (cimento ou cal hidratada). Apesar das vantagens econômicas e ambientais das CRAM, seu comportamento mecânico é complexo, pois diversas variáveis afetam sua rigidez. O objetivo deste estudo é avaliar a influência da temperatura, da frequência de carregamento, do estado de tensão e da umidade na rigidez das CRAMs. Quatro tipos de CRAMs foram coletados do campo durante a construção de um trecho experimental e ensaiadas em laboratório. Para análise do efeito da temperatura, o ensaio de módulo dinâmico foi realizado para obtenção das propriedades viscoelásticas das CRAMs e os resultados obtidos foram utilizados como dados de entrada para simulação computacional. Observou-se que a comportamento viscoelástico das CRAMs influencia a resposta mecânica do pavimento. Para avaliar o efeito da umidade e do estado de tensão, o ensaio de módulo de resiliência triaxial foi realizado em diferentes condições de cura. Juntamente com os ensaios de papel filtro e microtomografia por raio X observou-se que a sucção mátrica está relacionada com o módulo de resiliência desses materiais. Além disso, o efeito da dependência do estado de tensão das CRAMs foi avaliado por meio de simulação computacional e comparadas com medições in situ. Constatou-se que a elasticidade não-linear influencia significativamente o comportamento mecânico do pavimento.

Palavras-chave: Mistura reciclada a frio. Rigidez. Viscoelasticidade. Sucção mátrica. Elasticidade não-linear.

## ABSTRACT

The Brazilian reduced paved road density, the increasingly demand for highways, and the lack of investment in preventive maintenance practices accelerate the occurrence of pavement distresses. This imparts for poor riding quality highways, resulting in higher fuel consumption, greater emission of pollutant gases, and increasing operational costs. In this scenario, cold recycling practices may be a cost-effective and environmental friendly alternative for pavement rehabilitation. The cold recycled asphalt mixtures (CRAMs) produced by cold recycling techniques, are comprised by reclaimed asphalt pavement (RAP), bitumen stabilized agents (asphalt emulsion or foamed asphalt), and active fillers (cement or hydrated lime). Despite the economical and sustainable benefits, the CRAMs exhibit a complex mechanical behavior since numerous variables can influence its stiffness. Therefore, the purpose of this study is to evaluate the CRAM' stiffness dependency regarding temperature, load frequency, stress-state and moisture content variation. Four types of CRAMs were collected from the field during experimental test section construction and were evaluated by means of laboratory tests. For temperature evaluation, the CRAMs linear viscoelastic properties were investigated by means of dynamic modulus and the results were used as input data for computational simulation. It was observed that the CRAMs viscoelastic properties influence the pavement mechanical response. For moisture evaluation, triaxial resilient modulus tests were conducted at different curing conditions. In conjunction with the filter paper test and X-ray micro computed tomography, a correspondence was observed between matric suction and resilient modulus. Besides, the CRAMs stress-state dependency was evaluated by means of pavement simulation and compared with in situ measurements. It was observed that the non-linear elastic behavior of CRAMs substantially influences the pavement mechanical behavior.

Key words: Cold recycled asphalt mixtures. Stiffness. Viscoelasticity. Matric suction. Non-linear elasticity.

# LIST OF FIGURES

# LIST OF TABLES

## LIST OF ABBREVIATIONS

| | |
|---|---|
| AASHTO | American Association of State Highway and Transportation Officials |
| ABNT | Associação Brasileira de Normas Técnicas |
| AC | Asphalt concrete |
| AEMC | Análise Elástica de Múltiplas Camadas |
| ASTM | American Society for Testing and Materials |
| BSM | Bitumen stabilized material |
| CAM | Cold asphalt mixtures |
| CBTM | Cement-bitumen treated material |
| CCPR | Cold central plant recycling |
| CIR | Cold in-place recycling |
| CRAM | Cold recycled asphalt mixture |
| CTM | Cement treated material |
| DC | Degree of compaction |
| DSR | Dynamic shear rheometer |
| EMC | Equilibrium moisture content |
| ER | Expansion Ratio |
| FDR | Full depth reclamation |
| FEM | Finite element method |
| FFRC | Free-free resonant column |
| FHWA | Federal Highway Administration |
| FWD | Falling Weight Deflectometer |
| GCS | Graded crushed stone |
| H | Hydrated lime |
| HMA | Hot mix asphalt |
| HVS | Heavy Vehicle Simulation |
| IDT RM | Indirect tensile resilient modulus |
| ITS | Indirect tensile strength |
| LWD | Light Weight Deflectometer |

| | |
|---|---|
| ML | Moisture loss |
| MLET | Multilayer elastic theory |
| MM | Michaelis-Menten |
| OMC | Optimum moisture content |
| OPC | Ordinary Portland cement |
| RAP | Reclaimed asphalt pavement |
| RH | Relative humidity |
| RM | Resilient modulus |
| SBS | Styrene-butadiene-styrene |
| TSR | Tensile Strength Ratio |
| TTSP | Time-temperature superposition principle |
| Tx RM | Triaxial resilient modulus |
| UPV | Ultrasonic pulse velocity |
| WIM | Weigh-in-motion |
| WMM | Wet mix macadam |

# TABLE OF CONTENTS

# 1. INTRODUCTION

Currently, the road network is considered the main alternative in terms of transportation in Brazil, contributing with 61% and 95% of freight and passenger transportation, respectively. Although the road relevance, Brazil's paved road density is still low compared with other countries such as Colombia, Mexico and Russia. Only 12.3% from a total of 1.7 million km of road extension is paved (CNT, 2017), which may lead to highways over-demand.

From Figure 1 it is possible to observe that the federal roads extension increased 11.3% from 2007 to 2017. This road network evolution may be considered small in comparison with the fleet growth in Brazil, which corresponds to 102.4% within the same period (CNT, 2017). Therefore, the increasingly demand for highways in conjunction with traffic overload, climate variations, and the lack of investment in maintenance practices accelerate the appearance of pavement distresses. This scenario may contribute to more frequent rehabilitations or even reconstruction services, in order to guarantee pavement adequacy for its users in terms of structural and functional performance. According to the Global Competitiveness Report (SCHWAB, 2016), from the 138 analyzed countries, Brazil occupies the 111º global position rank regarding roads quality.

Figure 1 - Evolution of federal roads extension in Brazil from 2007 to 2017 (values in 1000 km)


Source: Adapted from CNT (2017)

Thus, the need for maintenance services during pavement early-life is not cost effective and oftentimes requires lane interdiction, resulting in operational issues. Furthermore, according to CNT (2017), 61.8% of the evaluated Brazilian highways present inadequate riding conditions, which is directly related with higher fuel consumption and polluting gases emission. In order to provide structural alternatives, pavement recycling is a sustainable option and is increasingly becoming a widespread rehabilitation practice. One of the existing recycling processes involves incorporating Reclaimed Asphalt Pavement (RAP), obtained from milled distressed asphalt pavements, into new mixtures. In countries like United States, Germany and Italy, the use of RAP is a common practice and is largely adopted in different types of mixtures (EAPA, 2018). Table 1 presents a summary of the RAP percentage used in different countries.

Table 1 - Percentage of RAP used in different countries

| Country | All RAP available in 2016 in tonnes | % of available RAP used in | | | |
|---|---|---|---|---|---|
| | | Hot and warm mix asphalt production | Half warm asphalt production | Cold recycling | Other civil engineering applications |
| USA | 74,200,000 | 94 | 0 | 0 | 6 |
| Germany | 12,000,000 | 87 | 0 | 0 | 13 |
| Italy | 9,000,000 | 20 | 0 | 30 | 50 |
| France | 6,370,000 | 70 | no data | no data | no data |
| Netherlands | 4,431,000 | 71 | 0 | 11 | 18 |
| Turkey | 3,551,167 | 2 | 0 | no data | 96 |
| Great Britain | 3,250,000 | 80 | no data | no data | 5 |
| Czech Republic | 1,800,000 | 17 | 0 | 30 | 53 |
| Sweden | 1,600,000 | 84 | 6 | no data | 5 |
| Austria | 1,400,000 | 40 | no data | no data | no data |
| Belgium | 1,240,000 | 81 | no data | no data | no data |
| Denmark | 1,150,000 | 65 | 0 | 0 | 35 |
| Finland | 1,150,000 | 100 | 0 | 0 | 0 |
| Norway | 1,112,000 | 37 | 0 | 0 | 63 |
| Spain | 490,000 | 67 | 1 | 0 | 33 |
| Hungary | 109,000 | 90 | 0 | 0 | 10 |
| Croatia | 80,000 | 50 | 0 | 50 | 0 |
| Slovenia | 56,000 | 43 | 0 | 0 | 57 |
| Slovakia | 54,000 | 98 | 0 | 0 | 2 |

Source: Adapted from EAPA (2018)

It is important to state that the recycling technique presents economic and environmental advantages. In terms of economic benefits, using RAP reduces costs of acquiring new aggregates. Besides, reduction in transportation costs is evident, since the RAP can be used at the same jobsite from which it was milled (COPELAND, 2010). When the most adequate recycling technique is applied for a specific location, followed by proper design and construction practices, costs savings of 30 to 50% can be obtained in comparison with conventional asphalt operations (FHWA, 2017).

Furthermore, the use of RAP reduces the consumption of virgin aggregates and decreases the amount of debris produced in landfills. Cold recycling, in particular, is more environmental friendly, since no heat is necessary for mixing and compaction purposes, minimizing greenhouse gases emission and energy consumption (GIANI et al., 2015). Figure 2 presents the energy consumption (in MJ/t) of different recycling techniques in comparison with the hot mix asphalt (HMA) production. It can be seen that pavement recycling indeed reduces the total required energy for pavement construction.

Figure 2 - Energy consumption for different pavement recycling techniques

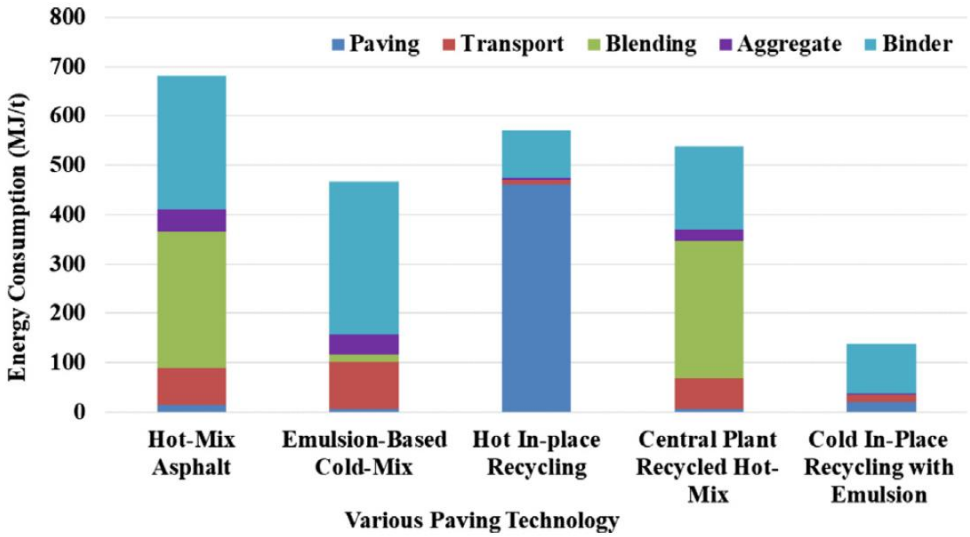


Source: Xiao et al. (2018)

Therefore, the recycling technique with RAP provides several advantages, being a sustainable and structural alternative for pavement rehabilitation. In Brazil, different studies related to asphalt pavement recycling have been conducted with: asphalt emulsion (SILVA, 2011), Portland cement (ARANHA, 2013), and foamed asphalt stabilization (GUATIMOSIM, 2015). Since this rehabilitation practice is not fully widespread in Brazil, numerous researches can be further conducted in order to better assess the mechanical behavior of this material, and better consider it into pavement design.

## 1.1. CLASSIFICATION OF COLD RECYCLING TECHNIQUES

Pavement recycling became more widespread after 1970 oil embargo (NAPA, 2007), mainly due to the increased asphalt costs, and the low availability of virgin aggregates near the construction jobsites (SONDAG; CHADBOURN; DRESCHER, 2002). Therefore, different techniques have been developed regarding more sustainable and cost-effective rehabilitation alternatives. The recycling practice can be categorized according to the (i) recycling temperature, (ii) milling process, (iii) location of recycling process, and (iv) type of stabilization.

For warm and hot recycling, the aggregates and asphalt binder must be heated in order to reduce the binder viscosity and guarantee proper mixing and compaction of the mixture. Temperature usually ranges from 70 to 120 ºC for warm recycling and above 120 ºC for hot recycling. Besides, rejuvenator agents are added to the mixture with the purpose of restoring some of the physicochemical properties of the aged binder of the RAP (KARLSSON; ISACSSON, 2006). Conversely, in cold recycling no heating is required. The aggregates can be mixed at ambient temperature with asphalt emulsion, or foamed asphalt. The South African guidelines for cold recycling recommend that the aggregate must be at minimum of 5 ºC for asphalt emulsion and 10 ºC for foamed asphalt (ASPHALT ACADEMY, 2009).

Considering the milled pavement depth, cold recycling can be executed by means of surface milling or full-depth reclamation (FDR), according to the level of severity of pavement distresses. In the former, only the asphalt concrete is removed from the existing pavement and mixed with bitumen stabilized agents and active fillers in order

to improve the mechanical properties of the recycled mixture. In the latter, the milling machine removes both the asphalt concrete and the underlying base course, that might be of unbound, or cement-treated material (GRILLI; GRAZIANI; BOCCI, 2012). The milling process can also be categorized in terms of temperature. Hot milling, which was first developed in the 1970's, presents several limitations, due to the high energy costs for heating the asphalt pavement prior to milling, and the great amount of smoke generated. Cold milling, on the contrary, does not require heating, reducing the construction costs (WIRTGEN, 2013).

Cold recycling can also be classified in terms of the location of the recycling process: cold in-place recycling (CIR), or cold central plant recycling (CCPR). In CIR, different machines are used to mill, mix and repave portions of the asphalt pavement in a single pass. The water tank, asphalt tank and recycler are followed by the vibratory and pneumatic-tired rollers to compact the layer, and a grader machine which levels the layer. On the other hand, the CCPR requires a mobile or central plant to recycle the milled material. In CCPR, the input materials can be selected, screened and stockpiled, which provides greater flexibility for gradation adjustments when necessary. With this higher control in comparison with CIR, the CCPR can be considered more reliable in terms of mix quality. However, due to the need for haulage trucks for transportation of the final mixture to the jobsite, this process may be less cost effective than CIR (WIRTGEN, 2012; FHWA, 2017). Figure 3 illustrates both the CIR and CCPR processes.

Figure 3 - Examples of (a) CIR and (b) CCPR process

(a) (b)

Source: FHWA (2017)

## 1.2. TEST PROCEDURES TO EVALUATE COLD RECYCLED ASPHALT MIXTURES STIFFNESS

Along this thesis, different tests were performed to evaluate the cold recycled asphalt mixtures (CRAMs) stiffness. Tests such as the indirect tensile resilient modulus, triaxial resilient modulus, dynamic modulus, and the backcalculated modulus from FWD data can be used to evaluate CRAM stiffness. However, the stress-state generated within the material and the boundary conditions in each of these tests can vary significantly (FU et al., 2011). In order to better understand CRAMs stiffness, the following topics summarize some of the aforementioned test procedures.

It is important to state that these tests should be used complementing each other, instead of being used individually for material characterization. Each of them can assess specific characteristics of CRAMs regarding stress state, temperature sensibility, curing mechanism, moisture effect, among others.

### 1.2.1. Indirect tensile resilient modulus (IDT RM)

The IDT RM is one of the most usual test methods for stiffness evaluation, primarily because of its cost effectiveness. The majority of the studies have been using the IDT RM for mix design purposes (KUNA; AIREY;THOM, 2017), better understanding of the curing mechanism (GRAZIANI et al., 2016), and temperature influence analysis (BOCCI et al., 2014). Nevertheless, the modulus obtained from the IDT RM test is oftentimes reported in literature with excessively high values (KHOSRAVIFAR et al, 2014).

Tabakovic et al. (2016) obtained resilient modulus values greater than 5000 MPa for foamed asphalt mixtures, which is considered impractical for this type of material. According to Fu et al. (2011), one possible reason for the stiffness overestimation is that the calculation of the horizontal tensile strains is based in the continuum mechanics, which might not be suitable especially for foamed asphalt treated materials that have a non-continuously bonded characteristic. Other test procedures such as the triaxial resilient modulus test, and the flexural beam test are more consistent with backcalculated modulus values. Additionally, these other test methods present a more

uniform stress distribution within the specimen geometry, differently of the IDT RM, in which the loading strips width and the distance between the measuring gauges may be too similar to the coarser aggregates dimensions (FU et al., 2011).

### 1.2.2. Triaxial resilient modulus

The triaxial resilient modulus test (Tx RM) is usually carried out with the objective of investigating the influence of the stress-state in CRAMs stiffness, which cannot be evaluated by the IDT RM tests. Different combinations of confining and deviator stresses are applied to the specimen by means of cyclic haversine loads, in order to simulate various stress state conditions. Usually, cylindrical specimens are used in a 2:1 (height:diameter) geometry relation.

Jenkins, Long and Ebels (2007) evaluated the influence of foamed asphalt and cement contents with respect to the stress state. It was found that even with 1% of cement addition, the resilient modulus of the specimens were highly dependent of the bulk stress. On the other hand, Bessa et al. (2016) conducted Tx RM tests in CRAMs stabilized with asphalt emulsion and, with 1% cement content, the resilient modulus was constant for all confining stresses.

Guatimosim et al. (2018) evaluated the curing time effect in CRAM samples comprised by RAP, crushed cement treated base aggregates, 1% of hydrated lime, and foamed asphalt. It was found that for shorter curing periods, the specimens presented greater dependency of the confining stress, due to the higher moisture content. At the final curing stages, the resilient modulus curves became flatter, but still dependent of the stress state. Similar results were reported by Fu et al. (2010).

The resilient modulus can also be assessed in terms of flexural tests in compacted beams. Fu et al (2011) compared the Tx RM with flexural beam resilient modulus results. The disparities observed from the results between the two test methods indicated that the aggregate particle orientation significantly influenced the stiffness determination. In addition, the stress state generated within the cylindrical and beam shape specimens during the test are considerably different. In the former, compressive

stresses are dominant while in the latter tensile stresses are generated at the bottom of the specimen.

### 1.2.3. Dynamic modulus

The dynamic modulus test is a laboratory test in which a specimen is subjected to a sinusoidal loading at varying temperatures and load frequencies in order to evaluate the material linear viscoelastic properties. Different specimen geometries and loading conditions have been used for this evaluation.

The most frequent dynamic modulus test is conducted in cylindrical specimens with 100 mm diameter and 150 mm height under a cyclic uniaxial compression stress-controlled condition. From the dynamic modulus results, some authors evaluated the CRAMs stiffness regarding the curing time and moisture content (KIM; IM; LEE, 2011), the type of recycling technique (DIEFENDERFER et al., 2016), the RAP content (GODENZONI; GRAZIANI; BOCCI, 2015), and its viscoelastic properties in comparison with HMA (KIM; LEE; HEITZMAN, 2009).

Smith and Braham (2017) performed the dynamic modulus test in both the IDT and uniaxial configuration. It was found that, for the CRAMs samples, the IDT stiffness master curves were lower than the uniaxial configuration. This result could be influenced by the sample geometry in the IDT.

Čížková et al. (2015) evaluated the stiffness of CRAMs stabilized with asphalt emulsion or foamed asphalt using a beam specimen in a four points flexural test equipment. Although this type of test better simulates the stress condition of a bounded compacted layer under traffic loading in comparison with an IDT configuration, the authors reported some difficulties during the specimens demolding and cutting, due to material loss and damage at the sample edges. Thus, the reproducibility of this type of test was partially impaired.

### 1.2.4. Backcalculated modulus

The backcalculated modulus, obtained from FWD data, are used for in situ evaluation of pavement layers' stiffness. By means of FWD deflection measurements, different values of layers moduli are simulated in order to fit the theoretical deflection basins with the measured ones. This iterative process is performed until an acceptable root mean square error (RMSE) value is obtained, which can vary from 2% to 10% (MARECOS et al., 2017).

Some authors have observed an increase in the backcalculated modulus over time due to the curing mechanism of the compacted layer in the field (PAPAVISILIOU; LOIZOS, 2013; GUATIMOSIM; VASCONCELOS; BERNUCCI, 2017). Godenzoni et al. (2017) obtained similar results and used the deflection measurements to calculate the Base Damage Index (BDI) of the CRAMs layers. Besides the increasing stiffness trend of the recycled layer, the BDI decreased over time, proving that the curing process imparts for greater modulus. Other researchers obtained similar results (ANDRADE; VASCONCELOS; BERNUCCI, 2016).

Loizos, Papavisiliou and Plati (2012) evaluated the influence of Falling Weight Deflectometer (FWD) load levels in the backcalculated modulus after curing of the compacted CRAM layer. The authors observed that within the FWD loading range of 40-80 kN, the backcalculated modulus of foamed asphalt stabilized mixtures may be considered constant. This result indicates that the studied recycled layer did not exhibit a stress dependency in situ.

### 1.2.5. Alternative methods

Other non-conventional test methods can also be used in order to assess CRAMs stiffness. In this case, no loading is applied in the specimen and its modulus is determined by indirect measurements.

Boz, Chen and Solaimanian (2017) used ultrasonic pulse velocity (UPV) testing to evaluate the curing effects on CRAMs stabilized with asphalt emulsion. In this testing, two transducers are used and the time required for the compressional wave to

propagate through the specimen is determined. The stiffness modulus is then calculated using a one-dimensional wave equation.

Fu et al. (2011), conducted free-free resonant column (FFRC) tests with the purpose of evaluating the stiffness of foamed asphalt materials. The FFRC test is similar to the UPV test, in which a wave propagates through the specimen. According to the authors, the Young modulus obtained from the FFRC tests overestimates the stiffness of the foamed asphalt materials, in comparison with the Tx RM and flexural tests. Albeit the high repeatability, the authors suggest that the results obtained from this indirect method are questionable for being used directly in the pavement design process.

## 1.3. PROBLEM IDENTIFICATION

Due to the RAP inherent variability and the existence of different stabilization agents, CRAMs present complex mechanical responses, since many factors can influence its stiffness.

The moisture content within CRAM mineral skeleton impacts asphalt dispersion during mixing, lubricates aggregate surfaces for compaction, and is directly related with the stress-state dependency and curing process. Various studies have been conducted with the goal of better understanding the curing mechanism, in which water evaporates and the final mix gains stiffness and strength during its service life (FU et al., 2010; GRAZIANI et al., 2016; GODENZONI et al., 2017; SAADOON; GARCIA; GÓMEZ-MEIJIDE, 2017). Many aspects can influence the curing process, considering the different types of aggregates and stabilization agents used.

The CRAM viscoelastic properties, which imparts for temperature and loading frequency dependency, are also discussed by researchers. Some authors state that CRAMs are granular materials with higher cohesion, since the low binder content do not dominate its mechanical behavior, being stress-state dependent (JOOSTE; LONG, 2007; FU; HARVEY, 2007; GUATIMOSIM et al., 2018). Conversely, other authors state that CRAMs viscoelastic properties may not be neglected, since it exhibits temperature and frequency dependency (LEANDRI; LOSA; DI NATALE, 2014; GODENZONI et al., 2017; NIVEDYA et al., 2018).

Therefore, the present thesis is not focused on damage evaluation (i.e. fatigue cracking, rutting), but on better understanding the influence of moisture, stress-state, temperature, and load frequency in CRAMs stiffness by means of laboratory tests and pavement simulation. A better comprehension of this mixture may contribute with future mechanistic-empirical design methods and construction purposes.

## 1.4. OBJECTIVES

The objective of this thesis is to investigate the influence of moisture content, stress-state, temperature and load frequency on CRAMs stiffness by means of laboratory and pavement simulation.

The specific objectives of this thesis are:

- Evaluate the influence of mixture composition on the mechanical behavior of CRAMs by means of triaxial resilient modulus test and dynamic modulus test.
- Analyze the effect of CRAMs viscoelastic properties on pavement structure mechanical response using computational simulations.
- Investigate the role of matric suction pressure in CRAMs specimens for better understanding of the curing mechanism.
- Evaluate if the linear or non-linear elastic behavior of CRAMs influence the pavement mechanical behavior by means of pavement simulation.

## 1.5. THESIS OUTLINE

This thesis is organized in five chapters:

Chapter 1 contains the classification of cold recycling techniques, a brief explanation of some test procedures to evaluate CRAMs stiffness, the problem identification, the general and specific objectives, and the thesis outline.

Chapter 2 presents a study of the effect of mixture composition on the mechanical behavior of CRAMs by means of triaxial resilient modulus and dynamic modulus tests. Part of Chapter 2 was submitted to the International Journal of Pavement Engineering.

The authors of the paper are André Kazuo Kuchiishi, Kamilla Vasconcelos, and Liedi Bernucci.

Chapter 3 presents an investigation of the influence of temperature in stiffness of CRAMs stabilized with foamed asphalt or asphalt emulsion by means of dynamic modulus tests, pavement simulation and temperature instrumentation. Part of Chapter 3 corresponds to an extended and improved version of the paper presented in 2018 at the International Society for Asphalt Pavements Conference and was submitted for the Special Issue of the Road Materials and Pavement Design journal. The authors of the paper are André Kazuo Kuchiishi, Camila C. S. Antão, Kamilla Vasconcelos, and Liedi Bernucci.

Chapter 4 presents the influence of matric suction in the stiffness of foamed asphalt stabilized mixtures by means of filter paper, X-ray microcomputed tomography, and triaxial resilient modulus tests. Part of Chapter 4 was submitted to the European Asphalt Technology Association in Granada, Spain, 2019, and accepted for publication for the Special Issue of Road Materials and Pavement Design journal. The authors of the paper are André Kazuo Kuchiishi, Camila C. S. Antão, Kamilla Vasconcelos, José Pires, Olga M. O. Araújo, Liedi Bernucci, and Ricardo T. Lopes.

Chapter 5 presents an investigation of the effect of non-linear elastic properties of CRAMs on the pavement structure mechanical response by means of pavement simulation and comparison with in situ measurements. This chapter is part of an ongoing research conducted by André Kazuo Kuchiishi, Camila C. S. Antão, Gabriel Souza, Kamilla Vasconcelos, and Liedi Bernucci and will be further submitted.

Chapter 6 presents the conclusions and recommendations for future work regarding CRAMs.

Appendix A presents the resilient modulus curves of the replicate samples of the four CRAMs studied. Appendix B presents the dynamic modulus master curves of the replicate samples of both asphalt mixtures and CRAMs. Appendix C presents the dynamic shear modulus master curves of the replicate asphalt binder samples for both asphalt mixture and CRAMs.

Some information may be repetitive from Chapter 2 to Chapter 5, especially for test section details, materials and sample preparation. It is worth noting that it was necessary since the chapters were written in the technical paper format and used the same materials for laboratory testing.

In order to better visualize the organization of this thesis, Figure 4 illustrates the materials and the test methods used in each chapter. The RAP or GCS identification on the materials names represent the more predominant type of aggregate selected within each base course material gradation. RAP is the aggregate obtained from the asphalt mixture milling process and GCS stands for graded crushed stone, comprised by virgin aggregate. The F and E indexes represent, respectively, foam and emulsion stabilization while the C and H indexes, represent cement and hydrated lime active fillers. The numbers that follow along with the aforementioned indexes represent the respective bitumen stabilizing agent and active filler contents (in percentage).

Figure 4 - Thesis organization

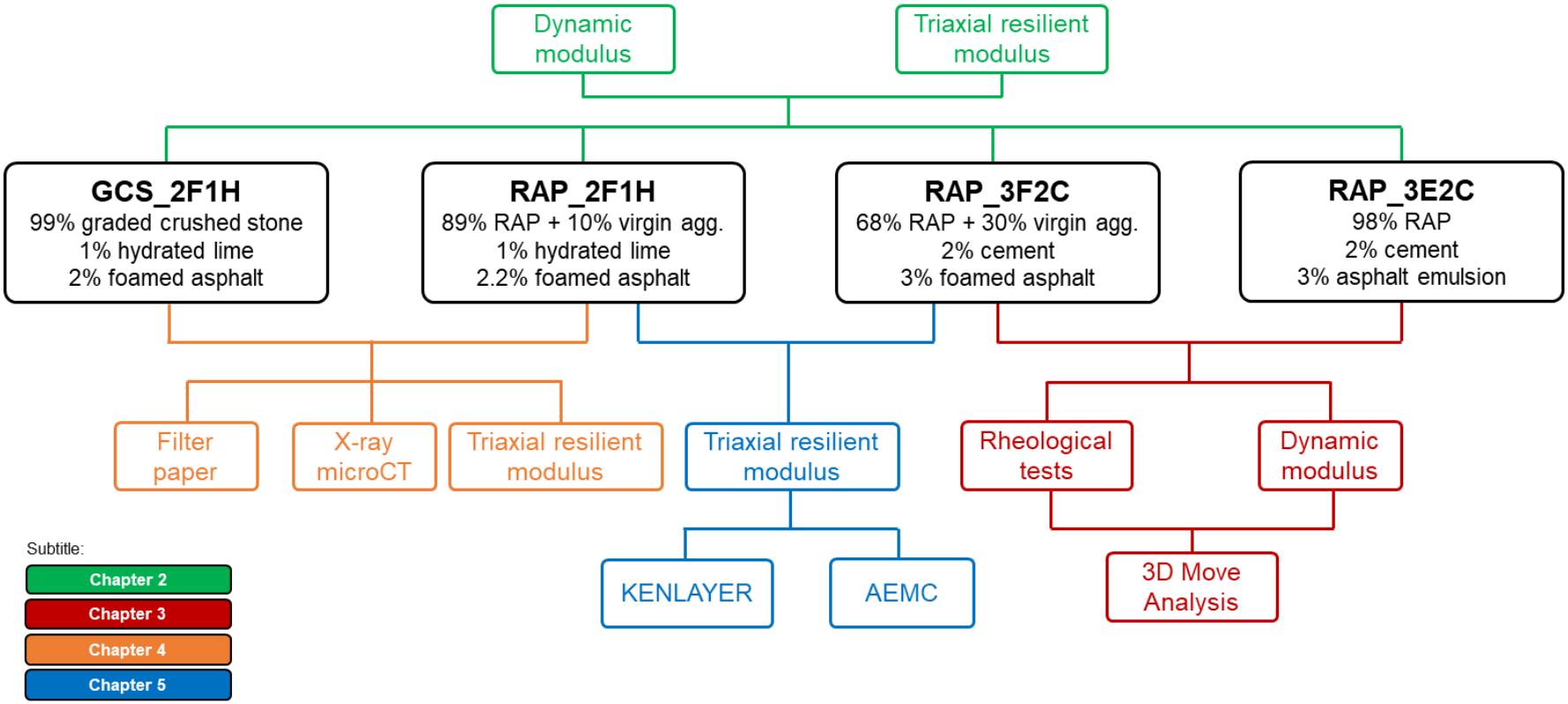


Source: Author

# 2. EFFECT OF MIXTURE COMPOSITION ON THE MECHANICAL BEHAVIOR OF COLD RECYCLED ASPHALT MIXTURES

## 2.1. INTRODUCTION

In general, cold recycled asphalt mixtures (CRAMs) are comprised by RAP, virgin aggregates (for gradation adjustment), stabilized with asphalt bitumen (asphalt emulsion, or foamed asphalt), active filler (cement Portland, or hydrated lime), or a combination of both. Despite of using asphalt and active filler, which increases mixture cohesion and stiffness, CRAMs are usually constructed as base course layers due to its low abrasion resistance against heavy traffic loading, especially in the initial curing period. Therefore, a hot mix asphalt layer is usually overlaid on top of the CRAM (MODARRES; RAHIMZADEH; ZARRABI, 2013).

Different types of mixtures can be produced with the cold recycling technique with respect to the bituminous and active filler contents. The CRAMs can be classified into four major categories with different mechanical properties (Figure 5), as described below. It is worth noting that, despite of the different types of active fillers, Figure 5 presents only the effect of cement, since it is subjected to the hydration reaction and stiffness increase.

- Bitumen Stabilized Material (BSM)
  BSMs present low bitumen and active filler contents (cement Portland ≤ 1%). Usually for BSMs the bitumen/cement (B/C) ratio content should be greater than 1 (B/C > 1). Different mechanical behaviors of BSMs are currently under discussion. Some researches state that they are considered as unbound granular materials with higher cohesion (FU; HARVEY, 2007; GUATIMOSIM et al., 2018) while others support that BSMs behave similarly to asphalt mixtures with viscoelastic characteristics (KIM; LEE; HEITZMAN, 2009; DIEFENDERFER et al., 2016, SMITH; GRAHAM, 2018).
- Cement Treated Material (CTM)
  CTMs are stabilized only with Portland cement, which increases the mixture strength and durability (XUAN et al., 2012). On the other hand, CTMs present

brittle behavior, susceptibility to shrinkage cracking, but increased permanent deformation resistance (CARDONE et al., 2015).

- Cement-Bitumen Treated Material (CBTM)

  CBTMs have higher dosages of cement than BSMs (B/C ≤ 1), which imparts for greater stiffness and strength and increased resistance to permanent deformation, but also have a small dosage of bituminous binder, reducing shrinkage susceptibility in comparison with CTMs (CARDONE et al., 2015). CBTMs can be placed between the HMA layer and the CTM, providing a gradual mechanical response transition from the surface to the underlying layer (MEOCCI et al., 2016).

- Cold Asphalt Mixtures (CAM)

  CAMs present higher bituminous content than BSMs and CBTMs, but limited cement content. Despite the differences between CAM and HMA compositions, the CAM exhibits some temperature and loading frequency dependency (GRILLI; GRAZIANI; BOCCI, 2012).

Figure 5 - Mechanical behavior of pavement mixtures with different cement and bitumen contents

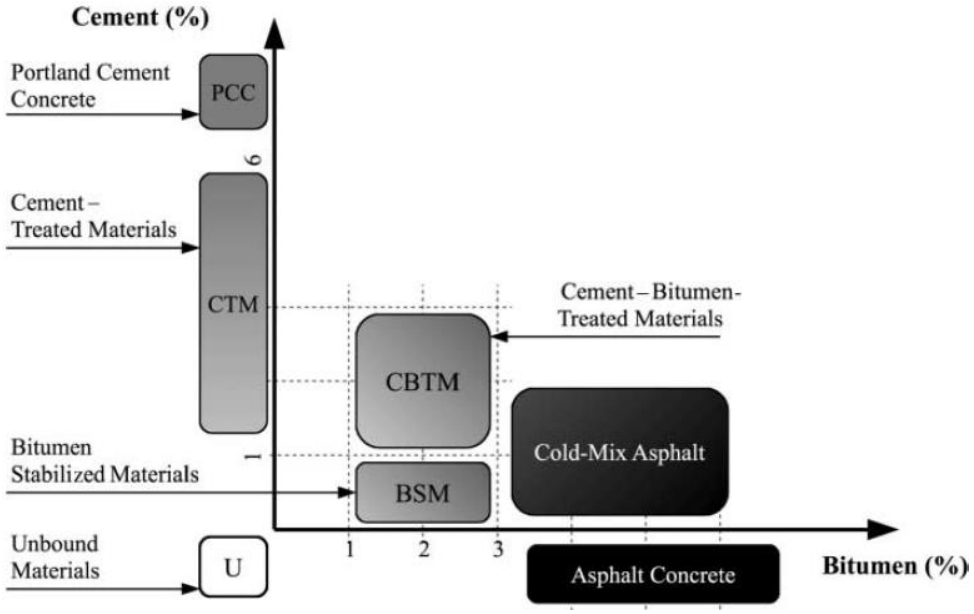


Source: Grilli, Graziani e Bocci (2012)

The great variability in terms of CRAM composition might influence its mechanical behavior when subjected to traffic loading. Several studies have being conducted in order to evaluate the effect of aggregate gradation (RASCHIA et al., 2018), RAP content (GODENZONI; GRAZIANI; BOCCI, 2015), and cold recycling technique (DIEFENDERFER et al., 2016) on CRAMs mechanical behavior.

Some studies reported that the type and content of active filler and bitumen stabilizing agent might impart for significant mechanical properties variability (JOOSTE; LONG, 2007; BOCCI et al., 2014). Jenkins, Long and Ebels (2007), for example, observed that the addition of 0, 1 or 2% of active filler, increasingly enhanced the cohesion of foamed asphalt stabilized mixtures. Guatimosim et al. (2018) observed that a mixture composed by the blend of RAP, crushed cement treated material, foamed asphalt and 1% of hydrated lime resembled a granular material since its stiffness was dependent on the stress state. On the other hand, other researchers concluded that the addition of 1% of cement in CRAMs stabilized with asphalt emulsion produced a mixture independent of the stress state, since a single modulus value was obtained from triaxial resilient modulus tests at different confining pressures (BESSA et al., 2016; KUCHIISHI et al., 2017).

Since different combinations of CRAMs constituents affect its mechanical behavior, a better understanding of its stiffness is fundamental. For this purpose, CRAMs with different compositions regarding aggregate blends, bitumen stabilizing agents and active filler types were investigated by means of triaxial resilient modulus (Tx RM) test and dynamic modulus test. The aim of this study is to evaluate the influence of different mixture compositions on CRAMs stiffness assessment.

## 2.2. COLD RECYCLED ASPHALT MIXTURE COMPOSITION

### 2.2.1. Reclaimed asphalt pavement

Although different aggregate types can be used for bituminous stabilization, such as graded crushed stone, natural gravel, crushed cement-treated materials and others (EBELS, 2008; GUATIMOSIM, 2015), RAP is the most commonly used aggregate for

CRAMs. RAP consists of old milled pavement lumps which are comprised by aggregates and aged asphalt binder. From a visual inspection, it is not possible to distinguish RAP lumps composition which contributes with RAP inherent heterogeneity. The most common practice in order to reduce RAP variability in plant sites prior to mixing is to separate it into two or more stockpiles according to particle size. This provides greater flexibility to adjust RAP gradation (NAPA, 2007), specially for CCPR technique. Figure 6 illustrates RAP particles heterogeneity, with different possible compositions.

Figure 6 - Possible compositions of RAP lumps

Source: Tebaldi et al. (2012)

Besides RAP heterogeneity, its gradation is a variable hard to control since the milling machine speed and the pavement milled depth influence the RAP gradation (BONFIM, 2016). Kuchiishi et al. (2017) presented a study comparing cold recycled mixtures stabilized with asphalt emulsion with different gradations. It was observed that, as the finer particles content increased, the unconfined compressive strength (UCS) and the indirect tensile strength (ITS) increased significantly. Some studies have reported that the RAP obtained from the milling process present a coarser gradation (BONFIM, 2016; LOIZOS; PAPAVISILIOU; PLATI, 2012). Therefore, due to the low amount of fine particles, the addition of a percentage of fine virgin aggregates is usually required. This is necessary, as the asphalt binder disperses preferentially through the fine aggregates (ASPHALT ACADEMY, 2009). For foamed and emulsion asphalt stabilized mixtures, a minimum of 4% and 2% of fines (material passing the 0.075 mm sieve) is recommended, respectively (WIRTGEN, 2012). Table 2 presents the recommended gradation limits for emulsion and foam stabilization.

Table 2 - Recommended grading limits for emulsion and foam stabilized mixtures

| Sieve size (mm) | Ideal percent passing (%) | | | |
|---|---|---|---|---|
| | BSM-emulsion | | BSM-foam | |
| | Min. | Max. | Min. | Max. |
| 50 | 100 | 100 | 100 | 100 |
| 37.5 | 87 | 100 | 87 | 100 |
| 26.5 | 76 | 100 | 76 | 100 |
| 19.5 | 65 | 100 | 65 | 100 |
| 13.2 | 55 | 90 | 55 | 90 |
| 9.6 | 48 | 80 | 48 | 80 |
| 6.7 | 41 | 70 | 41 | 70 |
| 4.75 | 35 | 62 | 35 | 62 |
| 2.36 | 25 | 47 | 25 | 47 |
| 1.18 | 18 | 36 | 18 | 36 |
| 0.6 | 12 | 27 | 13 | 28 |
| 0.425 | 10 | 24 | 11 | 25 |
| 0.3 | 8 | 21 | 9 | 22 |
| 0.15 | 3 | 16 | 6 | 17 |
| 0.075 | 2 | 10 | 4 | 12 |

Source: Wirtgen (2012)

Despite the difficulties of using RAP in terms of its variability, numerous studies have reported improvements in the mechanical performance of CRAM with RAP incorporation. Wu et al. (2012) evaluated the stiffness of a base course material containing 0%, 20%, 40%, 60%, and 80% RAP, blended with crushed aggregate, and without the addition of asphalt binder, or active fillers. From the triaxial resilient modulus test at 20 ºC, the authors observed that the increase of RAP percentage provided an increase of the resilient modulus. Since one single gradation was selected, it suggests that the greater stiffness is related with the void content of the compacted sample. From X-ray computed tomography, it was observed that the 80% RAP mixture presented a considerable lower void content than the mixture with 100% crushed aggregate. Therefore, the addition of RAP leaded to higher compaction levels and, consequently, greater resilient modulus.

Grilli, Bocci and Graziani (2013) compared CTMs with 0%, 50%, and 80% RAP by means of mechanical tests. Although the addition of RAP reduced CTMs' resistance and stiffness, the authors concluded that the recycled materials still presented favorable mechanical properties. A better selection and integration of RAP with virgin

aggregates can provide mixtures with an increasingly RAP content, minimizing the consumption of natural resources. Furthermore, the authors state that the aged binder of the RAP imparted for greater temperature and frequency sensitivity of the mixtures.

Similarly, Sangiorgi et al. (2017) observed that the CRAM with 100% RAP and stabilized with asphalt emulsion presented lower resistance and stiffness than HMA samples, both used as base layer materials. Despite of these differences in terms of mechanical properties, the ITS values of the recycled mixture were greater than those limited by some Italian technical specifications for base layer materials using Cold Mix Asphalt, which restricts the RAP content. According to Sangiorgi et al. (2017), even with 100% RAP, the ITS values obtained were higher than the minimum specified.

Therefore, when adequate stabilization and construction practices are guaranteed, appreciable mechanical properties can be obtained from CRAMs. A proper selection and integration of RAP with virgin aggregates can provide mixtures with increasingly RAP content.

### 2.2.2. Bitumen stabilizing agents

For bitumen stabilization, asphalt emulsion or foamed asphalt are frequently used with the purpose of reducing the asphalt binder viscosity and provide adequate mixing and dispersion of the asphalt throughout the mixture. This is equivalent to the hot mix asphalt production, in which the asphalt binder is heated in order to reduce its viscosity (DIEFENDERFER et al., 2016).

Asphalt emulsion and foamed asphalt are very different in terms of production and dispersion. Figure 7 depicts the visual difference of asphalt dispersion between an asphalt emulsion stabilized sample and a foamed asphalt stabilized sample. In the former, a thin layer of asphalt binder completely covers the aggregates surface. In the latter, the foamed asphalt is non-continuously distributed, characterized by the localized bonds. Further discussion of both bitumen stabilizations are presented herein. It is important to state that for cold recycling, RAP is considered a “black rock”

and its aged binder content is not considered for mix design purposes (WIRTGEN, 2012).

Figure 7 - External appearance of an (a) asphalt emulsion stabilized sample and a (b) foamed asphalt stabilized sample

(a) (b)

Source: Author

2.2.2.1. Asphalt emulsion

The use of asphalt emulsion date back to the beginning of the 20$^{th}$ century, when the Swiss Physicist Dr. Ernest Guglielminetti promoted the use of emulsified hydrocarbons to coat the road surfaces in order to reduce dust generation. However, it was after Hugh Mackay's anionic bitumen emulsion patent, in 1922, that the use of asphalt emulsion increased significantly (EBELS, 2008).

Emulsion is a dispersion of an immiscible fluid into another fluid. For asphalt emulsions, the immiscible fluid is the asphalt binder, which is dispersed into the water phase. Because of the hydrophobic characteristic of the asphalt binder, an emulsifier is also added in order to provide a stable emulsion during manufacturing, storage, and transportation purposes (EBELS, 2008).

The emulsifier molecule is composed by a polar hydrophilic "head" and a non-polar hydrophobic "tail", illustrated in Figure 8. Depending on the electrostatic charge of the emulsifier, the asphalt emulsion can be classified as anionic, for negative charge, or cationic, for positive charge. In general, cationic emulsions are more frequently used,

since it generally reacts with more types of rock, being more aggregate-compatible than anionic emulsion types (EBELS, 2008).

Figure 8 - Cationic emulsifier molecule comprised of hydrophilic and hydrophobic portions

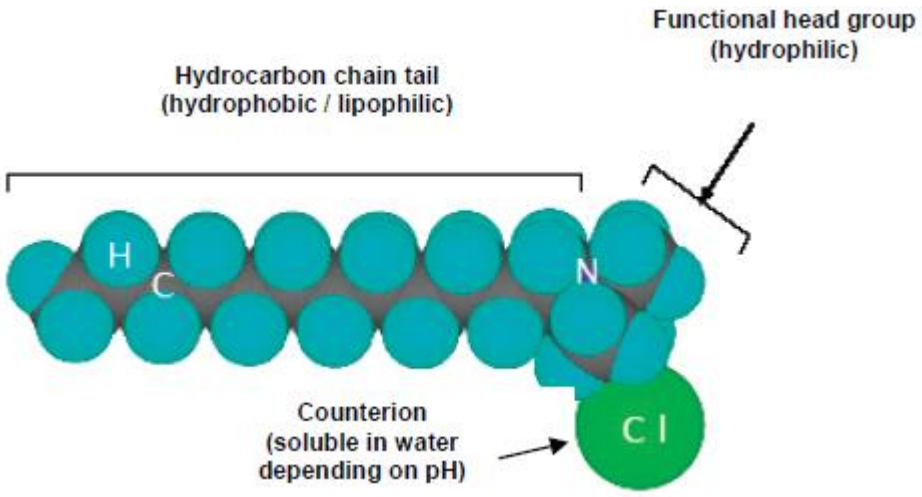


Source: James (2006)

The hydrophobic (or lipophilic) portion of the emulsifier molecule is adsorbed by the asphalt droplets surface, leaving the hydrophilic portion oriented towards the water phase. This configuration prevents the asphalt droplets to coalesce prior to compaction in the field, due to the repulsive electrostatic charge between the asphalt droplets. Figure 9 depicts the repulsive forces caused by positive electrostatic charges of a cationic emulsion type.

Figure 9 - Repulsive forces due to positive electrostatic charges in a cationic emulsion

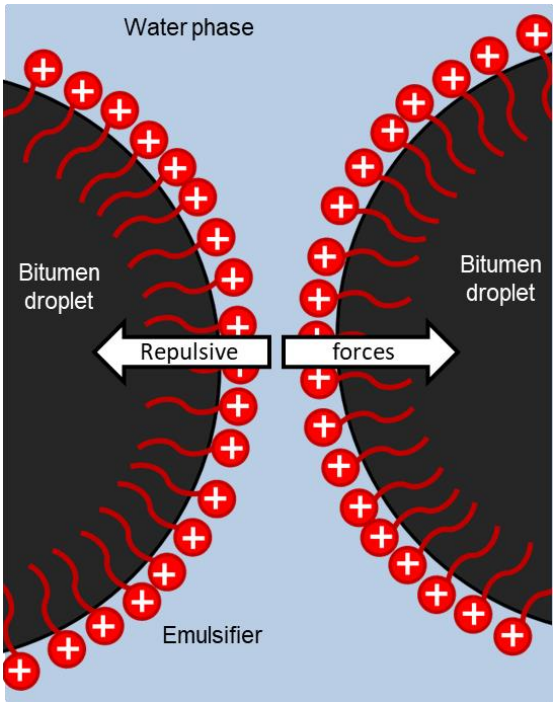


Source: Author

Since no heat is required for cold recycling purposes, the stability provided by the emulsifier is fundamental for proper mixing and compaction of CRAMs. Due to the opposite charges between asphalt emulsion and aggregates, the asphalt emulsion disperses throughout the mix, preferentially among the fine particles because of electrostatic attraction. This justifies the required minimum of 2% of material passing the 0.075 mm sieve in order to provide proper dispersion of asphalt emulsion (ASPHALT ACADEMY, 2009; WIRTGEN, 2012). After compaction, the reduction in the emulsifier repulsive charges (caused by water evaporation, cement catalyst behavior, or low emulsifier content) result in the coalescence of asphalt binder droplets. The transition in which asphalt changes from being dispersed in water to be covering the aggregates surface by a thin continuous asphalt film is known as “emulsion breaking” (EBELS, 2008). This process is visually identified when the color changes from dirty brown to black. The compaction of the mixture should be carried out prior to emulsion break, since the emulsion acts as a lubricant agent (WIRTGEN, 2012).

It is important to state that the breaking mechanism is different from the curing of the mixture. Despite both processes are related to moisture loss and occur simultaneously, the concepts regarding these two mechanisms are not the same. In the former process, the water within the emulsion evaporates and only the asphalt binder is left “painting” the coarse aggregates (JENKINS, 2000; ASPHALT ACADEMY, 2009). In the latter, the water evaporation corresponds to the reduction of moisture content increasing the bonding strength between asphalt mortar and aggregates (LIN et al., 2015) This will provide greater stiffness and tensile strength to the CRAMs stabilized with asphalt emulsion (WIRTGEN, 2012; BESSA et al., 2016).

#### 2.2.2.2. Foamed asphalt

Despite the different foaming methods that have been already invented, Dr. Ladis Csanyi, at the Bituminous Research Laboratory in Iowa State University, developed a foaming nozzle that permitted a more precise control of the materials quantity and the foaming process (CSANYI, 1957). Almost ten years later, Mobil of Australia acquired Dr. Csanyi’s nozzle patent, modified the process of foamed asphalt production and extended this technology to several countries (JENKINS, 2000). Currently, the foaming process have been extensively used, resulting in scientific studies in Brazil (GUATIMOSIM; VASCONCELOS; BERNUCCI, 2017), South Africa (DAL BEN; JENKINS, 2014), Greece (LOIZOS, 2006), Italy (GODENZONI et al., 2017), United States (KHOSRAVIFAR; SCHWARTZ; GOULIAS, 2014), and India (NIVEDYA et al., 2018).

The foamed asphalt is the result of the contact of water, air and hot asphalt binder inside an expansion chamber at high pressure. When the contact occurs, water turns into vapor and becomes trapped inside asphalt droplets (ASPHALT ACADEMY, 2009). At this state, the asphalt volume increases significantly, reducing its viscosity, and allowing proper mixing with aggregates at ambient temperature and at in situ moisture contents (JENKINS, 2000). The viscosity reduction is characterized by physical properties modification, while the chemical properties remain the same. According to Csanyi (1957), an asphalt binder with penetration grade between 85 and 100 will increase its penetration grade to 300 after foaming.

In order to guarantee the quality of the foamed mixture, binder with penetration grade between 60 and 200 are generally selected. However, in terms of asphalt requirements, the penetration index alone does not provide sufficient information to validate the use of an asphalt binder for the foaming process. Therefore, two additional properties are used: expansion ratio (ER) and half-life ($\tau_{1/2}$). The ER is a dimensionless value that indicates if the foam will disperse adequately throughout the mixture. It is defined as the ratio between the maximum volume of the foamed bitumen and its initial volume. The $\tau_{1/2}$ corresponds to the time, in seconds, needed for the maximum volume of the foamed bitumen to reduce by half. It is a measure of stability of the foam. Both the ER and $\tau_{1/2}$ are used to determine the optimum water content for the foaming process. An excessive amount of water increases the ER but decreases the $\tau_{1/2}$, compromising the stability of the foam, since a shorter period of time is available for foam dispersion. On the other hand, an insufficient water content provides greater stability but reduced ER. In this case, the viscosity of the foam is not low enough to provide a proper dispersion of the foam. A minimum of 8.0 times for ER and 6.0 seconds for $\tau_{1/2}$ are usually recommended (WIRTGEN, 2012).

During mixing, the asphalt droplets burst and tiny asphalt particles are produced, which disperse within the aggregate matrix. It is worth noting that this dispersion occurs exclusively throughout the fine particles, resulting in a mastic, since the tiny asphalt particles do not have enough energy to warm coarser aggregates. For this reason, a minimum of 4% of material passing the 0.075 mm sieve is required in order to guarantee adequate asphalt dispersion. When the percentage of fines is insufficient, many asphalt-rich lumps are formed, denominated “stringers”. At this condition, a poor mix is commonly produced (ASPHALT ACADEMY, 2009).

During compaction, the asphalt of the mastic is physically pressed against the coarser aggregates, bonding one particle to the other. Differently from asphalt emulsion, which covers the aggregate surface, the created bonds between mastic and aggregates are localized and non-continuously distributed. These bonds are referred as “spot welds” (COLLINGS; JENKINS, 2011; WIRTGEN, 2012).

### 2.2.3. Fillers

Fillers can be classified into inactive fillers or active fillers. Inactive fillers are mineral inert particles, such as rock flour, which are limited to a physical interaction with other components, mainly by supplementing the fines required for proper asphalt dispersion (ASPHALT ACADEMY, 2009). On the other hand, the active fillers chemically modify the mix properties. Besides the gradation adjustments, the active fillers can be used to improve adhesion of the asphalt to the aggregate, enhance dispersion of the asphalt, increase stiffness of the mixture, reduce moisture susceptibility, and accelerate curing of the compacted material (WIRTGEN, 2012).

Although different types of active fillers can be used (e.g. fly ash, blast furnace slag), Portland cement and hydrated lime are commonly preferred for cold recycling practices. Brown and Needham (2000) observed that CRAMs stabilized with asphalt emulsion containing cement and hydrated lime presented greater resistance to moisture damage, as the samples resisted better to the soaking cycles. The samples with different active fillers did not resist the second soak, indicating that cement and hydrated lime indeed impart for greater adhesion between binder and aggregate.

The need for cement or hydrated lime is determined in terms of the Tensile Strength Ratio (TSR) value. The TSR, calculated as the ratio between the $ITS_{WET}$ (24 hours soaking at 25 ºC) and the $ITS_{DRY}$ of the compacted samples, is expressed in percentage. If the TSR > 60%, no active filler is required in the mix design. If TSR < 60%, an active filler should be selected, and the preference for either cement or hydrated lime is undertaken regarding the type of mixture which contributes with more than 5% TSR increase (WIRTGEN, 2012).

Besides the increase of the CRAM's bearing capacity during its early-stages (BETTI et al., 2016), the use of cement as an active filler also accelerates the emulsion break. The hydration of cement compounds produces calcium silicate hydrate ($C_3S_2H_3$) and calcium hydroxide (CH or $Ca(OH)_2$). The calcium hydroxide, which is partly soluble, is then ionized producing calcium ion ($Ca^{2+}$) and hydroxide ($OH^-$). Thus, when cationic asphalt emulsion is used, the negatively charged hydroxides surrounds the positively charged cationic asphalt droplets, neutralizing the emulsifier agent (EBELS, 2008). This process accelerates the coalescence of the asphalt droplets and, consequently,

the emulsion break. Therefore, when high cement content is adopted, special care should be taken in order to avoid rapid emulsion break prior to mixture compaction.

Despite the influence of the emulsion water phase in cement hydration, some studies have investigated the chemical interaction between the two compounds. From X-ray diffraction analysis, Du (2012) observed that the cement paste (cement + water) and the cement asphalt mastic (cement + emulsion) presented similar diffraction patterns. As can be seen in Figure 10, these diffraction patterns present peaks located in similar positions. In conjunction with Fourier-transform infrared spectroscopy tests, it was observed that the combination of cement and asphalt emulsion does not produces new crystalline substances, being restricted to a physical interaction. Similar discussions are presented in Montepara and Giuliani (2001) and Garilli et al. (2016).

Figure 10 - X-ray diffraction patterns for cement paste and cement asphalt mastic

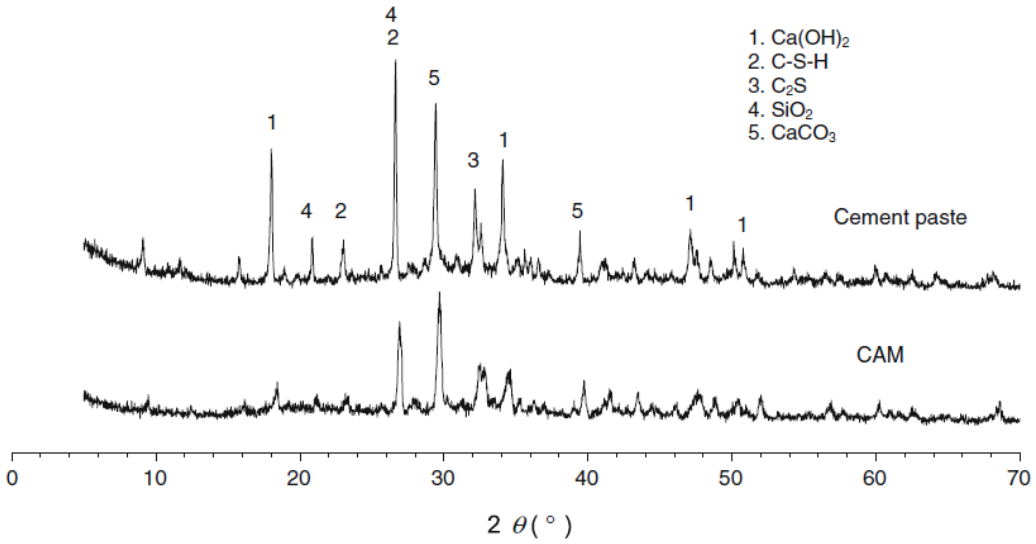


Source: Du (2012)

Albeit the advantages of using cement as an active filler, drawbacks with stockpiling the CRAMs are current. The South African guideline (ASPHALT ACADEMY, 2009) recommends that after binder stabilization, the mixture should be only temporary stockpiled. For asphalt emulsion stabilization, a maximum of two days is suggested for

stockpiling practices. Regarding foamed asphalt mixtures, the CRAM can be stockpiled for several days if the moisture content is maintained close to the optimum moisture content (OMC), and if the material remains uncompacted (ASPHALT ACADEMY, 2009). Schwartz and Khosravifar (2013) observed that CRAMs with cement as active filler and foamed asphalt stabilization presented lower ITS values for longer stockpiling periods. This was attributed to the breakage of cementitious bonds that were developed during storage time. In terms of CRAMs stabilized with asphalt emulsion, stockpiling practices are not recommended and hydrated lime can be used instead.

Nonetheless, differently from cement, hydrated lime is not comprised by tricalcium ($C_3S$) or dicalcium ($C_2S$) silicate, which react with water, producing $C_3S_2H_3$ and $Ca(OH)_2$. It means that the addition of hydrated lime as an active filler does not contribute with stiffness increase in contact with water, as it occurs when cement is used. Therefore, mixtures with cement (ordinary Portland cement, OPC) are stiffer than those with hydrated lime, as shown in Figure 11. Even though, the hydrated lime has specific surface area 10 times greater than has the cement (CINCOTTO, 2007). The presence of higher amounts of fine aggregates provides a better dispersion of the asphalt throughout the mix (ASPHALT ACADEMY, 2009).

Figure 11 - Stiffness modulus of CRAMs with different types of active filler

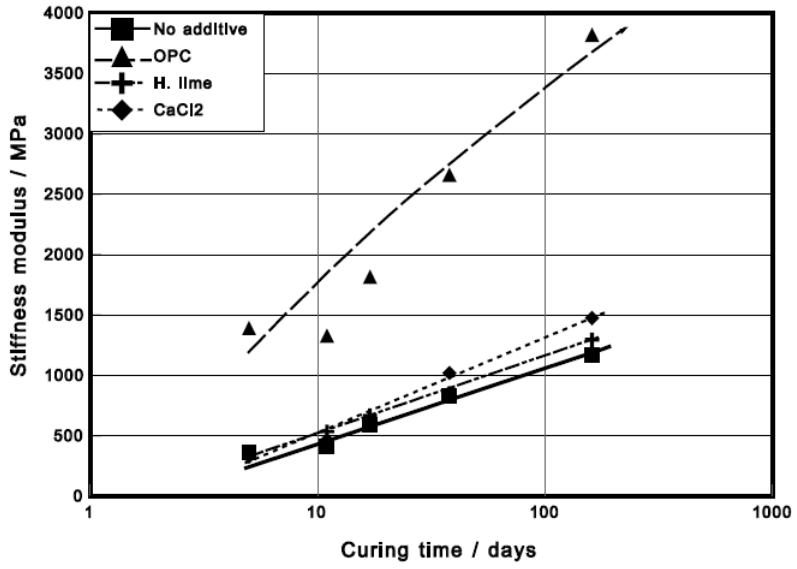


Source: Brown and Needham (2000)

## 2.3. MATERIALS

### 2.3.1. Pavement structure and material preparation

The materials used for this study were collected from the experimental test section in Fernão Dias highway, located at Extrema city, in Minas Gerais. The test section was constructed in the right lane (heavy traffic lane) of a two-lane segment in Fernão Dias highway (BR 381). Fernão Dias is a federal highway under Autopista Fernão Dias concession, and is considered a high traffic highway in Brazil, connecting São Paulo and Belo Horizonte cities.

The total length of the experimental test section is 800 m and is comprised by different pavement structures with 100 m length each. The pavement structures differ from each other in terms of the materials used for the pavement layers and its thickness. Among the eight test sections, four of them are composed by bitumen stabilized base course materials with different types of bitumen stabilizing agents, active filler, and aggregate composition. Figure 12 illustrates the location of the four bitumen stabilized test sections with different codes for base course material identification.

Figure 12 - Location of the experimental test sections

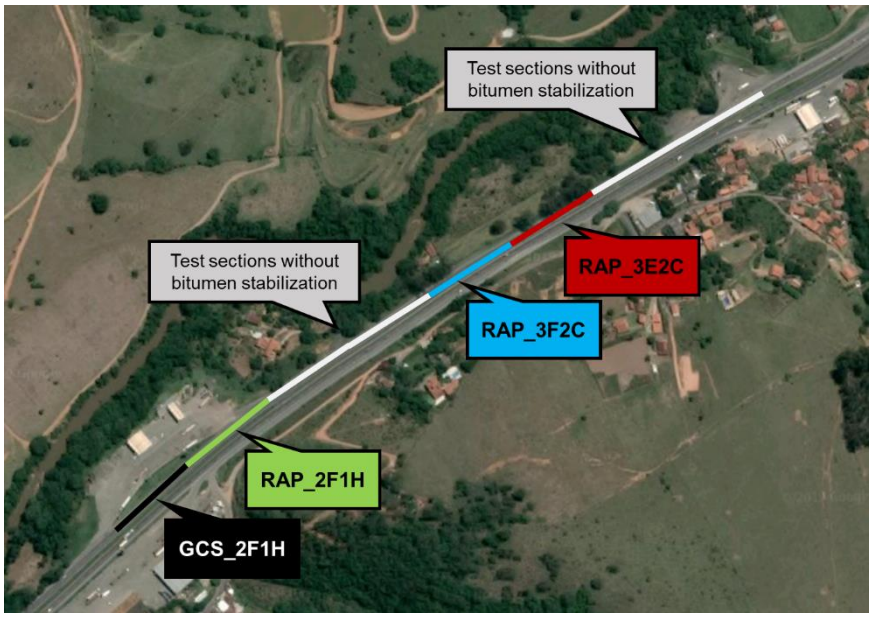


Source: Google, 2018

The RAP or GCS identification represent the more predominant type of aggregate selected within each base course material gradation. RAP is the aggregate obtained from the asphalt mixture milling process and GCS stands for graded crushed stone, comprised by virgin aggregate. The F and E indexes represent, respectively, foam and emulsion stabilization while the C and H indexes, represent cement and hydrated lime active fillers. The numbers that follow along with the aforementioned indexes represent the respective bitumen stabilizing agent and active filler contents (in percentage).

Differently from the RAP_2F1H and GCS_2F1H materials, above which a 30 mm gap-graded layer was compacted, an asphalt concrete layer of 125 mm thickness was placed on top of the RAP_3F2C and RAP_3E2C base courses. Figure 13 illustrate the proposed structural rehabilitation solution for the four bitumen stabilized test sections.

Figure 13 - Pavement structures of the (a) RAP_2F1H, (b) GCS_2F1H, (c) RAP_3F2C, and (d) RAP_3E2C

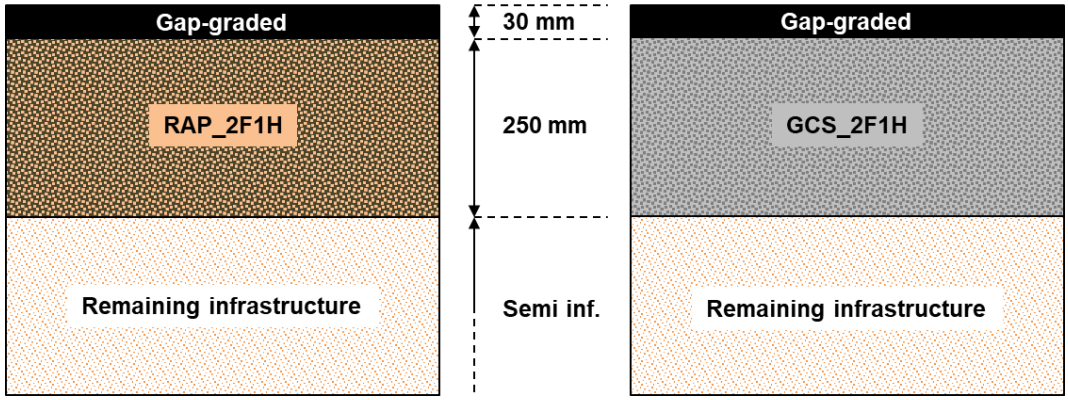


(a) (b)

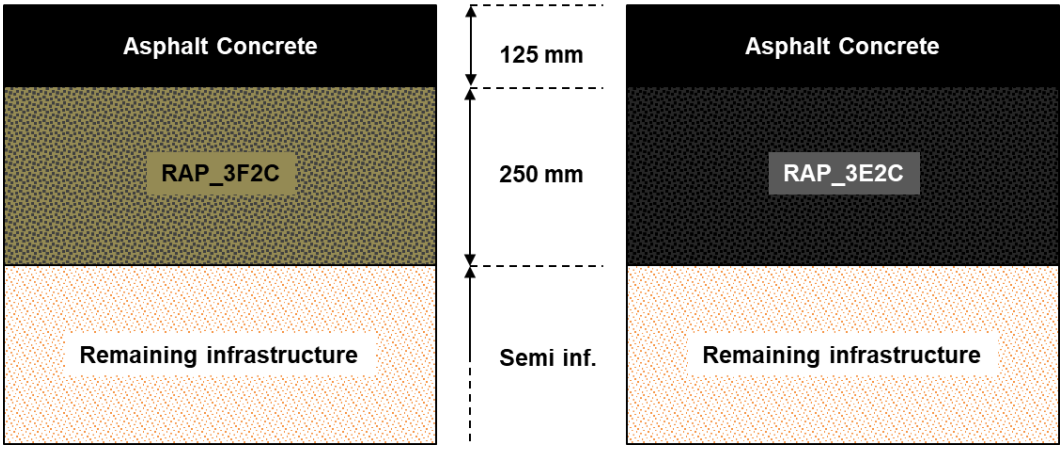


(c) (d)

Source: Author

The RAP_2F1H and GCS_2F1H test sections were constructed in July 2017 and the construction details will be further presented in Chapter 4. The RAP_3F2C and RAP_3E2C segments were built in December 2014 and further information regarding construction practices can be found in Andrade (2017). It is worth mentioning that the RAP used in the mixtures with hydrated lime or cement are not the same, since the test sections were constructed in different years.

Contrarily to the RAP_2F1H and GCS_2F1H, which were already stabilized with foamed asphalt, the RAP_3F2C and RAP_3E2C 'raw' materials were transported separately to the Laboratory of Pavement Technology, at Escola Politécnica of Universidade de São Paulo. Those mixtures could not be hauled after stabilization due to cement addition, which hydrates, impairing mixture and compaction procedures.

For the gap-graded mixture, used as wearing course in the RAP_2F1H and GCS_2F1H segments, a SBS-modified binder was selected and classified according to the Brazilian standards as 60/85 (minimum softening point/elastic recovery). For the asphalt concrete mixture, a neat binder with penetration index 30/45 was used. The asphalt binder content of the gap-graded and asphalt concrete mixtures was 5.7% and 4.3%, respectively.

For the RAP_3F2C, 30% of fine aggregate blend (100% passing the 2.36 mm sieve) was added in order to guarantee a minimum of 4% passing the 0.075 mm sieve.

However, with the higher amount of fines, the gradation curve of the mixture exceeded the limits recommended by Wirtgen (2013). Besides, an 85/100 penetration grade binder was used for foaming purposes. For the RAP_3E2C, the final gradation curve also exceeded the recommended limits, although no fine virgin aggregates were added for gradation adjustments. This may be attributed to the milling process, which might have produced a higher amount of RAP fines. In addition, a slow-setting cationic emulsion was selected (62.3% of nominal binder content).

The RAP binder content of both RAP_3F2C and RAP_3E2C mixtures is equal to 5.0% and it was determined by means of the ignition method (ASTM D6307-16). For the RAP_2F1H mixture, the RAP binder content could not be determined since the mixture was collected already after the foamed asphalt have been added. In this case, it would not be possible to separate the binder from the foamed asphalt from the RAP aged one. Table 3 presents the mixture composition and Figure 14 presents the gradation curves of the four bitumen stabilized materials. The asphalt content on Table 3 does not account for the RAP aged binder content of RAP_3F2C and RAP_3E2C mixtures.

Table 3 - Mixture composition of the four bitumen stabilized materials

| Mixture composition | Unit | RAP_2F1H | GCS_2F1H | RAP_3F2C | RAP_3E2C |
|---|---|---|---|---|---|
| RAP | % | 89.0 | 0.0 | 68.0 | 98.0 |
| Virgin aggregate | % | 10.0 | 99.0 | 30.0 | 0.0 |
| Active filler | % | 1.0 | 1.0 | 2.0 | 2.0 |
| Asphalt content | % | 2.2 | 2.0 | 3.0 | 3.0 |
| Maximum specific density | g/cm³ | 1.914 | 2.168 | 2.060 | 2.006 |
| OMC | % | 7.8 | 5.3 | 5.3 | 5.5 |

Figure 14 - Gradation curves of the four bitumen stabilized materials

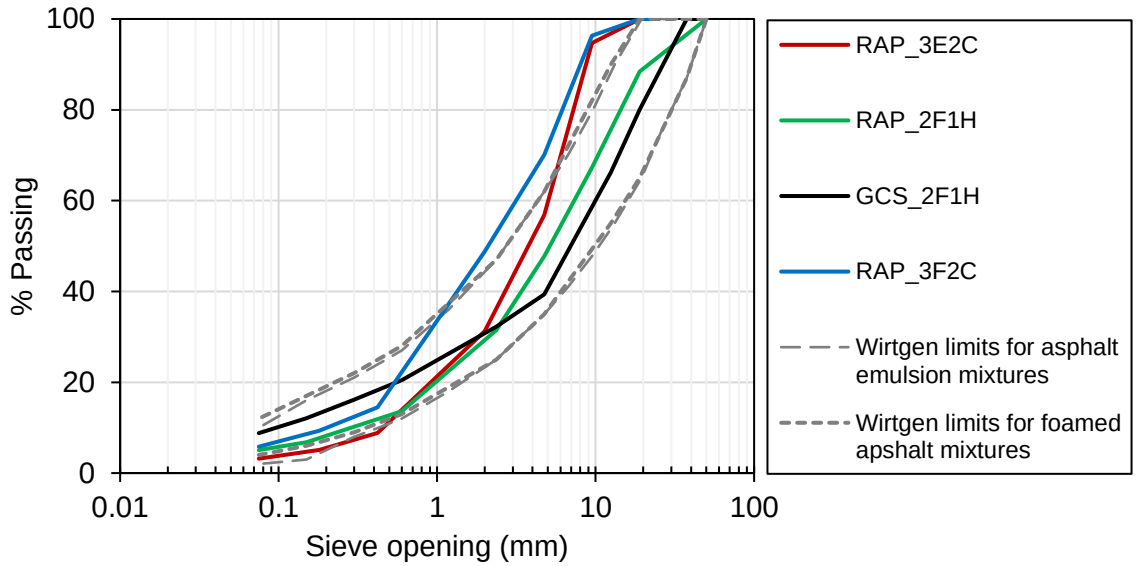


The RAP collected from the field was oven dried at 40 ºC for 24h and then further fractionated. Prior to compaction of the RAP_3E2C material, RAP and cement were first added and mixed inside a metal container, followed by water and asphalt emulsion. The materials were thoroughly revolved until a homogeneous mixture was obtained.

For the RAP_3F2C, the foaming machine Wirtgen WLB 10S was used (Figure 15a). The asphalt for the foaming process (Figure 15b) was heated until 165 ºC was reached within the whole system, and it was further used to adjust the machine foaming rate. After that, the water for foaming was determined by means of the Expansion Ratio (ER) and Half-life ($\tau_{1/2}$) parameters. A 2.6% of water content for foaming was then selected, providing an ER of 24 times and a $\tau_{1/2}$ of 14.3 seconds, greater than the recommended values of 8 times and 6 seconds by Wirtgen (2012). The RAP, cement, and the virgin aggregate blend were then placed into the Wirtgen pugmill WLM 30 and revolved (Figure 15c). Afterwards, the water was added, followed by the foamed asphalt. A total of approximately 25 kg was produced per batch and the foamed stabilized mixture was further conducted to specimen compaction. Both the foaming and compaction processes were conducted at Copavel Consultoria de Engenharia Ltda.

Figure 15 - (a) Wirtgen WLB 10s foaming machine and placement of the (b) binder and (c) aggregates

(a) 


(b)

(c)

Source: Author

### 2.3.2. Compaction

The equipment used for compaction was a Bosch GSH 11 VC vibratory hammer with 1700 W power and approximately 30 kg weight. The base course materials were laid inside the molds, compacted, extracted and stored inside PVC tubes and sealed into plastic bags in order to maintain the moisture inside. For the dynamic modulus test, specimens with 100 mm diameter and 150 mm height were prepared.

The number of layers and the compacted time per layer (in seconds) are defined according to the specimen size. It is worth noting that the vibratory hammer used in this thesis has small differences in comparison with the recommended South African one, especially with respect to the power rating specification. Besides, both types of specimen geometry (100 mm x 150 mm and 100 mm x 200 mm) are not specified in the guidelines (ASPHALT ACADEMY, 2009). Therefore, the number of layers and the compacted time were trial and error determined for each type of base course material.

Table 4 presents the number of layers, compaction time, dry bulk density achieved, and the degree of compaction (DC).

Table 4 - Assessment of vibratory compaction method

| Material | Specimen height (mm) | Replicate (-) | No. of layers (-) | Compaction time/layer (s) | Dry bulk density (g/cm³) | Maximum specific density (g/cm³) | DC (%) |
|---|---|---|---|---|---|---|---|
| RAP_2F1H | 150 | 1 | 2 | 5 | 1.981 | 1.914 | 104 |
| | | 2 | | 5 | 1.979 | | 103 |
| | 200 | 1 | | 7 | 1.973 | | 103 |
| | | 2 | | 7 | 1.975 | | 103 |
| GCS_2F1H | 150 | 1 | 2 | 15 | 2.161 | 2.168 | 100 |
| | | 2 | | 15 | 2.168 | | 100 |
| | 200 | 1 | | 20 | 2.147 | | 99 |
| | | 2 | | 20 | 2.146 | | 99 |
| RAP_3E2C | 150 | 1 | 2 | 15 | 2.091 | 2.006 | 104 |
| | | 2 | | 15 | 2.057 | | 103 |
| | 200 | 1 | | 20 | 2.037 | | 102 |
| | | 2 | | 20 | 2.058 | | 103 |
| RAP_3F2C | 150 | 1 | 2 | 7 | 2.055 | 2.060 | 100 |
| | | 2 | | 7 | 2.056 | | 100 |
| | 200 | 1 | | 10 | 2.049 | | 99 |
| | | 2 | | 10 | 2.053 | | 100 |

### 2.3.3. Curing

Due to the cement addition in the RAP_3E2C and RAP_3F2C mixtures, a longer curing period was adopted in order to guarantee total hydration of the cement. Cardone et al. (2015) observed increasingly stiffness values for CRAMs cured at 40 ºC during 28 days. Therefore, for the mixtures with cement addition, the same curing procedure was adopted. For the RAP_2F1H and GCS_2F1H materials, the specimens were cured at 40 ºC for seven days. Thus, the mixtures with either hydrated lime or cement Portland addition were fully cured prior to testing.

## 2.4. RESULTS AND DISCUSSION

### 2.4.1. Triaxial resilient modulus

The triaxial resilient modulus test (Tx RM) was conducted according to the Brazilian standard DNIT ME 134/10, which comprehend a wider range of pressure combinations in comparison with AASHTO T307-99 for base or subbase materials. In this test, a 100 mm diameter and 200 mm height specimen is subjected to cyclic haversine loading, with load period of 0.1 second and rest period of 0.9 second. Different combinations of confining and deviator pressure are used, in order to simulate various stress state conditions. Prior to the test, a conditioning stage is required in order to reduce plastic deformation during the test. All the Tx RM tests were performed at ambient temperature (around 25 °C). For sample preparation, a thin layer of plaster was used to level the top and bottom of the specimens.

The resilient modulus (RM) can be expressed in terms of the confining pressure ($\sigma_3$) and two regression coefficients, $k_1$ and $k_2$ (Equation 1).

$$RM = k_1 \sigma_3^{k_2} \quad (1)$$

Figure 16 presents the mean resilient modulus curves of the four bitumen stabilized base courses. Two replicates of each material were tested and the resilient modulus curves of the replicate specimens can be found in Appendix A. Table 5 presents the regression coefficients $k_1$ and $k_2$ along with the coefficient of determination ($R^2$).

Figure 16 - Resilient modulus curves of the four bitumen stabilized base courses

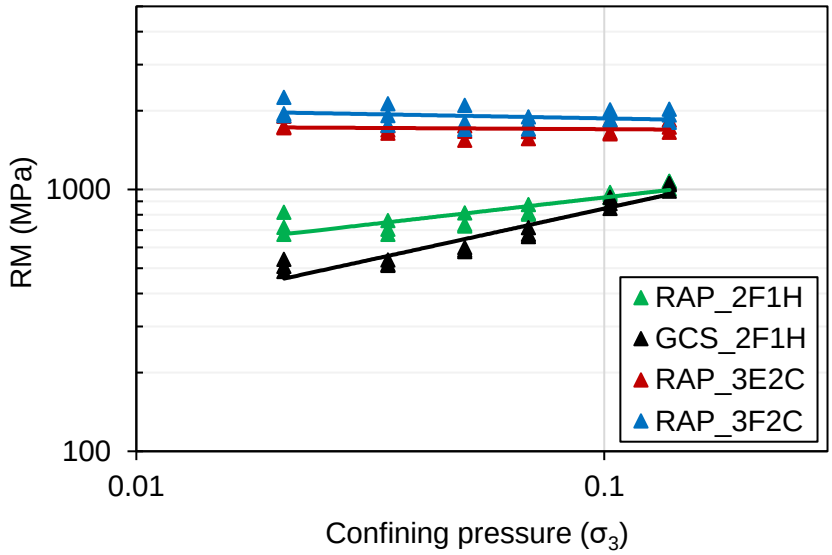


Table 5 - Regression coefficients of the RM model

| Mixture | $k_1$ | $k_2$ | $R^2$ |
|---|---|---|---|
| RAP_2F1H | 1493.8 | 0.205 | 0.76 |
| GCS_2F1H | 2077.6 | 0.391 | 0.90 |
| RAP_3E2C | 1661.2 | -0.010 | 0.01 |
| RAP_3F2C | 1733.2 | -0.032 | 0.08 |

From Figure 16, it can be seen that the RAP_3E2C and RAP_3F2C mixtures (with 2% Portland cement) are considerably stiffer than the RAP_2F1H and GCS_2F1H ones (with 1% hydrated lime). While the former have a modulus of approximately 2000 MPa, the latter exhibit a modulus lower than 1000 MPa. The difference in stiffness between these two groups of mixtures can be attributed to the presence of cement, which imparts greater stiffness after the hydration reaction. Other researchers have already observed significantly stiffness increase after cement addition in either asphalt emulsion (BROWN; NEEDHAM, 2000) and foamed asphalt stabilized mixtures (BETTI et al., 2016).

The base course materials can also be compared in terms of the confining pressure dependency. From Figure 16, it can be seen that the mixtures without cement addition

(RAP_2F1H and GCS_2F1H) present a stress-dependent behavior since different modulus values are obtained for different confining pressures. In this sense, these mixtures behave similarly to granular materials. The confining pressure dependency can also be depicted by the increased $k_2$ coefficient values presented in Table 5. On the other hand, RAP_3E2C and RAP_3F2C mixtures are independent of the confining pressure and its mechanical behavior resemble a cemented material, in which a single modulus value is obtained for different confining pressures. For these mixtures, the $k_2$ coefficient values are close to zero and the $R^2$ is low, indicating a reduced confining pressure dependency.

This difference regarding the mechanical behavior can also be attributed to the type of active filler used. The hydration reaction of the 2% Portland cement content used in the RAP_3E2C and RAP_3F2C mixtures imparts for a reduced stress-state dependency. Similar results were obtained for mixtures with 1% cement content (BESSA et al., 2016; KUCHIISHI et al., 2017). Since the hydrated lime in RAP_2F1H and GCS_2F1H mixtures does not react in the same manner as cement, these mixtures exhibit a granular mechanical behavior and reduced modulus values in comparison with RAP_3E2C and RAP_3F2C ones.

It is important to state that, although the Tx RM test properly distinguishes the mixtures with and without cement, conducting it solely for CRAMs stiffness assessment might lead to deceptive conclusions. Although the Tx RM test is faster to be performed in comparison with the dynamic modulus test, Figure 16 indicates that the RAP_3E2C and RAP_3F2C are structurally equivalent since the resilient modulus curves are similar to each other. In other words, from an elastic evaluation, both mixtures could be considered identical in terms of its mechanical behavior. However, the dynamic modulus master curves presented next shows that these mixtures cannot be considered the same when viscoelastic analysis is conducted.

### 2.4.2. Linear viscoelastic properties

The dynamic modulus test was performed according to the AASHTO T342-11. The 100 mm diameter and 150 mm height specimen is subjected to a sinusoidal load under

six different frequencies (25, 10, 5, 1, 0.5, 0.1 Hz) and four temperatures (54, 37.8, 21.2, 4.4 ºC). The test is conducted in a stress-controlled condition, and the loads are selected with the purpose of guarantying that the axial deformation would be within the range of 50 to 150 με, which should correspond to the linear viscoelastic region. The axial deformation is measured by two extensometers vertically aligned with the specimen and placed at diametrically opposed positions in relation to each other.

The dynamic modulus test was performed for the RAP_2F1H and GCS_2F1H materials at the OMC for one specimen of each mixture (initial curing condition). For the final curing condition, two specimens of each base course material was tested. After the curing period, the specimens were kept in a plastic bag to avoid moisture variation and were placed inside the environmental chamber at the first test temperature (4.4 ºC) prior to test initiation (Figure 17a). An overnight period was required in order to the specimen reach the 4.4 ºC temperature. For the remaining test temperatures, 21.1, 37.8 and 54 ºC, it was necessary to wait three, two and one hour, respectively, for temperature stabilization. After the stabilization time, the test could be conducted (Figure 17b).

Figure 17 - (a) Specimen inside plastic bag before test and (b) sample inside environmental chamber during test

(a) (b)

Source: Author

The complex modulus (E*) is defined as the ratio between the applied stress and the measured strain, and is represented by an imaginary number comprised by a real part (E', or storage modulus) and an imaginary part (E", or loss modulus). Equation 2 presents the complex modulus, as follows.

$$E^* = \frac{\sigma_0 e^{i\omega t}}{\varepsilon_0 e^{i(\omega t - \varphi)}} = \frac{\sigma_0}{\varepsilon_0}\cos\varphi + i\frac{\sigma_0}{\varepsilon_o}\sin\varphi = E' + iE'' \quad (2)$$

Where: E* is the complex modulus

$\sigma_0$, $\varepsilon_0$ are the stress and strain amplitudes, respectively

ω is the angular frequency

t is time

φ is the phase angle

E' is the storage or elastic modulus (real part)

E" is the loss or viscous modulus (imaginary part)

The dynamic modulus (|E*|) can then be calculated, as presented by Equation 3.

$$|E^*| = \frac{\sigma_0}{\varepsilon_0} = \sqrt{(E')^2 + (E'')^2} \quad (3)$$

In order to determine the dynamic modulus master curves, the shift factors ($a_T$) at each temperature are calculated and the results are shifted to a reference temperature (21.1 ºC). Then, the sigmoidal model proposed by Pellinen, Witczak and Bonaquist (2004) was used for fitting the dynamic modulus data. Equation 4, Equation 5 and Equation 6 present the dynamic modulus sigmoidal model, the shift factor polynomial equation, and the reduced frequency calculation, respectively.

$$\log|E^*| = \delta + \frac{\alpha}{1 + e^{\beta - \gamma\log(f_r)}} \quad (4)$$

$$\log(a_T) = \alpha_1 T^2 + \alpha_2 T + \alpha_3 \quad (5)$$

$$\log(f_r) = \log(f) + \log(a_T) \quad (6)$$

Where: |E*| is the dynamic modulus

$f_r$ is the reduced frequency

δ, α, β, and γ are the sigmoidal model coefficients

$a_T$ is the shift factor at a temperature T

$\alpha_1$, $\alpha_2$ and $\alpha_3$ are the shift factor polynomial equation coefficients

T is the temperature

f is the test frequency

Figure 18 present the |E*| values at OMC conducted at the initial curing stages of both RAP_2F1H and GCS_2F1H. The test could not be performed at 54 °C due to the reduced stiffness of the specimens.

Figure 18 - Dynamic modulus at OMC for (a) RAP_2F1H and (b) GCS_2F1H specimens

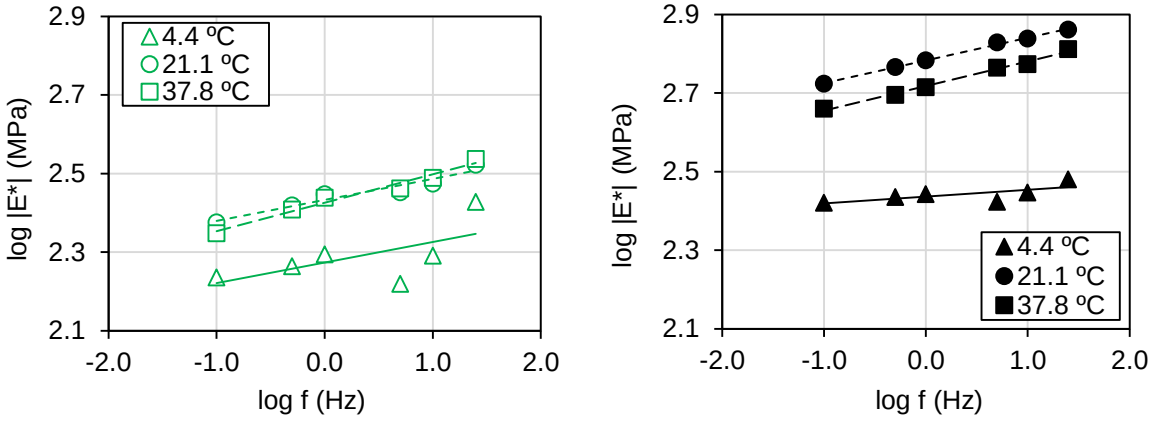


From Figure 18, not expected results were obtained, since the specimen exhibited higher modulus for higher temperatures. Considering that the dynamic modulus test requires several hours to be completed, these results can be attributed to the moisture

loss during the test execution. As water evaporates the stiffness increases, hindering the effects of stiffness reduction caused by temperature elevation, expected in viscoelastic materials. Therefore, the master curves of the RAP_2F1H and GCS_2F1H mixtures could not be constructed for the OMC condition.

The dynamic modulus and phase angle master curves for the fully cured specimens are presented in Figure 19 and Figure 20, respectively, at the reference temperature of 21.1 ºC. Two replicates of each mixture were tested, but only one specimen result is presented for better visualization. The dynamic modulus master curves of the replicate samples can be found in Appendix B. Table 6 presents the sigmoidal model and shift factor equation regression coefficients for the dynamic modulus data. Figure 19, Figure 20, and Table 6 also presents the results for the asphalt concrete and the gap-graded used as the wearing course mixtures of the test sections.

Figure 19 - Dynamic modulus master curves

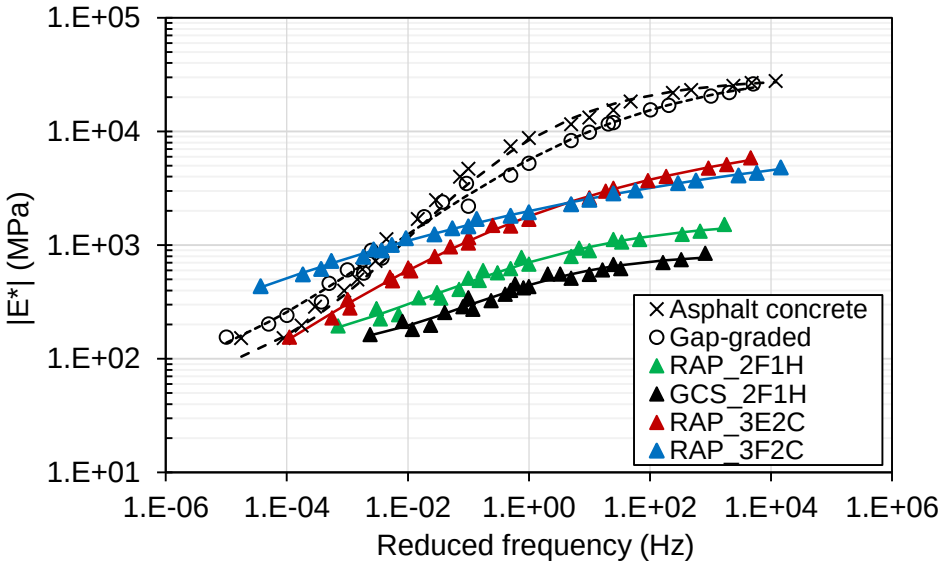

Figure 20 - Phase angle master curves

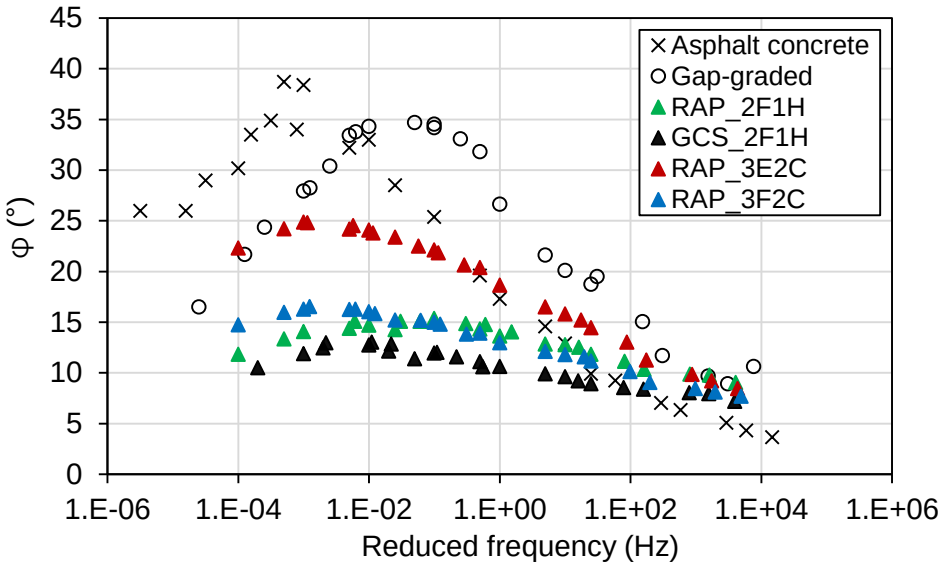


Table 6 - Sigmoidal model and shift factor equation regression coefficients

| Material | Sigmoidal model coefficients | | | | Shift factor polynomial equation coefficients | | |
|---|---|---|---|---|---|---|---|
| | α | β | γ | δ | $\alpha_1$ | $\alpha_2$ | $\alpha_3$ |
| Gap-graded | 3.094 | -1.014 | 0.464 | 1.482 | 0.0006 | -0.1649 | 3.0699 |
| Asphalt concrete | 2.780 | 1.410 | 0.719 | 1.690 | 0.0012 | -0.1960 | 3.4500 |
| RAP_2F1H | 1.314 | -0.920 | 0.590 | 1.908 | 0.0011 | -0.1434 | 2.4718 |
| GCS_2F1H | 0.905 | -0.815 | 0.828 | 2.020 | 0.0009 | -0.1144 | 2.0102 |
| RAP_3E2C | 4.485 | -1.553 | 0.306 | -0.448 | 0.0011 | -0.1739 | 3.0486 |
| RAP_3F2C | 9.594 | -2.351 | 0.151 | -5.460 | 0.0009 | -0.1615 | 2.8133 |

From Figure 19, it can be observed that the time-temperature superposition principle (TTSP) was valid for all the bitumen stabilized materials. Besides, the gap-graded and asphalt concrete mixtures present a greater modulus variation for different reduced frequencies, indicating a greater temperature and frequency dependency in comparison with the base courses. This was expected, since the asphalt mixtures presented higher asphalt binder content.

It can also be observed from Figure 19 that the RAP_2F1H and GCS_2F1H mixtures cannot be considered as purely elastic materials, since the modulus varies for different temperature and load frequency combinations. This viscoelastic characteristic is

evident even for the GCS_2F1H mixture, which is comprised by only 2% of foamed asphalt and no aged binder, since virgin aggregates were used instead of RAP. Besides, the modulus of these two mixtures is also dependent on the stress-state, as depicted from the triaxial resilient modulus test. Therefore, these mixtures present a complex mechanical behavior, since they resemble both an asphalt material with viscoelastic properties and a granular material with non-linear elastic properties. Similar conclusions were presented by Jenkins and Yu (2009) and Colings and Jenkins (2016).

At higher reduced frequencies (or low temperatures) both RAP_3E2C and RAP_3F2C have similar modulus. However, for lower reduced frequencies (or high temperatures), the RAP_3F2C modulus is substantially greater, since the asphalt becomes more fluid and the mechanical properties of the specimen are then dominated by the aggregate gradation (PELLINEN; WITCZAK; BONAQUIST, 2004). Considering that the RAP_3F2C have a finer gradation than the RAP_3E2C (Figure 14), the smaller particles fill the voids left by the coarser ones, creating a more imbricated aggregate skeleton. At this condition, the specimen is more load resistant, especially at higher temperatures (KUCHIISHI; VASCONCELOS; BERNUCCI, 2018).

It is worth noting that a significant difference is observed between RAP_3E2C and RAP_3F2C mixtures from the dynamic modulus master curves than from the triaxial resilient modulus curves. This difference is attributed to the different viscoelastic properties of these mixtures, which is not depicted from the Tx RM test, in which a single temperature and load frequency combination was used. In this sense, the Tx RM results would indicate that these mixtures are structurally equivalent, which is not true. The RAP_3E2C mixture exhibit a wider modulus variation in contrast with the other base course materials, which might be related with the form of asphalt dispersion within the mixture. Although only a thin layer of asphalt covers the aggregate surface after emulsion breaking, the temperature and frequency variation have a major influence in comparison with the foamed asphalt materials, in which the asphalt is non-continuously distributed as spot welds within the mixture. Similar results were reported by Ebels (2008) and Leandri, Losa and Di Natale (2014).

From Figure 20, it can be seen that the foamed asphalt stabilized base courses (RAP_2F1H, GCS_2F1H, RAP_3F2C) presented similar values of phase angle, indicating that these mixtures present similar viscoelastic behavior, differently from the emulsion stabilized mixture (RAP_3E2C), which has higher phase angle values. This result reinforces the idea that the form of the asphalt binder dispersion significantly influences the viscoelastic properties of CRAMs. The increased phase angle values (mixture with asphalt emulsion) show a higher dependency of temperature and frequency variation while the reduced phase angle values (mixtures with foamed asphalt) suggest a lower dependency.

Comparing the mixtures with foamed asphalt, the ones with hydrated lime (RAP_2F1H and GCS_2F1H) presented lower phase angle values in comparison with the one with cement (RAP_3F2C).This indicates that the modulus dependence of temperature and frequency variation of the former are lower than the latter. In terms of stiffness, the RAP_3F2C modulus is considerably higher than the RAP_2F1H and GCS_2F1H mixtures, due to the presence of 2% cement, which hydrates and imparts for greater stiffness in comparison with the other two mixtures, which do not have Portland cement as active filler.

The dynamic modulus shift factor curves also confirm the differences regarding the viscoelastic properties of the mixtures (Figure 21). Since the shift factor value is directly proportional to the temperature dependency of the material, i.e. higher shift factors lead to higher temperature susceptibility, it can be seen from Figure 21 that the asphalt mixtures exhibited higher shift factor values while the mixtures with hydrated lime presented the lowest ones.

Figure 21 – Dynamic modulus shift factor curves

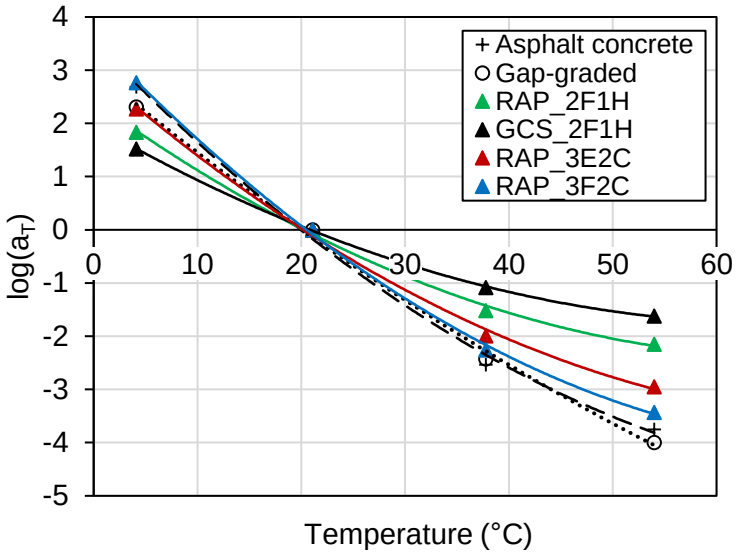


The Black space (Figure 22a) and the Cole-Cole plane (Figure 22b) can also be used for viscoelastic properties evaluation. For the Black space plot, dynamic modulus (|E*|) and phase angle (φ) data are used. For the Cole-Cole graph, the elastic (E') and viscous (E") portion of the complex modulus (E*) are plotted.

Figure 22 - (a) Black space and (b) Cole-Cole plane

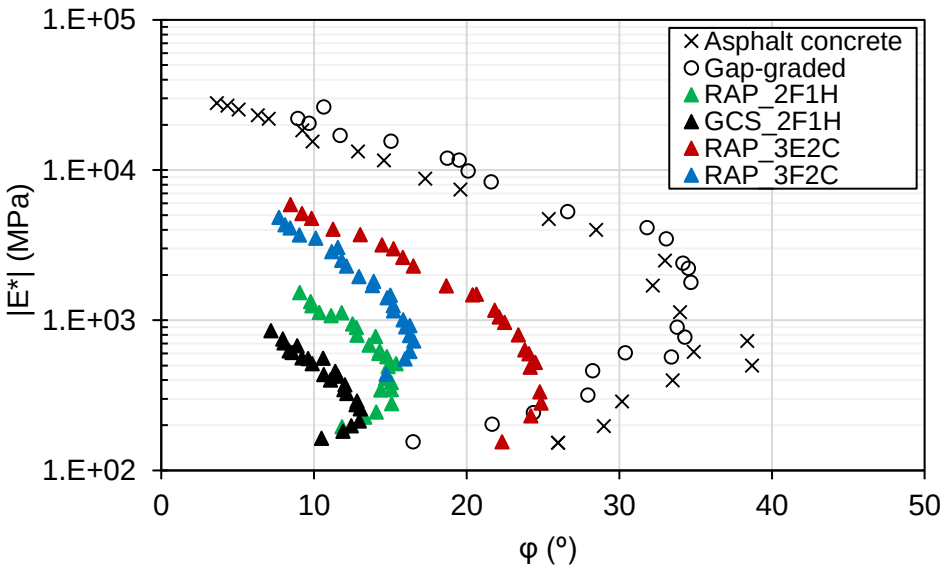


(a)

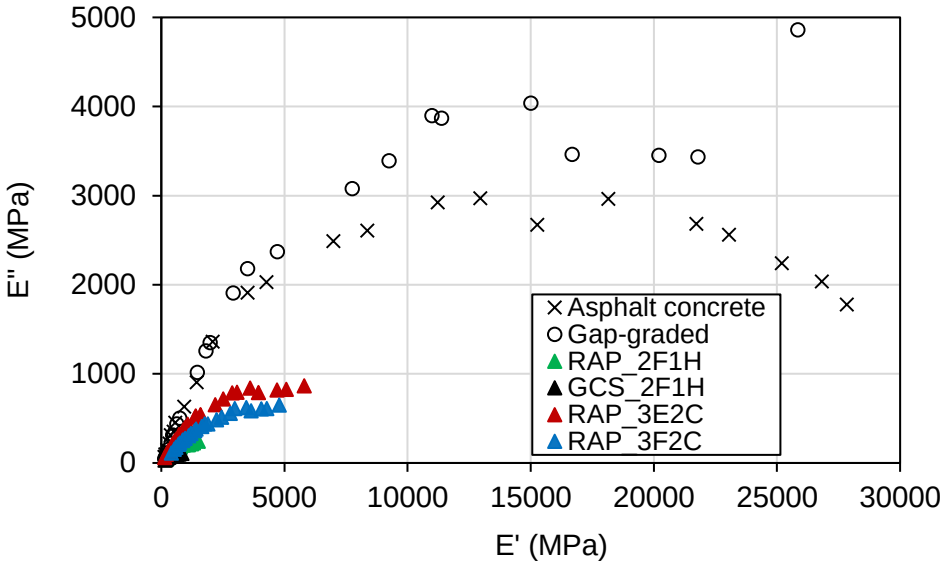


(b)

From the Black space (Figure 22a), the asphalt concrete and gap-graded mixtures exhibited higher phase angle values, due to its higher asphalt content. For the bitumen stabilized materials, the RAP_3E2C present greater values of phase angle, indicating major temperature dependency, as already depicted in Figure 20. On the other hand, the RAP_3F2C, RAP_2F1H and GCS_2F1H mixtures have lower phase angle values than the RAP_3E2C, but similar values among themselves. This reinforces the fact that the type of asphalt binder and the form of its distribution within the mixture indeed influence the CRAMs viscoelastic characteristics. Therefore, the Black space can be useful for indicating differences regarding viscoelastic properties of the RAP_3E2C and RAP_3F2C mixtures, which are considered structurally similar according to the Tx RM test results.

From the Cole-Cole plane (Figure 22b), the bitumen stabilized materials presented the lowest values of E” and E’. Therefore, although its lower dynamic modulus slope indicates a more elastic behavior, with increased E’ values, their |E*| and phase angle results are reduced in comparison with the asphalt mixtures. In this case, both E’ (or |E*|×cosφ) and E” (or |E*|×sinφ) will also have limited values. Seeing that the dynamic modulus test was not conducted at temperatures lower than 4.4 °C, the Cole-Cole curves do not present the full bell-shaped format.

## 2.5. SUMMARY AND FINDINGS

Four types of CRAMs composition were evaluated with different types and contents of active filler, bitumen stabilizing agent, aggregate gradation, and optimum moisture content. Those CRAMs mechanical behavior were analyzed by means of triaxial resilient modulus and dynamic modulus tests. The following findings can be drawn:

- The type of asphalt binder, active filler and aggregate gradation substantially influenced the mechanical behavior of the CRAMs.
- The mixtures with cement presented a mechanical behavior similar to cemented mixtures with a constant modulus value for different confining pressures. The mixtures without cement exhibited a behavior similar to a granular material, with increasing modulus for increasing confining pressure. Besides, the mixtures with cement presented increased modulus values in comparison with the ones without cement
- The RAP_2F1H and GCS_2F1H resemble both an asphalt material, with temperature and load frequency dependency, and a granular material, with stress dependency.
- From the triaxial resilient modulus results, the RAP_3E2C and RAP_3F2C mixtures with cement addition seemed to be structurally similar, since they presented equivalent modulus values. However, from dynamic modulus test results, the differences between the RAP_3E2C and RAP_3F2C mixtures become more evident. This result is attributed to the different viscoelastic characteristics, primarily due to the form of the binder distribution within these mixtures.
- The dynamic modulus master curves and the Black space showed to be useful in order to identify differences regarding the viscoelastic properties of CRAMs and type of bitumen stabilizing agent.

# 3. INFLUENCE OF VISCOELASTIC PROPERTIES OF COLD RECYCLED ASPHALT MIXTURES ON PAVEMENT RESPONSE BY MEANS OF TEMPERATURE INSTRUMENTATION *

## 3.1. INTRODUCTION AND BACKGROUND

Cold recycled asphalt mixtures (CRAMs) have been extensively used in pavement structures, mainly as base course materials. Since CRAMs are comprised by reclaimed asphalt pavement (RAP) aggregates, and does not require mixture heating for proper mixing procedure, the cold recycling technique provides several sustainable benefits, for instance: lower virgin aggregate consumption, reduction of the polluting gases emission, reduction on aggregate transportation costs (in-situ recycling), and greater reclamation levels of milled aggregates (COPELAND, 2011; LEE; CHOU; CHEN, 2012).

Nonetheless, the mechanical behavior of CRAMs is complex since different variables may affect its stiffness. Therefore, the assessment of CRAMs stiffness is difficult, and depending on the assumed mechanical behavior, different modes of distresses must be considered in the design process. If the CRAMs is believed to be a granular material, it is expected that the major distress mode will be permanent deformation. On the other hand, if CRAM is considered as a bound-like material with viscoelastic properties that resemble the behavior of an HMA, then permanent deformation and fatigue cracking might be the distress modes (NIVEDYA et al., 2018). Thus, the CRAM mechanical behavior is dependent of several factors that are not fully understood, as they are highly dependent on the CRAM composition, as already described in Chapter 2.

According to the Asphalt Academy (2009), since the asphalt is non-continuously distributed within the CRAM, no temperature sensitivity should be expected. Besides,

---

* "Influence of viscoelastic properties of cold recycled asphalt mixtures on pavement response by means of temperature instrumentation" by André K. Kuchiishi, Camila C. S. Antão, Kamilla Vasconcelos and Liedi Bernucci. Extended and improved version of the paper presented in 2018 at ISAP Conference and submitted for the Special Issue of the Road Materials and Pavement Design journal.

for construction purposes, the stabilized material after compaction presents similar void content in comparison with a conventional granular one; therefore, it should also be treated as granular, but with higher cohesion.

Guatimosim et al. (2018) concluded that the mechanical behavior of the blend of RAP with crushed cement treated base material and foamed asphalt stabilization is similar to an unbound granular material, due to its modulus dependency on confining pressure at different curing conditions. In this case, since permanent deformation may be the primary distress mode, permanent deformation tests were further conducted in order to assess the curing process.

In contrast, Leandri, Losa and Di Natale (2015) conducted dynamic modulus tests in CRAMs stabilized with whether asphalt emulsion or foamed asphalt. Besides the temperature and load frequency dependency of the recycled mixtures, the dynamic modulus master curves were used as input data for pavement analysis simulation in ViscoRoute 2.0 software. It was concluded that, if the viscoelastic properties of CRAMs were considered, a good fit was obtained between the predicted stresses and strains and the measured ones by field instrumentation, especially for CRAMs stabilized with asphalt emulsion.

Nivedya, Veeraragavan and Krishnan (2016) compared a CRAM stabilized with foamed asphalt with a Wet Mix Macadam (WMM). According to the authors, the CRAMs presented unexpected Tx RM results, with decreasing modulus values for increasing confining pressures. Therefore, the stress-dependent behavior was not suitable for CRAM characterization, and the dynamic modulus tests indicated that the CRAM is essentially similar to a bituminous material, with respect to temperature and frequency dependency. Other researchers also suggested that the CRAMs viscoelastic properties should not be neglected (STIMILLI et al., 2013; CIZKOVA et al., 2015; GODENZONI; GRAZIANI; PERRATON, 2016).

Vorobeiff (2005), on the other hand, developed an interim design model for foamed stabilized materials, considering three distress modes related with either granular and bound asphalt materials: (i) fatigue cracking, (ii) rutting, and (iii) shrinkage cracking. The design method, which involves different distress modes in its calculation, is based on the assumption of a two-phase behavior for the CRAM layer: precracking and

postcracking. At the first phase, the CRAM layer has greater modulus values, while at the second phase, the integrity of the material reduces, decreasing the CRAM modulus.

This two-phase hypothesis was first suggested by Liebenberg and Visser (2003, 2004) which evaluated CRAM stabilized with asphalt emulsion and cement. At the first phase, named “effective fatigue phase”, the CRAM behaves similarly to a lightly cemented material in which fatigue takes place as the primary distress mode. At the second phase, referred as “equivalent granular phase”, the CRAM layer is already cracked and its stiffness reduces, being comparable to a granular material and susceptible to rutting distress. Figure 23 illustrates the two-phased behavior.

Figure 23 - Hypothesis of "effective fatigue phase" and "equivalent granular phase"

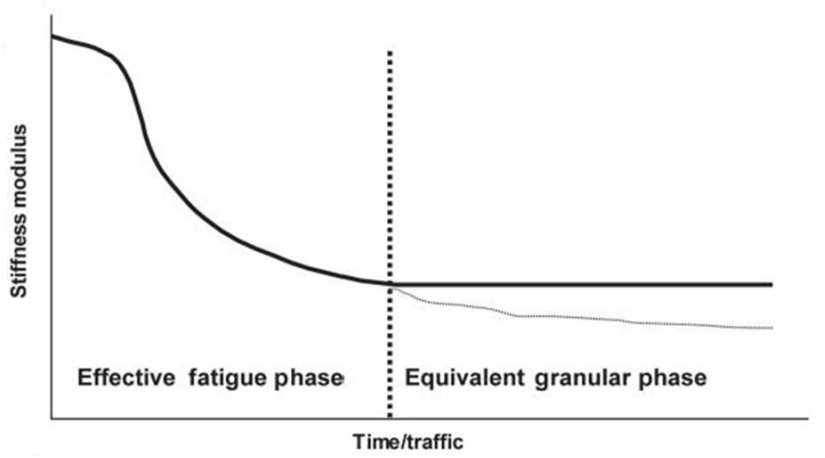


Source: Pérez, Medina, Ángel del Val (2013)

Nevertheless, the hypothesis was first assumed by Liebenberg and Visser (2003, 2004) regarding CRAMs stabilized with asphalt emulsion and 2% of cement content. This higher cement dosage imparts for a more bound-like behavior (in which fatigue cracking may be dominant) and is above the limits of the current South African and German specifications for BSMs, which suggest a maximum of 1% of cement (ASPHALT ACADEMY, 2009; WIRTGEN, 2012). In addition, the stiffness reduction described in Figure 23 relies on accelerated pavement testing results from Heavy

Vehicle Simulation (HVS) tests, in which the heavy accelerated loading would contribute with the significant stiffness reduction (EBELS; JENKINS; COLLINGS, 2005).

Therefore, the proposed mechanical behavior was found to be not suitable for CRAMs characterization. Based on several studies regarding curing mechanisms and considering that the permanent deformation distress would be more likely to occur in the first curing stages, Ebels, Jenkins and Collings (2005) proposed a new stiffness development hypothesis (Figure 24). The first phase, named “curing phase”, is defined by the increase of stiffness due to the curing process (see Section 3.2). In the second phase, “stiffness reduction phase”, although the CRAM may exhibit some viscoelastic characteristics, fatigue cracking would not be the main distress. Figure 24 indicates that the two-phase hypothesis proposed by Liebenberg and Visser (2003, 2004) is within the “curing phase”, in which the material stiffness is not fully developed and the occurrence of fatigue cracking suggested by the authors would be incorrect.

Figure 24 - Hypothesis of “curing phase” and “stiffness reduction phase”

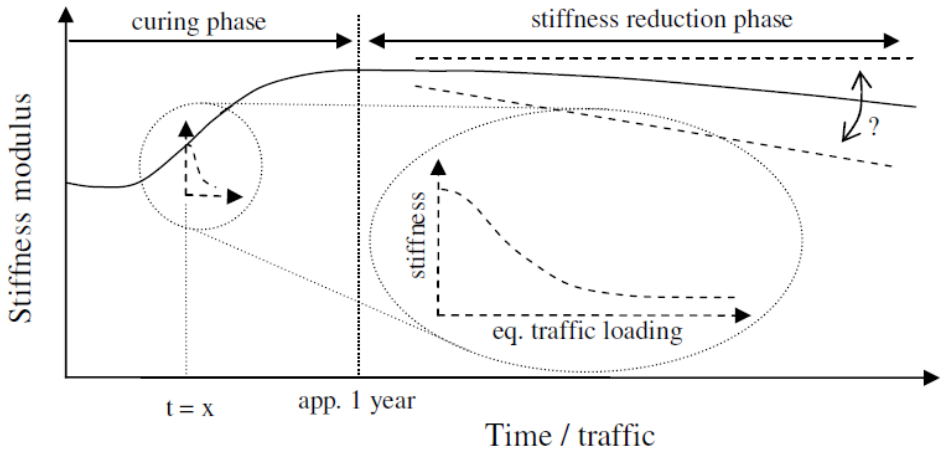


Source: Ebels, Jenkins and Collings (2005)

Beyond the granular- or asphalt-like behavior discussion, there is no consensus in terms of the assumption of whether the CRAM should be considered an elastic or viscoelastic material. This consideration is directly related with design purposes, in

which modulus values are attributed to the material. With an elastic approach, the CRAM may be characterized by a single modulus value. However, if a viscoelastic approach is considered, climatic conditions and load frequency are fundamental parameters for pavement design.

Collings and Jenkins (2011) suggested a visco-elasto-plastic characterization, since Tx RM tests indicate a stress-state dependency (elasto-plastic behavior) and the dynamic modulus tests indicates a temperature and loading time dependency (visco-elastic behavior). The authors highlight that the recycled material cannot be considered as purely elastic, even with the addition of 1% of cement.

Ebels (2008) conducted several four-point bending beam tests in order to investigate flexural stiffness and viscoelastic characteristics of CRAMs. Different types of binder, RAP content and cement content were used. It was found a significant influence of the elastic or viscoelastic properties regarding those variables. For greater amounts of RAP, the emulsion mixes exhibited a more viscoelastic behavior, while with 1% of cement addition, the recycled material became more elastic with whether emulsion or foamed asphalt treatment. In addition, the use of foamed asphalt imparted for a more elastic behavior in comparison with asphalt emulsion. Table 7 summarizes those findings.

Table 7 - Summary of the influence of different variables on the mechanical properties of emulsion and foamed asphalt mixes

| Experimental variable | Emulsion mixes | Foamed bitumen mixes |
|---|---|---|
| Increasing %-RAP | more elastic<br>more time/temp. dependent | no significant effect |
| Adding 1% cement | more elastic | more elastic |
| Type of binder | Emulsion A ≈ Emulsion B<br>Foam more elastic than emulsion | |

Source: Ebels (2008)

Therefore, it can be seen that the CRAMs exhibit a complex mechanical behavior and different models have been proposed in order to better assess its stiffness. In addition, despite of the several approaches that have been suggested regarding the primary distress mode, the present study is not focused on the investigation of fatigue cracking or permanent deformation. Since numerous variables affect CRAMs behavior, the goal of this study is to characterize the CRAMs in terms of its viscoelastic characteristics and use these properties for the analysis of pavement response under different temperature conditions. As different approaches have been used for CRAMs characterization, a better understanding of the mechanical behavior of this material is necessary. This will provide a more accurate representation of CRAMs behavior, reducing the chances of early distresses during pavement field performance.

## 3.2. EXPERIMENTAL TEST SECTIONS

### 3.2.1. Materials and pavement structure

The materials used for this study were collected from the experimental test section in Fernão Dias highway (BR 381), located at Extrema city, in Minas Gerais, Brazil. The test section was constructed in the right lane (heavy traffic lane) of a two-lane segment.

Approximately 370 mm of the old pavement was milled and the RAP produced was further used to construct two experimental test sections. Both of them are comprised by an asphalt concrete (AC) layer as the wearing course but different CRAMs as base course materials: (i) asphalt emulsion mixture (RAP_3E2C) and (ii) foamed asphalt mixture (RAP_3F2C). The proposed rehabilitation structures are presented in Figure 25 along with the layers' thicknesses. The structure under the milled pavement is referred as "remaining infrastructure".

Figure 25 - Pavement structure of the (a) RAP_3F2C and (b) RAP_3E2C test sections

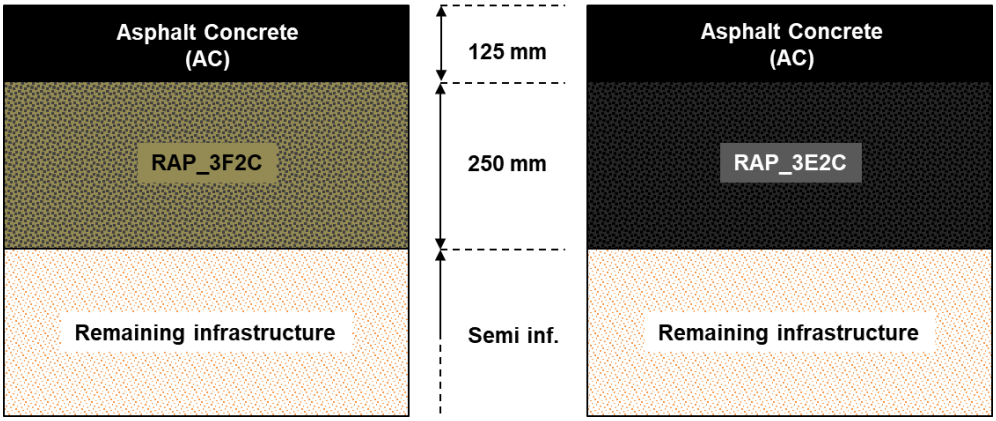


(a) (b)

Source: Author

Figure 26 presents the gradation curves and the limits recommended for both asphalt emulsion and foamed asphalt stabilized mixtures. Although the gradation curves exceeded the limits recommended by Wirtgen (2012), it was decided to prioritize field representation, and the samples' aggregate composition followed the gradation used in the field.

Figure 26 - Gradation curves of the RAP_3E2C and RAP_3F2C

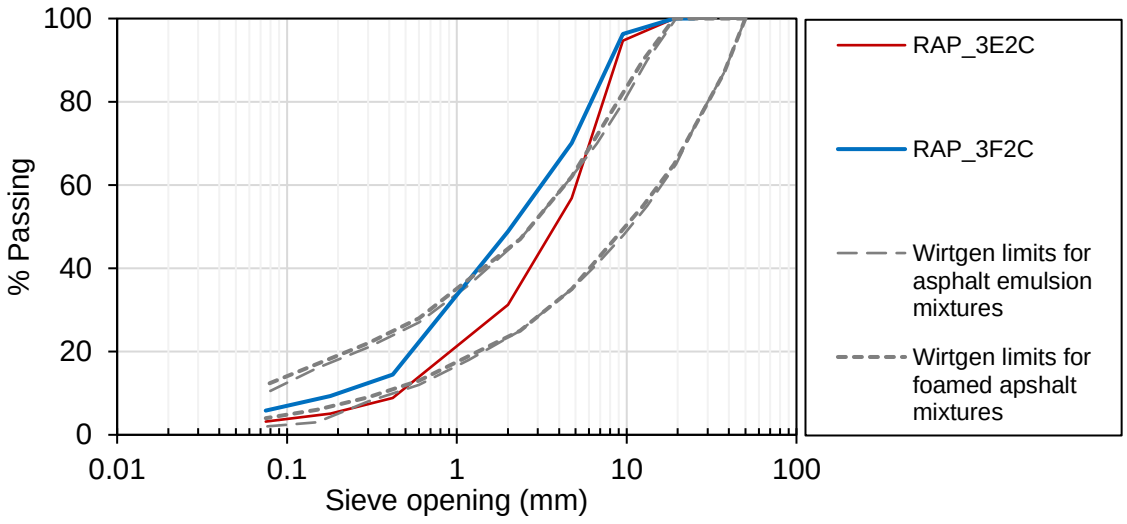

A Proctor hammer was used to produce the specimens with 100 mm diameter and 150 mm height with modified compaction energy. The RAP_3E2C samples were prepared by mixing 98% of RAP and 2% of Portland-limestone cement by dry aggregate weight. A slow-setting cationic emulsion was selected (62.3% of residual binder content) with 3% emulsion content by dry aggregate weight. The moisture content was 5.5% by dry aggregate weight. The curing procedure proposed by Bessa et al. (2016) was slightly modified with an additional curing time. The samples were initially stored unsealed at 60 ºC for 3 days in order to ensure water evaporation. After that they were sealed and cured for three additional days at 60ºC. Since the core of the samples might have higher moisture content than the border, the additional sealed procedure ensures that the moisture is uniformly distributed within the sample geometry.

The RAP_3F2C mixture have an aggregate blend of 68% of RAP, 30% of fine aggregate blend and 2% of Portland-limestone cement by dry aggregate weight (the same used for the RAP_3E2C samples). The addition of fine aggregate blend is required for the RAP_3F2C, because the asphalt binder dispersion occurs exclusively throughout the finer particles. Therefore, for a proper dispersion of asphalt binder, the amount of finer particles required is greater than RAP_3E2C, in which the dispersion of the asphalt binder occurs preferentially throughout the finer particles (Asphalt Academy, 2009). The binder for the foaming process has 85/100 penetration grade with 3% asphalt content by dry aggregate weight. For the foaming process, 2.6% of foaming water was necessary, and 6.5% for moisture content by dry aggregate weight was selected for compaction. The RAP_3F2Cs samples were cured at 40 ºC, unsealed, until they reached 60% of the OMC (Guatimosim, 2015). After that, the specimens were sealed and kept at 25 ºC.

### 3.2.2. Pavement instrumentation and data acquisition

In order to evaluate the temperature distribution within the pavement structure, a total of four temperature thermoresistors were installed at different depths. For temperature measurement, PT100 sensors from PID Brasil Automação Industrial Ltda. were selected. The asphalt pavement was sawed at the desired depths and the sensors

were placed at the bottom of the cuts. Three thermoresistors were installed within the AC layer (3, 7.5 and 9.5 cm) and one at the top of the RAP_3F2C base layer (13 cm).

The temperature data acquisition could not be performed at the AC and RAP_3F2C layer simultaneously, due to practical field limitations. Therefore, the measurements were conducted separately for each layer. Although there was no sensors in the RAP_3E2C layer, it was assumed that the temperature data is equivalent at the top of both base course materials, since the pavement structures are comprised by the same AC layer in terms of composition and thickness. Table 8 presents the maximum and minimum temperatures recorded between 12:30 and 15:30 PM at different seasons throughout the year. A 1 Hz recording frequency was used, providing one temperature measurement per second.

Table 8 - Measured temperature at different pavement depths using temperature instrumentation

| Sensor depth (cm) | Layer | Temperature (max. - min., in °C) Summer 12/13/2017 | Fall 5/4/2018 | Winter 8/2/2018 |
|---|---|---|---|---|
| 3.0 | AC | 55.6 - 46.1 | * | * |
| 7.5 | | 49.6 - 39.9 | * | * |
| 9.5 | | 48.8 - 39.0 | * | * |
| 13.0 | RAP_3F2C or RAP_3E2C | * | 30.5 - 26.1 | 24.7 - 20.9 |

The collected temperature data were used as reference for the selection of analysis temperature for pavement simulation. For the AC layer, the sensor placed at approximately mid-depth (7.5 cm) was selected as representative of the whole layer. From Table 8, it can be seen that, at this depth, the temperature ranges from 50 to 40 °C during summer (December/17). For the base courses, the temperature at the top of the layer ranges from 25 to 30 °C during fall (May/2018), and from 20 to 25 °C during winter (August/2018).

Based on the aforementioned temperature data, different temperature combinations were used for pavement simulation. Twagira (2010) observed a difference of 5 °C

between the mid-depth of a 25 cm asphalt emulsion mixture and a wearing course with only 6 cm thickness (2 cm of an ultra-thin friction coarse over 4 cm of an HMA). Therefore, since there was no data available for the AC during fall or winter and for the base courses during summer, a difference of 10 °C was adopted as a reasonable estimative of the temperature difference between the AC and base course mid-depth temperatures, considering the greater AC layer thickness in comparison with Twagira's (2010). The temperature combinations used for pavement simulation will be further presented.

## 3.3. TESTING PROGRAMME

### 3.3.1. Laboratory testing

#### 3.3.1.1. Mixture linear viscoelastic characterization

To evaluate the viscoelastic properties of RAP_3E2C and RAP_3F2C mixtures, the dynamic modulus test was conducted (AASHTO T342-11) after the curing process was completed. The 100 mm diameter and 150 mm height specimen was subjected to a sinusoidal load under six different frequencies (25, 10, 5, 1, 0.5 and 0.1 Hz) and four temperatures (54, 37.8, 21.1 and 4.4 ºC). The test is conducted in a stress-controlled condition, and the loads are selected with the purpose of guarantying that the axial deformation would be within the range of 50 to 150 με. Two replicates of each material were tested.

In order to determine the dynamic modulus master curves, the sigmoidal model (Equation 7) proposed by Pellinen, Witczak and Bonaquist (2004) was used for fitting the dynamic modulus data and the parameters δ, α, β and γ were determined by means of an optimization tool in Microsoft Excel. The $f_r$ parameter is the reduced frequency and is calculated using Equation 8, in which f is the test frequency and $a_T$ is the shift factor. Figure 27 and Figure 28 presents the dynamic modulus and phase angle master curves, respectively, for the AC, RAP_3F2C and RAP_3E2C mixtures at the reference temperature of 21.1ºC. Two replicates of each mixture were tested, but only one

specimen result is presented for better visualization. The dynamic modulus master curves of the replicate samples can be found in Appendix B

$$\log|E^*| = \delta + \frac{\alpha}{1 + e^{\beta - \gamma\log(f_r)}} \quad (7)$$

$$\log(f_r) = \log(f) + \log(a_T) \quad (8)$$

Figure 27 - Dynamic modulus master curves of AC, RAP_3E2C and RAP_3F2C mixtures

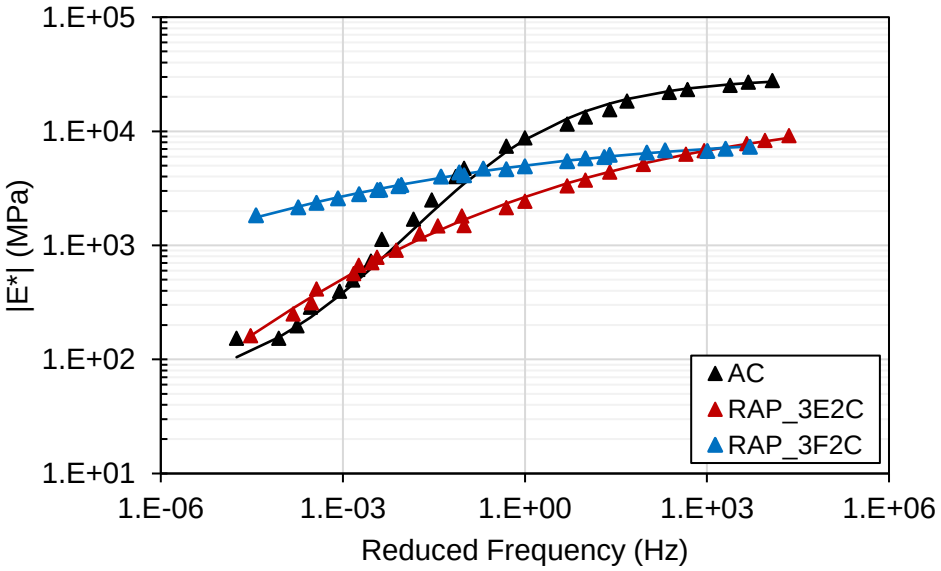

Figure 28 – Phase angle master curves of AC, RAP_3E2C and RAP_3F2C mixtures

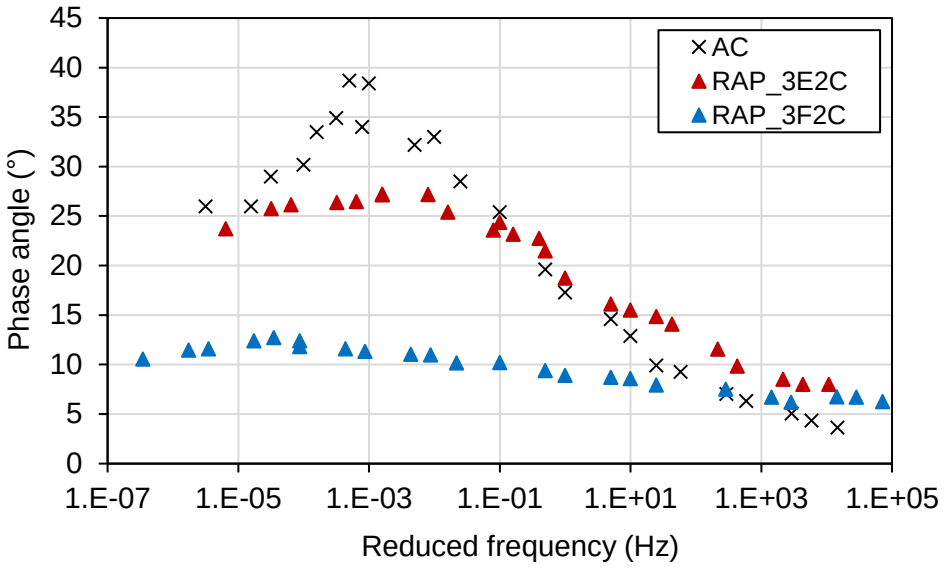


At low reduced frequencies, the AC presents the lowest dynamic modulus values. However, at high reduced frequencies, the AC dynamic modulus is higher than the one from the CRAMs. It indicates that the AC is more thermo-sensitive than the CRAMs, due to its steeper master curve slope.

From Figure 27 it can be observed that the time-temperature superposition principle (TTSP) is valid for both the base course materials. Comparing the CRAMs master curves, despite both mixtures presented good fit with the sigmoidal model, the master curves are quite distinct from each other, with the RAP_3F2C being less thermo-sensitive than the RAP_3E2C one. This result can also be observed in Figure 28, in which the phase angle values are higher for the RAP_3E2C mixture in comparison with the RAP_3F2C, indicating a higher temperature susceptibility. At high reduced frequencies, or low temperatures, the dynamic modulus of both mixtures is similar. On the other hand, at low reduced frequencies, or high temperatures, the dynamic modulus of RAP_3F2C is higher than the RAP_3E2C. This behavior was also observed in the literature (EBELS, 2008; LEANDRI; LOSA; DI NATALE, 2015) and could be partially explained by the gradation curves of each material. At higher temperatures, the binder becomes more fluid and the mechanical properties of the samples are dominated by the aggregate gradation (PELLINEN; WITCZAK;

BONAQUIST, 2004). Considering that the RAP_3F2C mixture have higher content of finer aggregates, the smaller particles fill in the voids created by the coarse particles, creating a more imbricated aggregate skeleton which will improve load resistance.

The RAP_3E2C master curve also suggests that the aggregate composition influences the dynamic modulus results. Since RAP is a combination of aggregates and aged binder, the total asphalt content within the mixture increases as RAP content increases. Considering RAP_3E2C have higher RAP content (98%) than RAP_3F2C (68%), the binder content of the former is greater than the latter. In this case, as temperature increases, the RAP_3E2C stiffness decreases faster, which describes the master curve higher slope for this type of mixture. For the RAP_3F2C, as the binder content is lower, the temperature increase will not significantly reduce its stiffness. It is important to note that despite the significant difference in RAP content between CRAMs, the RAP_3E2C and RAP_3F2C are different mixtures, with distinct gradation curves, aggregate blending, and asphalt content.

In addition, the higher temperature dependency characteristic of RAP_3E2C might be related with the form of binder dispersion within the mixture. Although only a thin layer of asphalt covers the aggregate surfaces after emulsion breaking, the temperature and frequency variation have a major influence in comparison with the foamed asphalt materials, in which the asphalt is non-continuously distributed and referred as spot-welds.

#### 3.3.1.2. Asphalt binder linear viscoelastic properties

The asphalt binders used for the asphalt concrete layer and the bitumen stabilized base courses were tested by means of the Dynamic Shear Rheometer (DSR), with the purpose of evaluating its viscoelastic properties. Those properties are used as input parameters at the 3D-Move Analysis software for pavement simulation.

The asphalt binders from the hot mix asphalt layers and the RAP_3F2C mixture were collected inside metal cans, facilitating its manipulation and sample preparation. For the RAP_3E2C mixture, the asphalt binder residue was necessary to be obtained,

since after emulsion breaking only the residue remains covering the aggregates. This procedure was conducted in accordance with the Brazilian standard ABNT NBR 14896/12.

Afterwards, asphalt binder specimens of 25 mm diameter and 1 mm height were molded and placed between the parallel plates of the DSR. The test was conducted from 40 to 80 ºC with frequency ranging from 0.1 to 10 Hz at a strain level of 0.1 %. The described procedure is in accordance with the ASTM D7175-15 standard. Two replicates of each asphalt binder were tested. Figure 29 presents some of the stages of the asphalt binder testing.

Figure 29 - Images of the (a) DSR, (b) specimen molding, (c) specimen placement, and (d) test gap of 1 mm

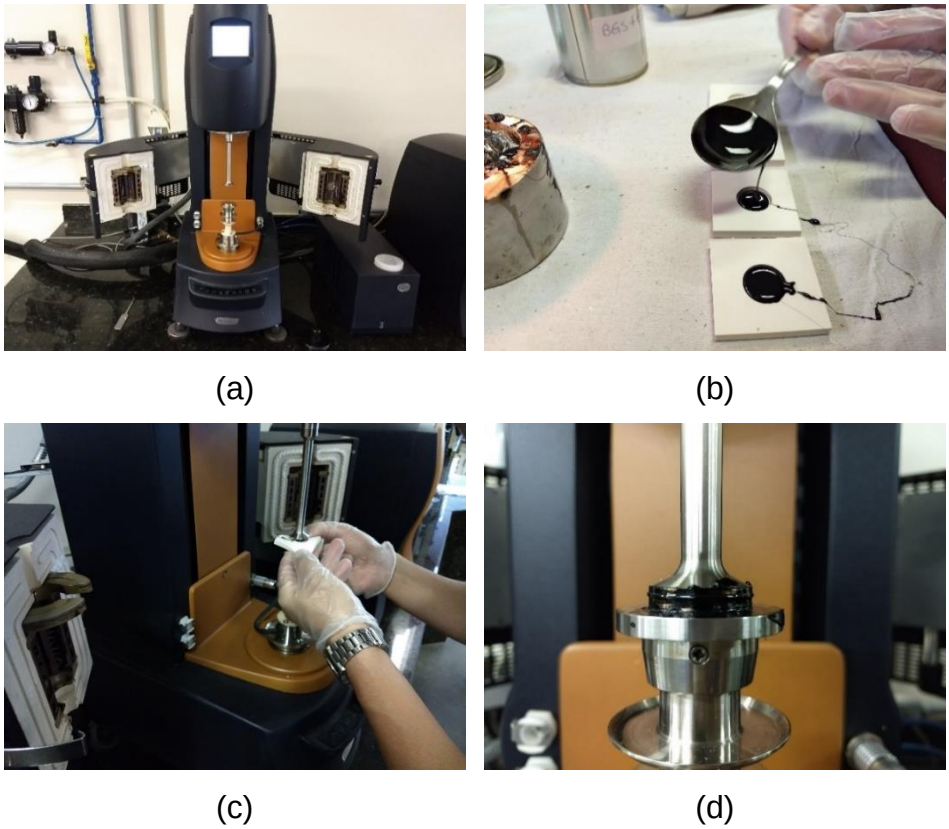

(a) (b)

(c) (d)

Source: Author

Figure 30 presents the dynamic shear modulus master curves (|G*|) of the asphalt binders from the surface and base course layers at the reference temperature of 40 ºC. Although two replicates of each mixture were tested, only one sample result is presented for better visualization. The dynamic shear modulus master curves of the replicate samples can be found in Appendix C.

Figure 30 - Dynamic shear modulus master curves

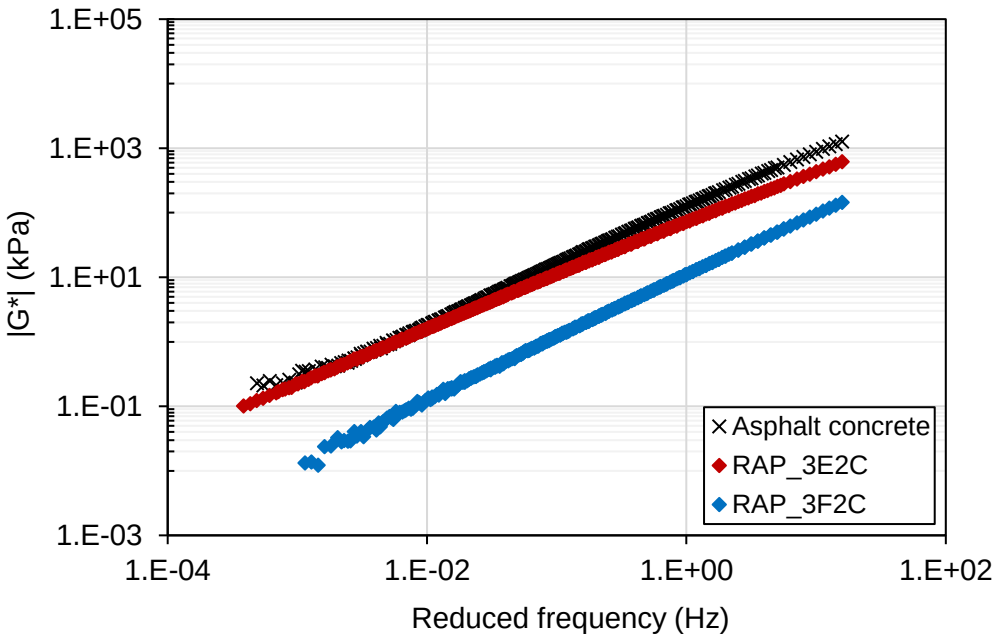


From Figure 30, the AC layer asphalt binder is stiffer in comparison with the binders used in the base course layers. The RAP_3F2C binder exhibited the lower |G*| master curves, mainly due to its low viscosity and high penetration grade. The RAP_3E2C binder, on the other hand, presented high |G*| values, which can be related to the process of obtaining the asphalt emulsion residue. The elevated temperature might have aged the binder residue during the evaporation process, increasing its stiffness.

### 3.3.2. 3D Move Analysis 2.1 simulation

The 3D-Move Analysis V2.1 software is a continuum-based finite-layer approach to evaluate the pavement response to moving loads with different speeds, tire-pavement contact areas, and temperature conditions (SIDDHARTHAM; YAO; SEBAALY, 1998). The 3D-Move software has been used to validate pavement responses and to compare field with pavement-modelled data (SIDDHARTHAM et al., 2005; HAJJ et al., 2010; ULLOA et al., 2013; ABDO; JUNG, 2016).

The pavement structures with RAP_3E2C and RAP_3F2C, presented in Figure 25, were reproduced at 3D-Move software. The Poisson ratio of 0.35 was adopted for the AC, RAP_3F2C and RAP_3E2C materials based on literature data (LOIZOS; PAPAVASILIOU; PLATI, 2012; 2016), and 0.45 for the remaining infrastructure. During the construction period, the Light Weight Deflectometer (LWD) test was performed over the remaining infrastructure after the milling process. The resulting modulus of 118 MPa was used as input data for the remaining infrastructure modulus. For the tire-pavement contact configuration, a circular contact area was selected, with radius of 0.107 m and tire pressure of 560 kPa, and a semi-axle configuration was used with 20 kN/tire uniformly distributed. Although the maximum speed limit is 80 km/h, a low speed of 40km/h was selected in order to simulate the worst case scenario for traffic loading. The viscoelastic properties of the AC, RAP_3E2C and RAP_3F2C, in terms of dynamic modulus master curves, were used as input data for 3D-Move Analysis simulation. For the binder input data, a dynamic shear rheometer (DSR) was used and the $|G^*|$ and $\delta$ parameters were determined at different temperatures and frequencies.

The simulation was conducted in order to assess the temperature effect in the strain at the bottom of the wearing course, since most of the fatigue models for flexible pavements use the tensile strain as input data. In addition, the strain at the bottom of the base course was also evaluated with the purpose of better understanding the mechanical behavior of the CRAMs under different temperature conditions. In both cases, the point of analysis for strain calculation is vertically aligned with the semi-axle outer tire centerline.

The simulation scenarios were divided into three stages. At first, the pavement structures were compared in terms of the strain measured at the bottom of the AC

layer, considering the base course layers (RAP_3E2C and RAP_3F2C) as either elastic or viscoelastic materials. At this stage, the backcalculated modulus and the dynamic modulus results were used as input data for the elastic and viscoelastic analysis, respectively. The temperatures of 30 ºC for the AC and 20 ºC for the base layers were selected, respectively.

Secondly, the influence of temperature on pavement response was evaluated by analysing the strain at the bottom of the AC and base course layers. Five temperature conditions were used: (i) W(50)B(40), (ii) W(40)B(30), (iii) W(30)B(20), (iv) W(25)B(15), and (v) W(20)B(10). The “W” and “B” letters correspond respectively to the wearing and base courses and the numbers represent the temperatures, in degree Celsius, used in the simulation for each layer. Those combinations were based on the temperature data collected in situ by means of temperature instrumentation.

At last, two temperature combinations were simulated: (i) W(25)B(15) and (ii) W(15)B(25). The first one corresponds to the day period, in which the wearing course is warmer than the base layer due to solar radiation. The second condition simulates the night period with no solar radiation, in which the surface layer is colder in comparison with the base course, since the former is more susceptible to climate variation than the latter. This temperature inversion is commonly observed between day and night periods and has been already reported in the literature (RAMADHAN; WAHHAB, 1997; ASAEDA; CA, 2000; ARIAWAN; SUBAGIO; SETIADJI, 2015; YINFEI; SHENGYUE; JIAN, 2015).

## 3.4. RESULTS AND DISCUSSION

### 3.4.1. Elastic vs. Viscoelastic

Figure 31 presents the longitudinal and transversal strain values obtained at the bottom of the AC layer. The positive values correspond to the tensile strain and the negative values correspond to the compressive strain. It is worth noting that the CRAMs elastic and viscoelastic behavior are depicted by the “EL” and “VE” notations, respectively.

The RAP_3F2C and RAP_3E2C structures are presented in Figure 31a and Figure 31b, respectively.

Figure 31 - Longitudinal and transversal strains at the bottom of the AC for the (a) RAP_3F2C and (b) RAP_3E2C structures

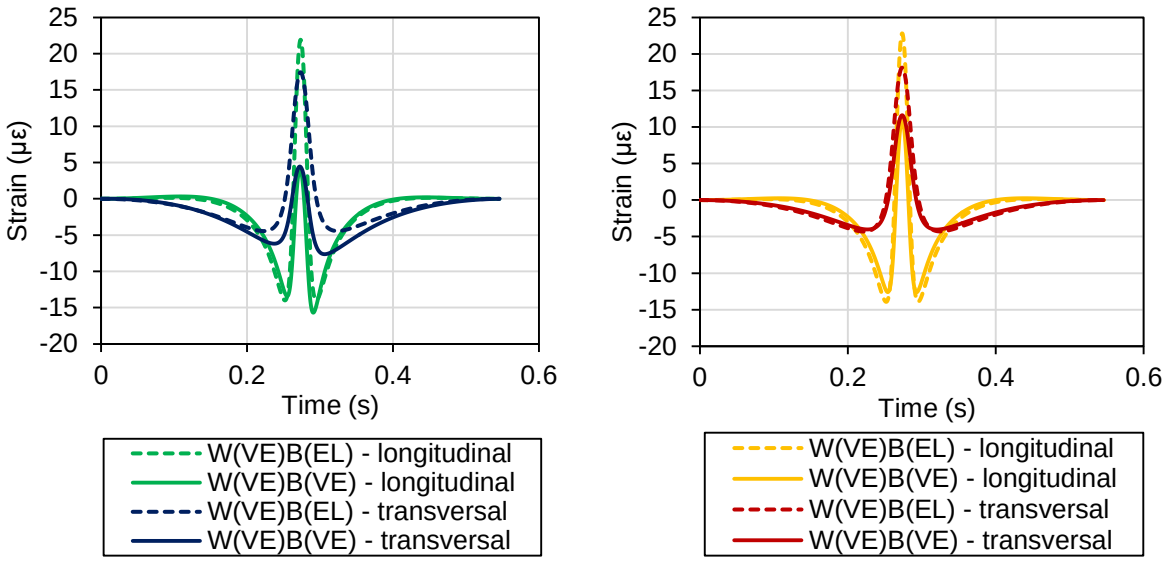


From both pavement structure results, it can be observed that, as the vehicle load approaches the analysis point, an increase of the compression strain occurs at the bottom of the AC layer. After that, when the load is vertically aligned with the analysis point at the bottom of the AC, a maximum tensile strain is obtained followed by a compression strain peak as the load moves away. The same strain pattern was observed by Nasimifar et al. (2017). The authors obtained good correlations between measured and predicted longitudinal strains at the bottom of the AC layer by means of 3D-Move simulation.

Figure 31 shows that, considering the CRAM as an elastic material, the longitudinal and transversal tensile strains at the bottom of the AC layer increase and, consequently, a more robust structure would be necessary to resist traffic loading. This suggests that neglecting the viscoelastic properties of the CRAMs might result in overdesigned pavement structures, which requires higher material consumption and

higher construction costs. Although CRAMs require lower binder content, its viscoelastic properties play a major role in the tensile strain at the bottom of the AC layer. Considering the frequency and temperature dependency of those materials result in a more reliable characterization.

### 3.4.2. Temperature variation

The further analysis will focus on the longitudinal strains since they were greater than the transversal ones in the viscoelastic scenario previously discussed. Figure 32 presents the predicted longitudinal strains at the bottom of the RAP_3F2C (Figure 32a) and RAP_3E2C (Figure 32b) layers under different temperature combinations.

Figure 32 - Longitudinal strain at the bottom of the (a) RAP_3F2C and (b) RAP_3E2C layers at different temperatures

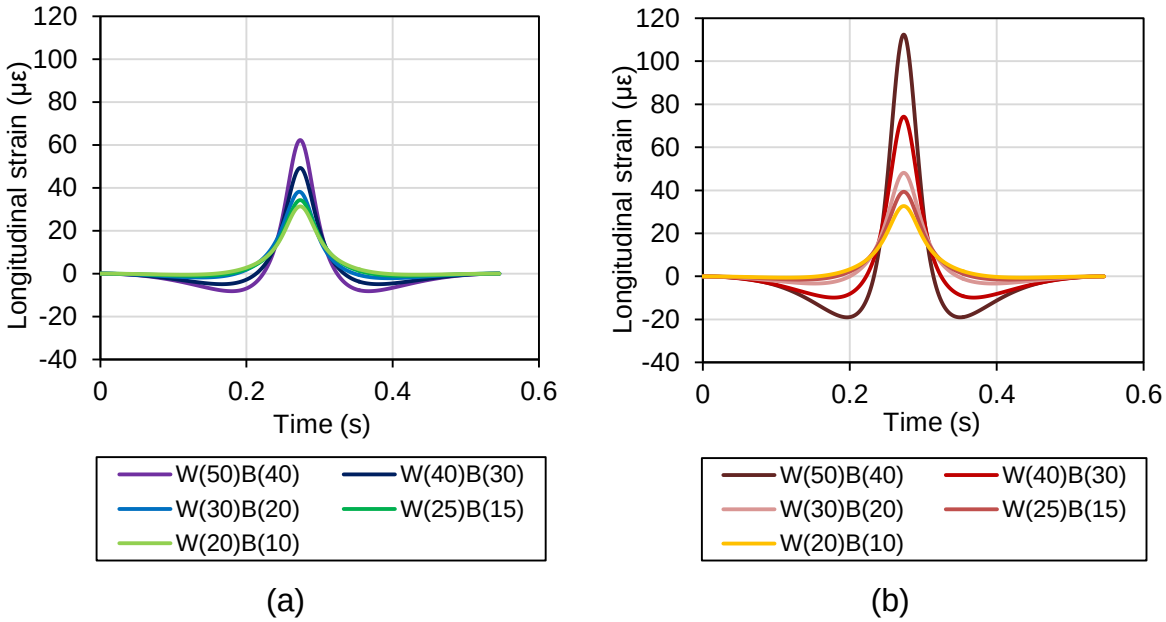


For all the temperature combinations, a tensile strain peak was observed at the bottom of the RAP_3F2C and RAP_3E2C layers, which means that CRAMs exhibit enough cohesion to resist tensile stresses. This result contradicts the hypothesis that the CRAMs behaves similarly to an unbound granular material. The increased cohesion of

the studied base course materials might be attributed to the high cement content (2%), above the limits recommended by Wirtgen (2013) for bitumen stabilized materials. The gain in CRAMs stiffness by the addition of Portland cement has already been observed in previous studies (BROWN; NEEDHAM, 2000; BETTI et al., 2016; KUCHIISHI et al., 2017).

In addition, both Figure 32a and Figure 32b demonstrate the temperature dependency of the CRAMs, since the tensile strain varies according to the temperature condition simulated. As temperature rises, the tensile strain at the bottom of the RAP_3E2C layer exhibit a greater variation in comparison with the RAP_3F2C, because of its higher temperature susceptibility. Besides, the longitudinal strain magnitudes are higher for the RAP_3E2C layer. This might be attributed to the lower stiffness of the emulsion stabilized mixture in comparison with the foamed mixture at higher temperatures, as already illustrated by the dynamic modulus master curves.

On the other hand, the trend in tensile strain at the bottom of the AC layer differs from RAP_3F2C to RAP_3E2C simulations. Figure 33 presents the predicted strains for the test sections with RAP_3F2C (Figure 33a) and RAP_3E2C (Figure 33b).

Figure 33 - Longitudinal strain at the bottom of the AC for the (a) RAP_3F2C and (b) RAP_3E2C structures at different temperatures

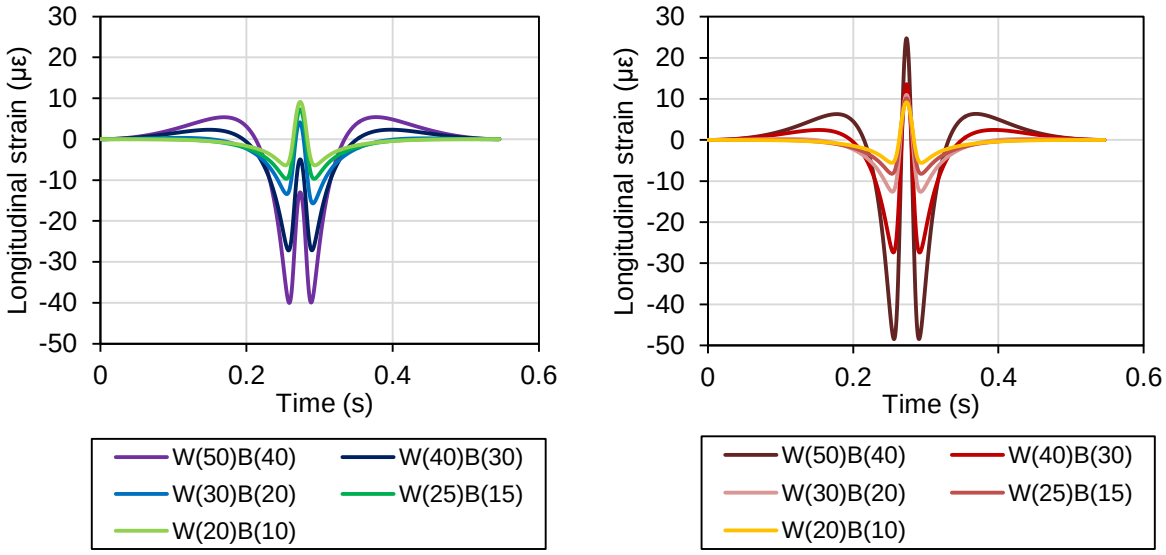


(a) (b)

From both Figure 33a and Figure 33b, it can be observed that as temperature increases, the tensile strain at the bottom of the AC layer decreases in the RAP_3F2C test section, but increases in the RAP_3E2C one. This result is attributed to the different temperature dependency of both base course materials and its relative stiffness in comparison with the wearing course. In order to evaluate the layers' stiffness at different temperatures, isochronous master curves were constructed using the dynamic modulus test output data. The reference frequency of the isochronous master curves was determined by converting the vehicle speed into a loading time, using Brown's model, and the loading time to frequency, using a time-frequency interconversion relation. Brown's model is presented in Equation 9, in which t is the loading time (seconds), d is the depth of AC's bottom layer (0.124 m) and v is the vehicle speed (40 km/h).

$$\log(t) = 0.5d - 0.2 - 0.94\log(v) \quad (9)$$

The resulting loading time was converted using the relation $t = 1/\omega = 1/2\pi f$. Although different equations might be used for conversion from time to frequency domain, this relation is considered accurate and has been widely used in the field of rheology (DONGRÉ; MYERS; D'ANGELO, 2006; KATICHA et al., 2008). Therefore, the corresponding frequency of 7.0 Hz is then calculated. Since the frequency of 5 Hz of the dynamic modulus test is the most similar to the calculated one, isochronous master curves for the tested materials were determined at the reference frequency of 5 Hz. For the construction of the isochronous master curves, a second-degree polynomial equation was fitted, as described by Equation 10, and the coefficients a, b and c were derived using a linear regression calculation. Additionally, Equation 11 was used to shift the temperature data (T) to a reduced temperature ($T_r$) by means of shift factor values ($a_T$).

$$\log \mathrm{E}(T) = a.T^2 + b.T + c \quad (10)$$

$$\log(T_r) = \log(T) + \log(a_T) \quad (11)$$

Figure 34 presents the isochronous master curves of the AC, RAP_3F2C and RAP_3E2C at the reference frequency of 5 Hz, and the regression coefficients are indicated in Table 9 along with the calculated modulus at different temperature combinations and modular ratios ($E_{AC}/E_{RAP\_3E2C/RAP\_3F2C}$). A good fitting was obtained, with $R^2 \geq 0.97$. Godenzoni et al. (2017) also used CRAMs isochronous master curves for stiffness assessment, but related with temperature correction of FWD measurements.

Figure 34 - Isochronous master curves at the reference frequency of 5 Hz

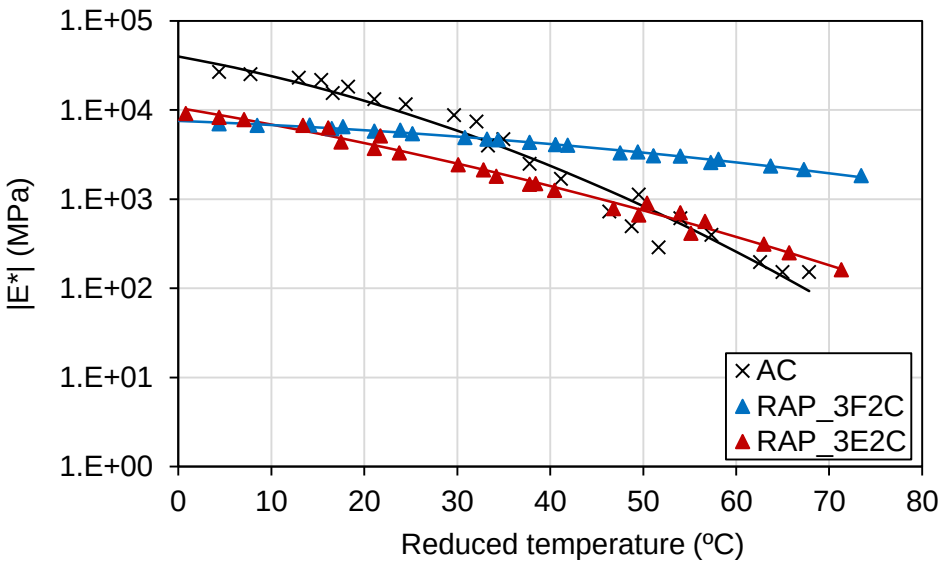

Table 9 - Regression coefficients of the isochronous master curves (5 Hz), calculated modulus, and modular ratio

| Pavement structure | Regression coefficients | | | Calculated modulus (MPa) | | | | |
|---|---|---|---|---|---|---|---|---|
| | a | b | c | W(20) B(10) | W(25) B(15) | W(30) B(20) | W(40) B(30) | W(50) B(40) |
| AC | -0.000291 | -0.018995 | 4.600302 | 12700 | 8775 | 5863 | 2367 | 835 |
| RAP_3E2C | -0.000110 | -0.017517 | 4.023822 | 6881 | 5450 | 4262 | 2509 | 1405 |
| Modular ratio ($E_{AC}/E_{RAP\_3E2C}$) | - | - | - | 1.8 | 1.6 | 1.4 | 0.9 | 0.6 |
| AC | -0.000291 | -0.018995 | 4.600302 | 12700 | 8775 | 5863 | 2367 | 835 |
| RAP_3F2C | -0.000063 | -0.003945 | 3.877972 | 6795 | 6376 | 5939 | 5041 | 4156 |
| Modular ratio ($E_{AC}/E_{RAP\_3F2C}$) | - | - | - | 1.9 | 1.4 | 1.0 | 0.5 | 0.2 |

Figure 33b shows that the tensile strain values at the bottom of the AC layer decreases as temperature increases in the RAP_3F2C pavement structure. It can be explained by RAP_3F2C relative stiffness values in comparison with AC layer, depicted by the modular ratio, which is defined as the ratio between the modulus of the wearing course ($E_{AC}$) and the base course ($E_{RAP\_3E2C}$ or $E_{RAP\_3F2C}$). As temperature rises, the RAP_3F2C stiffness exhibit a lower reduction in comparison with the AC, because of its reduced thermo-sensitivity. Therefore, the RAP_3F2C will become increasingly stiffer than the AC, reducing the modular ratio. From Table 9, it can be seen that even at the highest temperature combination, the RAP_3F2C modulus is greater than 4000 MPa, providing a substantial bearing capacity in comparison with the AC's (835 MPa). This means that, for higher temperatures (or lower modular ratios), the AC layer behaves essentially as a load transfer material and the traffic loading is primarily resisted by the RAP_3F2C layer, due to its higher stiffness and lower temperature susceptibility. Walubita and Van der Wen (2000) also observed decreasing tensile strains for lower modular ratios until compressive strains were obtained. The authors suggested that the thin surface layer acted as a load transfer component within the simulated pavement structure.

On the other hand, the RAP_3E2C structure presented a different trend regarding temperature variation and tensile strain at the bottom of the AC. For higher temperature combinations, the tensile strain increased. Although the modular ratio decreased similarly to the RAP_3F2C simulations, the inverted trend may be attributed to the

stiffness magnitude of the RAP_3E2C layer being considerably lower than RAP_3F2C ones, especially at higher temperatures. This occurs because the RAP_3E2C is more thermo-sensitive than the RAP_3F2C due to its higher master curve slope (as shown in Figure 27 and in Figure 34), which means that the stiffness decrease rate of the former is greater than the latter. At the highest temperature combination, the modulus of the RAP_3E2C is 1400 MPa, almost three times lower than RAP_3F2C at the same condition. Therefore, as temperature rises, the RAP_3E2C stiffness decreases, resulting in a faster reduction of the bearing capacity and, consequently, greater tensile strains at the bottom of the AC layer. Mejłun, Judycki and Dołżycki (2017), observed the same tensile strain trend by means of pavement mechanical simulations of a typical Polish flexible pavement structure using different models for viscoelastic materials.

Thus, even though the modular ratio of both pavement structures follow the same trend, the differences between the CRAMs temperature susceptibility impart for opposite mechanical responses after a certain temperature. The magnitude of CRAMs stiffness and its relation with AC's plays a major role in the pavement mechanical behavior. In addition, it can be said that the use of an RAP_3E2C layer would be more beneficial in terms of fatigue cracking in lower temperatures conditions, since lower tensile strains are developed. Conversely, at higher temperatures, the tensile strains could be minimized by using RAP_3F2C as base course layers. This means that the selection of the most adequate CRAM during the design process should consider field climate conditions, seeing that the CRAMs viscoelastic properties cannot be neglected.

### 3.4.3. Wearing course and base course temperature inversion

Since the deeper layers are less susceptible to temperature variation, a longer period is required for them to reach peak temperatures. This indicates that the wearing and base course may eventually invert temperatures during a 24h-period (LI; LIU; SUN, 2017). Therefore, the temperature combinations of W(25)B(15) and W(15)B(25) were used with the purpose of evaluating the effects of this temperature inversion in pavement mechanical response. Figure 35 presents the predicted longitudinal strains for the test sections with RAP_3F2C (Figure 35a) and RAP_3E2C (Figure 35b).

Figure 35 - Longitudinal strain at the bottom of the AC for the (a) RAP_3F2C and (b) RAP_3E2C structures

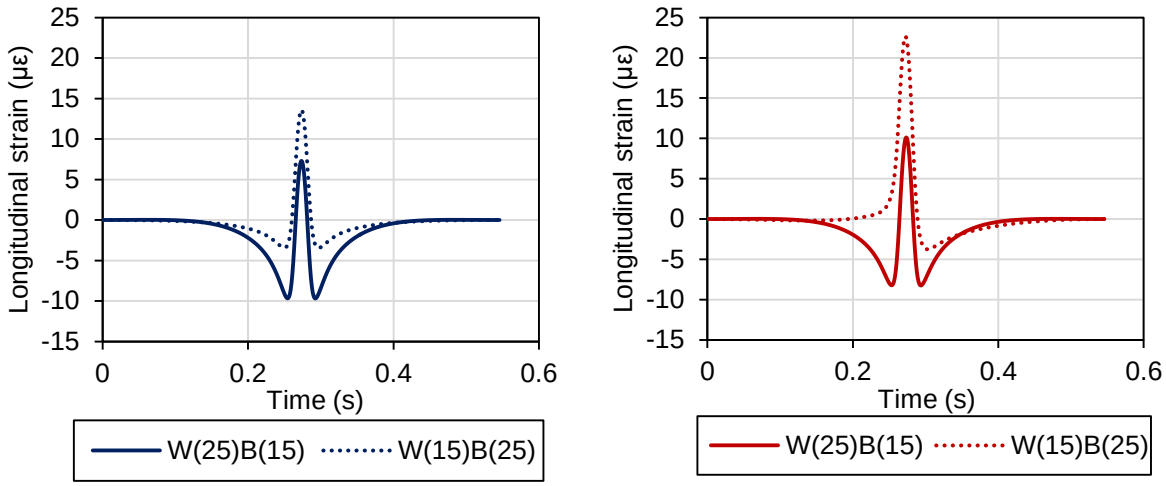


From Figure 35a and Figure 35b it can be seen that temperature inversion approximately doubles the tensile strain at the bottom of the AC, increasing from 7.29 to 13.59 με for the RAP_3F2C test section and from 10.12 to 22.64 με for the RAP_3E2C one. This inversion reduces the base course stiffness but increases the AC's. Since the AC is over a base course material with low bearing capacity, the tensile strain is increased (Walubita & Van der Ven, 2000).

It is worth noting that although the traffic volume usually reduces at night, the traffic overload is an issue that should be addressed, especially for the test sections at Fernão Dias highway. Bosso (2018) analyzed a two-years database (Sep/2015-Feb/2017) from a Weigh-in-Motion system located in the experimental test sections and observed that the passage of overloaded axles (above the legal limits) was primarily concentrated after 9:00 PM and before 6:00 AM. The author suggests that the main reason is the low activity of vehicle weighing stations in this period, which reduces the drivers' probability of being penalized by overloaded axles.

Keeping this in mind, the viscoelastic properties of CRAMs are of great importance, since the reduction of its stiffness during night maximizes the tensile strain at the

bottom of the AC. Although traffic volume is low, the overloaded axles might accelerate the occurrence of fatigue cracking of the asphalt layer. The use of RAP_3F2C as base course layers would be useful, seeing that lower tensile strains are generated at the bottom of the AC layer in comparison with the RAP_3E2C simulated structure.

## 3.5. SUMMARY AND FINDINGS

The paper herein presents the characterization of CRAMs in terms of its viscoelastic properties by means of dynamic modulus tests. These properties were used as input data for 3D-Move Analysis, simulating different temperature combinations based on temperature instrumentation data collected from the experimental test section. The following findings can be drawn:

- Both RAP_3E2C and RAP_3F2C are thermo-sensitive materials and its viscoelastic properties cannot be neglected. The differences between the CRAMs master curves can be attributed to gradation, RAP content characteristics, and form of asphalt binder dispersion within the CRAM specimens.
- Considering the CRAMs as elastic materials, the tensile strain at the bottom of the AC is maximized. This result in greater material consumption since a more robust pavement structure would be necessary to resist traffic loading. If the viscoelastic properties are considered in mechanical analysis, a greater bearing capacity is obtained, depicted by the reduced tensile strains.
- Tensile strains were observed at the bottom of the RAP_3E2C and RAP_3F2C layers, which contradicts the hypothesis that CRAMs should be considered as unbound granular materials. Besides, the temperature increase resulted in greater tensile strains at the bottom of the base course layers.
- For increasingly temperatures, the tensile strains at the bottom of the AC layer decreased for the RAP_3F2C test section, but increased for the RAP_3E2C one. The lower temperature susceptibility of the RAP_3F2C imparts for greater stiffness at higher temperatures in comparison with the AC layer, which essentially behaves as a load transfer material. Since the RAP_3E2C exhibit

greater stiffness reduction for higher temperatures than RAP_3F2C, the tensile strain at the bottom of the AC increased, seeing that RAP_3E2C does not provide a substantial bearing capacity as RAP_3F2C does.

- RAP_3F2Cs and RAP_3E2Cs could be more beneficial in colder and warmer sites, respectively, because of the reduced tensile strains at these conditions. Therefore, the selection of the most adequate CRAM during the design process should consider climatic conditions.
- The temperature inversion between AC and CRAM layers that usually occurs at night periods maximizes the tensile strain at the bottom of the AC. Considering the overloaded axles in this periods, the occurrence of fatigue cracking of the asphalt layer could be accelerated. RAP_3F2Cs may be used as a rehabilitation alternative to minimize the tensile strains increase caused by temperature inversion.

# 4. INVESTIGATION OF THE MATRIC SUCTION ROLE ON THE CURING MECHANISM OF FOAMED ASPHALT STABILIZED MIXTURES *

## 4.1. INTRODUCTION

Moisture has a major role with respect to cold recycled asphalt mixtures (CRAMs) mixing and compaction. For the mixtures stabilized with foamed asphalt, moisture suspends the fines and facilitates their contact with asphalt, enhancing asphalt dispersion during the mixing process. For asphalt emulsion stabilized mixtures, moisture reduces the absorption of the emulsion water by the aggregates, avoiding premature emulsion breaking and extending the time period for material mixing, transportation, and compaction. In terms of compaction, water imparts for greater workability of CRAMs, since it lubricates the contact between aggregates, reducing the shear strength, thus allowing densification. In this case, the optimum moisture content (OMC) is fundamental in order to provide proper densification of the material (ASPHALT ACADEMY, 2009). On the other hand, for excessive amounts of water (moisture content > OMC), agglomerations of granular material can be formed impairing asphalt dispersion (KUNA; AIREY; THOM, 2017).

The moisture content is also strongly related to the mechanical performance of CRAMs. In general, the higher the amount of water within the mixture, the lower is its modulus. The increase of stiffness and strength is obtained with moisture loss in a mechanism named “curing” (JENKINS, 2000).

From backcalculated modulus, Papavisiliou and Loizos (2013) observed a stiffness increase of the CRAM layer stabilized with foamed asphalt over time. It happens due to water evaporation during the curing process. In addition, the enhanced CRAM stiffness contributed with a reduction of the tensile strain at the bottom of the asphalt

* “Investigation of the matric suction role on the curing mechanism of foamed asphalt stabilized mixtures” by André K. Kuchiishi, Camila C. S. Antão, Kamilla Vasconcelos, José Pires, Olga M. O. Araújo, Liedi Bernucci and Ricardo T. Lopes. Submitted to European Asphalt Technology Association, Granada, Spain, 2019, and accepted for publication for the Special Issue on the Road Materials and Pavement Design journal.

concrete overlay, confirming the curing process. Meocci et al. (2016) reported similar results from backcalculated moduli of CRAMs stabilized with asphalt emulsion.

In laboratory, Graziani et al. (2018) evaluated the mechanical properties evolution of CRAMs stabilized with asphalt emulsion at different curing stages. A correlation was found between the indirect tensile strength values (ITS) and the water loss during water evaporation, since the two measurements increased at the same rate. This indicates that the strength of CRAMs is directly related to moisture content and further investigation should be conducted in order to assess for field curing.

In spite of the numerous studies evaluating curing of CRAMs, the curing process is not thoroughly understood, since several mechanisms that impart for stiffness and strength increase may be occurring simultaneously. Besides, the different types of bitumen stabilizing agents and active fillers allow producing CRAMs with distinct compositions, increasing its mechanical behavior complexity.

Therefore, a better understanding of the curing mechanism is of paramount importance, since it contributes with the development of standardized laboratory curing procedures and with construction practices. Consequently, the time required for early strength evolution and traffic opening can be reduced (FU et al., 2010; SAADOON; GARCIA; GÓMEZ-MEIJIDE, 2017).

## 4.2. LITERATURE REVIEW

### 4.2.1. Curing considerations

According to Jenkins (2000), the curing mechanism is the process in which the compacted mixture, stabilized with asphalt emulsion or foamed asphalt, releases water by means of evaporation, particle charge repulsion, or pore-pressure induced flow paths. When the moisture content decreases, an increase in stiffness and strength is observed.

Several factors can influence the moisture loss such as temperature, relative humidity, pH value of the mixture, type and content of active filler, among others (GRAZIANI et

al., 2016) and, therefore, lead to different CRAMs mechanical properties. Cardone et al (2015) evaluated the mechanical properties of cement-bitumen treated materials (CBTMs) with 3% of asphalt emulsion and two cement contents (1 and 2%), using specimens cured at 20 or 40 °C. It was concluded that the 40 °C cured specimens presented lower stiffness in comparison with the 20 °C cured ones, mainly for the mixtures with 2% of cement. The authors suggest that for higher temperatures the hardened cement may be less uniform and have higher porosity, resulting in decreased modulus.

Bessa et al. (2016) investigated the influence of curing temperature in CRAMs samples stabilized with asphalt emulsion, in order to propose a design method for this type of material. The specimens were cured at 25, 40, 60 and 100 °C during different periods of time. The authors observed an increase in the ITS values when the curing temperature raised from 40 to 60 °C. Conversely, at 100 °C the ITS reduced, which was attributed to excessively high rates of moisture loss, preventing the cement to hydrate. In addition, the authors also highlighted that higher curing temperatures (above the binder softening point) may induce redistribution of the asphalt binder within the specimen, changing its permeability.

García et al. (2013) evaluated the effect of different relative humidity (35, 70 and 90%) on the mechanical properties of emulsion stabilized samples. For mixtures without cement, a greater variability of the remaining water for different relative humidity curing processes was observed. Lower relative humidity values resulted in to an increased rate of moisture loss and, consequently, higher compressive strength especially in the initial curing period. For the mixtures with cement addition, the evaporable water content reduced due to the hydration reaction, producing samples with lower sensitivity for relative humidity.

Although controlling environmental conditions during the laboratory analysis is easier, controlling the curing process in field is a lot more complex and several procedures are recommended by different agencies and research groups. Since the moisture content significantly affects the mechanical behavior of CRAMs, the South African guidelines recommend that the overlay of the asphalt surface layer must be laid down only after 2-4 weeks after compaction of the CRAM layer (ASPHALT ACADEMY, 2009). This is

usually the curing time required for the upper 100 mm portion of CRAM compacted layer to reach 50% of the OMC. The Asphalt Recycling & Reclaiming Association recommends that the overlay should be executed only after a minimum of 3 days of curing or a moisture content lower than 3% for either cold-in place (CIR) and cold central plant recycling (CCPR) techniques (ARRA, 2016a, 2016b).

Kim, Im and Lee (2011) presented an extensive literature review regarding the residual moisture content and the curing period in situ that are usually recommended by most agencies worldwide. The presented values vary from 1.0-2.5% of residual moisture content, and from 4-45 days of curing period, indicating that there is no consensus in terms of field curing procedure. The differences between the curing recommendations might be attributed to different in situ aspects such as temperature, rainfall intensity, wind, layer thickness, level of compaction, and drainage characteristics of the material below the CRAM, that may influence the curing process in the field (KIM; IM; LEE, 2011).

During its service life, the compacted CRAM layer will cure until its moisture reaches the long-term equilibrium moisture content (EMC). According to Twagira (2010), the EMC ranges from 40-50 % of the OMC, and at this stage full bonding between the mastic and aggregates is developed, maximizing the mixture stiffness. Besides, after the evolution of those bonds, water cannot easily diffuse into the interface. Figure 36 illustrates the increase of the CRAM' stiffness (represented by the resilient modulus, $M_r$) as moisture content (MC) reaches the EMC along time.

Figure 36 - Relationship between moisture content (MC), equilibrium moisture content (EMC) and the CRAM stiffness ($M_r$)

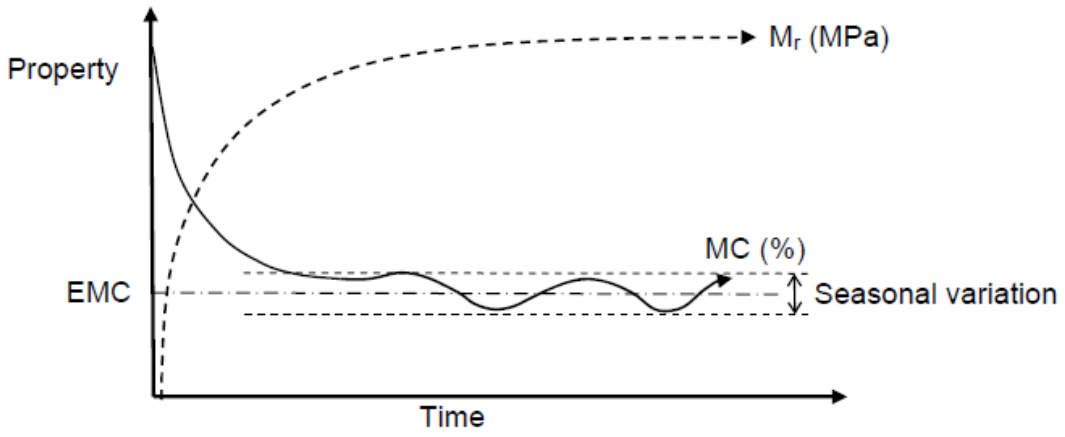


Source: Ebels and Jenkins (2007)

However, predicting the EMC and when it will be reached is difficult. According to Ebels (2008), 18 months might be required until EMC is reached; Twagira (2010) suggests that it would be necessary 24 to 36 months, whilst Moloto (2010) estimates that this period could reach up to 60 months. Those differences reported in the literature indicate that predicting the proper EMC in which stiffness is maximized is not a simple task. Jenkins (2000) tried to predict the field moisture content from data of five different roads after 6 to 24 months after construction. However, significant variability was found between field and predicted EMCs, since elements like seasonal variation and groundwater depth were not considered. Other studies have also derived different models in order to adequately predict EMC, but properties like heat transfer coefficient and evaporation coefficient were not considered (TWAGIRA, 2010).

Therefore, precisely reproducing field-curing conditions in laboratory is difficult. In addition, the great variability of CRAMs compositions in terms of aggregates, asphalt binder and active filler types and contents hinders the development of a unified laboratory curing protocol. Consequently, several laboratory curing procedures have been used worldwide, with different temperatures, curing periods, relative humidity, and for different specimen geometries. Table 10 presents a comprehensive review of some of the curing procedures used in different countries.

Table 10 - Summary of some CRAMs curing procedures

| Country | Source | Bitumen stabilizing agent | Specimen diameter/height (mm/mm) | Curing Method |
|---|---|---|---|---|
| Brazil | DNIT 169/2014 | Foam | 100 x 63.5 | 72h at 40 °C |
| | Marcandali et al. (2013) | Emulsion | 100 x 63.5 | 24h at 60 °C + 2h at room temperature (inside the mold) |
| | Bessa et al. (2016) | Emulsion | 100 x 200 | 24h at 60 ºC |
| | Guatimosim et al. (2018) | Foam | 100 x 200 | Dry curing: 3, 7, 14, 28 and 60 days at 25 °C (specimens unsealed) |
| | | | | Humid curing: 1, 7 and 28 days at 25 °C (specimens sealed) |
| China | Lin et al. (2015) | Emulsion | 150 x 100 | Early-stage curing: 24, 48, 72 and 120h at room temperature (60 or 90% RH); specimens sealed except the tops<br>Long-term curing: 168h at 60 °C |
| | Wang et al. (2018) | Emulsion | 100 x 63.5 | 1, 2, 3 and 4 days at 60 °C |
| Czech Republic | Cizkova et al. (2015) | Foam or emulsion | 150 x NS | 1 day at 20 °C (90-100% RH) + 7, 14 and 28 days at 20 °C (40-70% RH) |
| Germany | Wirtgen (2012) | Foam | 100 x 63.5 or 150 x 95 | Curing Dry: 72h at 40 °C or until constant mass |
| | | Foam | 150 x 95 | Field simulation: 20h at 30 °C or until 50% of OMC |
| | | Emulsion | 100 x 63.5 or 150 x 95 | Curing Dry: 72h at 40 °C or until constant mass |
| | | Emulsion | 150 x 95 | Field simulation: 24h at 30 °C or until 50% of OMC |
| Greece | Papavisiliou and Loizos (2013) | Foam | 100 x 40 | 72h at 40 °C + 6 months at ambient temperature (55-65% RH) |
| India | Nivedya et al. (2018) | Foam or emulsion | 100 x 63.5 | 72h at 40 °C |
| Ireland | Tabakovic et al. (2016) | Foam or emulsion | 150 x 75 | 28 days at 40 °C (specimens sealed) |
| | | | | Without cement: 3 days at 50 °C (specimens unsealed) |
| | | | | With cement: 14 days at 20 °C (specimens unsealed) |

| | | | | |
|---|---|---|---|---|
| Italy | Graziani et al. (2016) | Foam or emulsion | 150 x 75 | 1, 3, 7, 14, 28 and 100 days at 25 °C and 40 °C (specimens unsealed) |
| | Bocci et al. (2014) | Emulsion | 150 x NS | 7, 14, 21, 28, 35 days at 20 °C |
| | Giuliani and Rasteli (2004) | Emulsion | 101.6 x 63.5 | 7 and 28 days at 20 °C |
| New Zealand | Alabaster et al. (2013) | Foam | 150 x 100 | 14 days at room temperature |
| | | Foam or emulsion | 150 x 300 | 28 days at 20 ºC (specimens sealed in double plastic bags) |
| South Africa | Asphalt Academy (2009) | Foam or emulsion | 100 x 63 | 72h at 40 °C (specimen unsealed) |
| | | Emulsion | 150 x 127 | 26h at 30 °C (specimen unsealed) + 48h at 40 °C (specimen sealed) |
| | | Foam | 150 x 127 | 20h at 30 °C (specimen unsealed) + 48h at 40 °C (specimen sealed) |
| | Jenkins (2004) | Foam | 150 x NS | 24h at 40 °C (specimen sealed) + 48h at room temperature (specimen in new dry plastic bag) |
| UK | Merrill et al. (2004) | Foam or emulsion | 150 x NS | 72h at 60 °C |
| | Brown and Needham (2000) | Emulsion | 100 x 63.5 | 16h (inside the mold) + different curing periods at 20 °C (55% RH) |
| USA | Fu et al. (2010) | Foam | 100 x 63.5 | 24h at 20 °C (specimen sealed) |
| | | | | 7 days at 40 °C (specimen unsealed) |
| | Fu and Harvey (2007) | Foam | 150 x 300 | More than 7 days at 50 °C |
| | Boz et al. (2017) | Emulsion | 100 x 50 | 14 days at 25 °C and 40 °C (specimens unsealed) or 3 days at 40 ºC (specimens unsealed) |
| | Kim et al. (2007) | Foam | 100 x 63.5 | 3 days at 40 °C (specimens unsealed) |

RH = Relative humidity

NS = Not specified

### 4.2.2. Mechanisms of loading resistance

According to Fu et al. (2009) the loading resistance capacity of mixtures stabilized with foamed asphalt and without Portland cement can be described by three mechanisms: (i) interlocking and frictional sliding of aggregates, (ii) bonding of foamed asphalt mastic and aggregates, and (iii) bonding in the mineral phase due to weak cementation and suction of residual water.

The first mechanism is related with the angle of internal friction obtained by means of monotonic triaxial tests. According to Fu et al. (2009), this mechanism is the less sensitive to moisture conditioning. Twagira (2010) observed that the samples conditioned with water (wet) exhibited only a slight reduction of friction angle values in comparison with the unconditioned ones (dry). Other researches have been conducted in order to assess CRAMs angle of internal friction regarding foamed asphalt content (GONZÁLEZ et al., 2012) and RAP content (DAL BEN; JENKINS, 2014).

The second mechanism is related to the adhesion theories, such as the electrostatic, mechanical, and weak boundary layer theories (HEFER; LITTLE; LYTTON, 2005). Fu et al. (2010) investigated the adhesion development of foamed stabilized CRAMs using different curing methods. From the image analysis of the specimens fractured faces after the ITS tests, it was found that the weakest region of the samples cured at sealed condition (without water evaporation) was at the mastic-aggregate interface, in which water impaired the bonding development. On the other hand, the samples cured at unsealed condition (with water evaporation), the weakest region corresponded to the mastic itself, and the fracture occurred within it.

Li et al. (2016) reported similar results for CRAM stabilized with foamed asphalt and further investigated the full bonds development by quantifying the fractured faces asphalt coverage (FFAC) at different curing periods. It was found that, for longer curing periods, the FFAC increased indicating that, as water evaporates, the adhesion between mastic and aggregates increased and a greater amount of energy would be necessary to break this bond. When adhesion becomes greater than the cohesion within the mastic, the fracture type changes from the mastic-aggregate interface to the mastic itself, increasing the FFAC value.

On the other hand, although some studies have already highlighted the relevance of the third mechanism related to soil-suction in the bearing capacity of pavement structures (OLOO, 1994; ZAPATA; PERERA; HOUSTON, 2009), most of them are more focused on a qualitative analysis for CRAMs (FU et al. 2009; Fu et al., 2010; KHOSRAVIFAR; SCHWARTZ; GOULIAS, 2014). This means that besides evaluating the CRAMs curing process solely by comparing mechanical test results at different curing stages, the present study will further investigate the influence of suction by means of a quantitative analysis in order to evaluate the effective role of suction in the stiffness of CRAMs.

### 4.2.3. Suction of residual water

The concept of residual water suction has been extensively studied in the field of unsaturated soil mechanics (FREDLUND, RAHARDJO, 1993). The unsaturated soils are comprised by three different phases: gas, liquid and solid. The gas phase corresponds to the fluid present in the pore space not occupied by a liquid. Similarly, the liquid phase corresponds to a fluid in the pore space which is not occupied by gas, and could be represented by any liquid or combination of liquids (e.g. water, oil). The solid phase, on the other hand, corresponds to the soil and aggregate particles and can range from finer particles such as silts and clays, to coarser particles such as sands or gravel.

The unsaturated soil zone, in which the unsaturated soil mechanics theory is valid, is usually located between the ground surface and the water table, and is commonly referred as “vadose zone”. The vadose zone depth is highly dependent on the climatic conditions (e.g. temperature, relative humidity, precipitation) and consists of a transition zone in which the soil is partially saturated (FREDLUND; RAHARDJO; FREDLUND, 2012). In terms of paving materials, the dynamic relation between the amount of water and gas inside the materials pores is supposed to cause approximately corresponding effects. For example, in the case of a material composed by mineral grains, asphalt and inherent pores with variable percentage of air and water, the variation of the water content/saturation degree can cause important changes in the general material behavior, such as changes in the internal permeability. In this

case, it is considered that the suction pressure can have a singular importance. The increase in the suction pressure indicates a higher contact force between the grains that, in turn, is influenced by the presence of the binder.

The suction pressure is generated inside the pore-water and can be divided into two suction components: (i) osmotic and (ii) matric. Total suction is then calculated as the sum of the two components, as described in Equation 12.

$$\psi = (u_a - u_w) + \pi \quad (12)$$

Where: Ψ is the total suction;
$(u_a\text{-}u_w)$ is the matric suction;
$\pi$ is the osmotic suction.

The osmotic suction is related with salt concentration inside the pore-water. For higher salt concentrations an osmotic gradient is then generated attracting water to the pore-water, in order to equalize the chemical potential between the high and low salt concentrated regions (MARINHO, 1994). In spite of the influence of osmotic suction on unsaturated soil properties, it is considered less significant in comparison with matric suction for most engineering problems (FREDLUND; RAHARDJO; FREDLUND, 2012). From Krahn and Fredlund (1972) results, it can be stated that moisture content variation has major influence in the matric suction rather than the osmotic suction. Therefore, Equation 12 can then be simplified into Equation 13 which is presented below.

$$\Delta\psi \approx \Delta(u_a - u_w) \quad (13)$$

Where: Ψ is the total suction;
$(u_a\text{-}u_w)$ is the matric suction.

According to Van Genuchten (1980), the matric suction can be described as the negative water pressure generated at the soil water as a result of capillarity and adsorption forces. During desaturation, air begins to take place of some of the voids that were previously filled with water. In the air-water interface, denominated contractile skin, surface tension is then generated due to intermolecular forces inside the water phase. However, the forces exerted in the molecules within the contractile skin are unbalanced, contrarily to the molecules located in the interior of the water. Due to the unbalanced forces, the contractile skin curves toward the interior of the water and create a meniscus, frequently observed in capillary rises, until equilibrium is reached. At this condition, the contractile skin may be described as a function of surface tension ($T_s$) and radius of curvature ($R_s$) (FREDLUND; RAHARDJO, 1993). Figure 37 shows the hypothetical internal structure of a foamed stabilized specimen and the relation between its different phases.

Figure 37 - Illustration of the interaction between the phases of the foamed stabilized mixtures at different scales

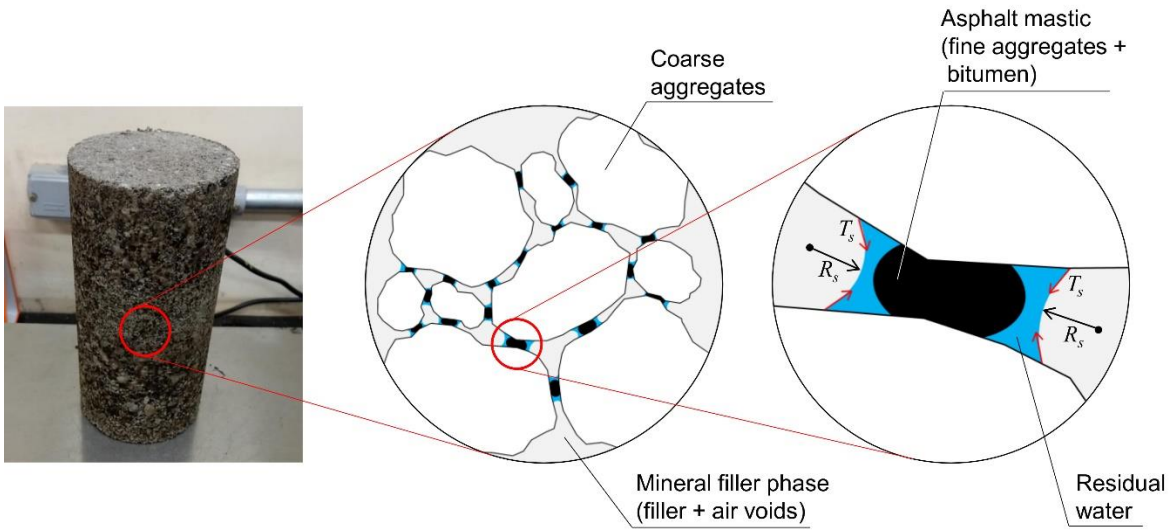


Source: Author

The matric suction can be calculated according to Equation 14, where $u_a$ and $u_w$ are the pore-air and pore-water pressures, respectively, $T_s$ is the surface tension, and $R_s$ is the radius of curvature of the contractile skin.

$$Matric\ suction = u_a - u_w = \frac{2T_s}{R_s} \quad (14)$$

Where: $u_a$ is the pore-air pressure;
$u_w$ is the pore-water pressure;
$T_s$ is the surface tension;
$R_s$ is the radius of curvature of the contractile skin.

It is worth noting that Equation 14 has a physical meaning. For higher moisture contents (or higher saturation levels), the difference of the pore-air and pore-water tend to zero. In this case, the contractile skin tends to be flat, increasing $R_s$ infinitely and reducing matric suction to zero (FREDLUND; RAHARDJO; FREDLUND, 2012). On the other hand, for lower moisture contents (or higher degrees of desaturation), the $R_s$ of the contractile skin decreases, increasing the matric suction. During the curing process, this matric suction increase imparts for greater contact force between the grains which might be occurring simultaneously to the adhesion development between mastic and aggregates.

Currently, several techniques for soil suction measurements can be used such as the filter paper, the tensiometer, the electrical or thermal conductivity sensors, psychrometers, and others. The filter paper method stands out due to its low cost, simplicity, no need for special equipment and reasonably accurate measurements (MARINHO, 1994; LEONG; HE; RAHARDJO, 2002; LU; LIKOS, 2004).

The filter paper is considered an indirect method for suction evaluation, since it measures the moisture transferred from the unsaturated material to the dried filter paper after an equilibrium period, and determines the suction values by means of calibration equations. Different equations have been developed in order to estimate the suction within the unsaturated sample as a function of the moisture (w). Table 11 presents some of the calibration equations for different lots of the Whatman Nº 42 filter paper relating the matric suction (Ψ) with the moisture content (w).

Table 11 - Calibration equations for different lots of the Whatman Nº 42 filter paper

| Source | Moisture content (w, in %) | Matric suction calibration equation (Ψ, in kPa) |
|---|---|---|
| Oliveira (2004) | w < 33% | log(Ψ) = 4.83 - 0.0839×w |
| | w ≥ 33% | log(Ψ) = 2.57 - 0.0154×w |
| Chandler et al. (1992) | w ≤ 47% | log(Ψ) = 4.84 - 0.0622×w |
| | w > 47% | log(Ψ) = 6.05 - 2.48×log(w) |
| ASTM 5298-16 | w < 45.3% | log(Ψ) = 5.237 - 0.0779×w |
| | w > 45.3% | log(Ψ) = 2.412 - 0.0135×w |

There are two methods for evaluating suction by means of the filter paper technique: (i) contact method and (ii) non-contact method (Figure 38). In the contact method, the filter paper remains in contact with the unsaturated sample, and water is transferred from the sample to the filter paper by means of capillary flow without breaking its continuity. In this situation, matric suction can then be determined. In the non-contact method, the filter paper and the sample are separated, so the air between them acts as an obstacle to water flow. In this case, since there is no contact, water vapor must overcome capillary and osmotic forces within the sample in order to be transferred to the filter paper. In this scenario, total suction is then obtained (MARINHO, 1994). Since the osmotic suction is less significant than matric suction, the contact method was then selected for suction evaluation in the present study.

Figure 38 - Representation of the (a) non-contact and (b) contact filter paper method

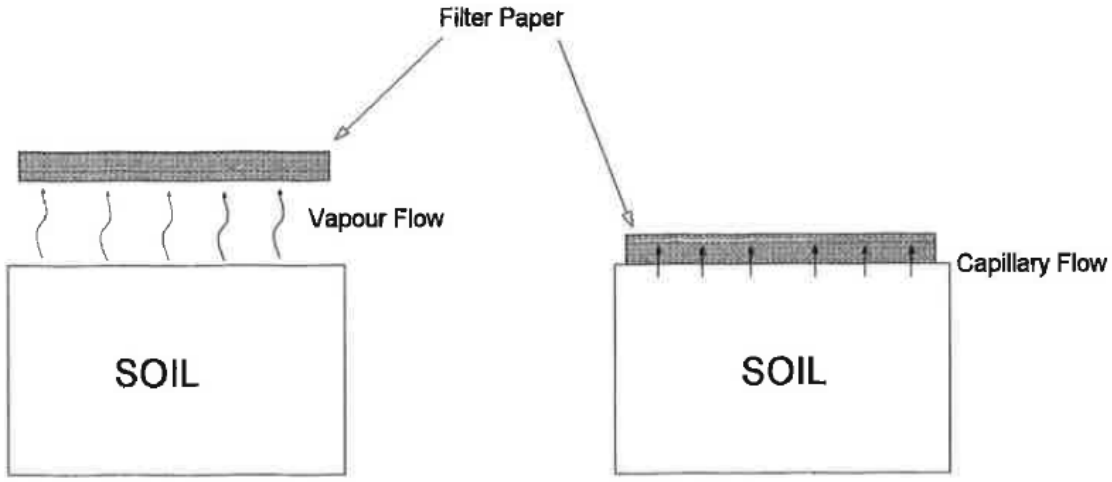


Source: Marinho (1994)

## 4.3. EXPERIMENTAL TEST SECTION AND MATERIALS

### 4.3.1. Experimental test section

The materials used for moisture investigation in the present study were collected from the field during construction of an experimental test section located at the city of Extrema, in Minas Gerais state, Brazil. The test section was constructed in the right lane (heavy traffic lane) of a two-lane segment in Fernão Dias highway (BR 381). Fernão Dias is a federal highway under Autopista Fernão Dias concession, and is considered a high traffic highway in Brazil, connecting São Paulo and Belo Horizonte cities.

The total length of the experimental test section is 800 m and is comprised by different pavement structures with 100 m length each. The pavement structures differ from each other in terms of the materials used for the base course layer, wearing course layer and layer thickness. Among the eight test sections, four of them are composed by bitumen stabilized base course materials with different types of bitumen stabilizing agents, active filler, and aggregate composition. Figure 39 illustrates the location of the four bitumen stabilized test sections with different codes for base course material identification.

Figure 39 - Location of the experimental test sections

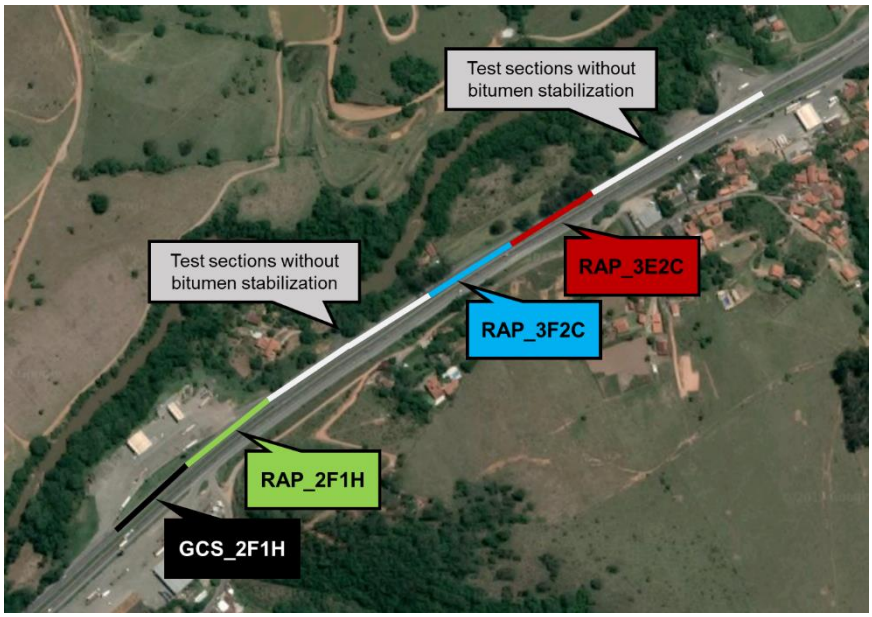


Source: Google, 2018

The RAP or GCS identification represent the more predominant type of aggregate selected within each base course material gradation. RAP is the aggregate obtained from the pavement milling process and GCS stands for graded crushed stone, which is a virgin aggregate. The F and E indexes represent, respectively, foam and emulsion stabilization while the C and H indexes, represent cement and hydrated lime active fillers. The numbers that follow along with the aforementioned indexes represent the respective bitumen stabilizing agent and active filler contents (in percentage). For the moisture analysis presented herein only the base course materials named RAP_2F1H and GCS_2F1H were used and the proposed rehabilitation structures are presented in Figure 40.

Figure 40 - Pavement structure of the (a) RAP_2F1H and (b) GCS_2F1H test sections

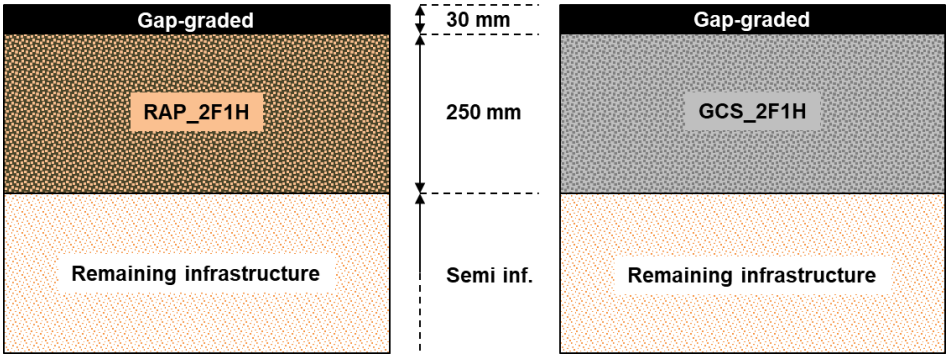


(a) (b)

Source: Author

Both RAP_2F1H and GCS_2F1H pavement structures were constructed following the same process. At first, 280mm depth of the old pavement was milled and the RAP produced was placed in stockpiles nearby the jobsite. Since the RAP was too heterogeneous it was not used in none of the test sections mentioned before. The RAP_2F1H and GCS_2F1H were previously stabilized with foamed asphalt and were hauled to the jobsite prior to compaction. In order to maintain the moisture content near the OMC and prevent water infiltration from precipitation, the base course materials were stockpiled and covered with an impervious blanket (Figure 41).

Figure 41 - Stockpiles covered with impervious blanket

Source: Author

Afterwards, the RAP_2F1H and GCS_2F1H were compacted in two layers, resulting in a 250 mm base course thickness. The first 150 mm layer was compacted by means of a padfoot roller followed by the pneumatic compaction roller. In the second layer of 100 mm thickness, the tandem compaction roller was used followed by the pneumatic compaction roller. In order to assess the dry bulk density and moisture content, degree of compaction and moisture content were determined in each layer of each test section. In comparison with the maximum specific density and OMC obtained in laboratory for mix design, no significant differences were observed with dry bulk density and moisture content from the field.

Subsequently, a light fog spray of diluted bitumen emulsion was applied with the goal of protecting the base course from surface damaging. After two days of curing, the base course materials were then overlaid with a 30 mm layer of gap-graded asphalt mixture. The construction stages mentioned above are depicted in Figure 42.

Figure 42 - Construction stages involving (a) pavement milling, (b) base course application, (c) base course compaction , and (d) gap-graded application


(a) (b)

(c) (d)

Source: Author

### 4.3.2. Materials

During the construction of the experimental test section, both RAP_2F1H and GCS_2F1H were already stabilized with foamed asphalt and were collected from the center of the stockpile in which moisture content was closer to the OMC. The RAP_2F1H and the GCS_2F1H were designed by JBA Engenharia e Consultoria Ltda. and Copavel Consultoria de Engenharia Ltda., respectively. Table 12 presents the gradation composition, foamed asphalt content, OMC and maximum specific density of the base courses obtained from the mix design. The gradation curves are within the recommended limits for foamed asphalt stabilized mixtures (WIRTGEN, 2012), as can be seen in Figure 43. The GCS_2F1H presents a relatively finer gradation. It is worth noting that, for both base course mixtures, the percentage of material passing the 0.075 mm sieve is higher than the minimum of 4% required for foamed asphalt stabilized mixtures (WIRTGEN, 2012).

Table 12 - Mixture composition of RAP_2F1H and GCS_2F1H

| Mixture composition | Unit | RAP_2F1H | GCS_2F1H |
|---|---|---|---|
| RAP | % | 89.0 | 0.0 |
| Virgin aggregate | % | 10.0 | 99.0 |
| Hydrated lime | % | 1.0 | 1.0 |
| Foamed asphalt content (pen. 50/70) | % | 2.2 | 2.0 |
| Maximum specific density | g/cm³ | 1.914 | 2.168 |
| Optimum moisture content (OMC) | % | 7.8 | 5.3 |

Figure 43 - Gradation curves of RAP_2F1H and GCS_2F1H

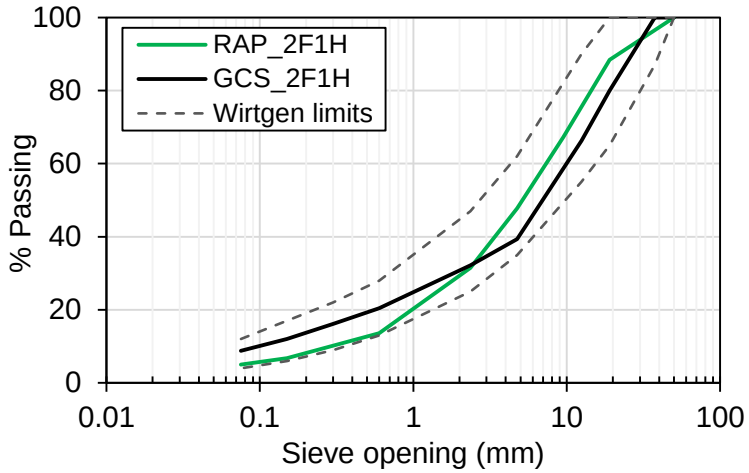


## 4.4. LABORATORY TESTING PROGRAMME

### 4.4.1. Material preparation

Ten bags of approximately 20 kg for each base course material were then transported to the Laboratory of Pavement Technology, at the Escola Politécnica of Universidade de São Paulo. The RAP_2F1H was quartered (Figure 44) according to the Brazilian specification DNER-PRO 199/96 and then replaced in sixteen sealed plastic bags to retain the moisture inside. The moisture content before the homogenization process was 4.38% and after the material was quartered the moisture reduced to 4.35%.

Figure 44 - Quartering process of RAP_2F1H

Source: Author

Due to the lower moisture content of GCS_2F1H, a mechanical rotary quartering machine was used instead, in order to quarter the material in a faster way and prevent excessive moisture loss. The material was disposed from the bags through a funnel and into a conveyor belt, which transported the material to a rotary table with sixteen compartments. The material inside the compartments was then placed in sealed plastic bags to retain the moisture inside. The moisture content before and after the mechanical quartering process was 3.66% and 3.46%, respectively. Figure 45 present some of the quartering stages.

Figure 45 - Quartering process of GCS_2F1H using a (a) mechanical rotary machine. Details of the material through the (b) funnel, (c) the conveyor belt and the (d) compartments

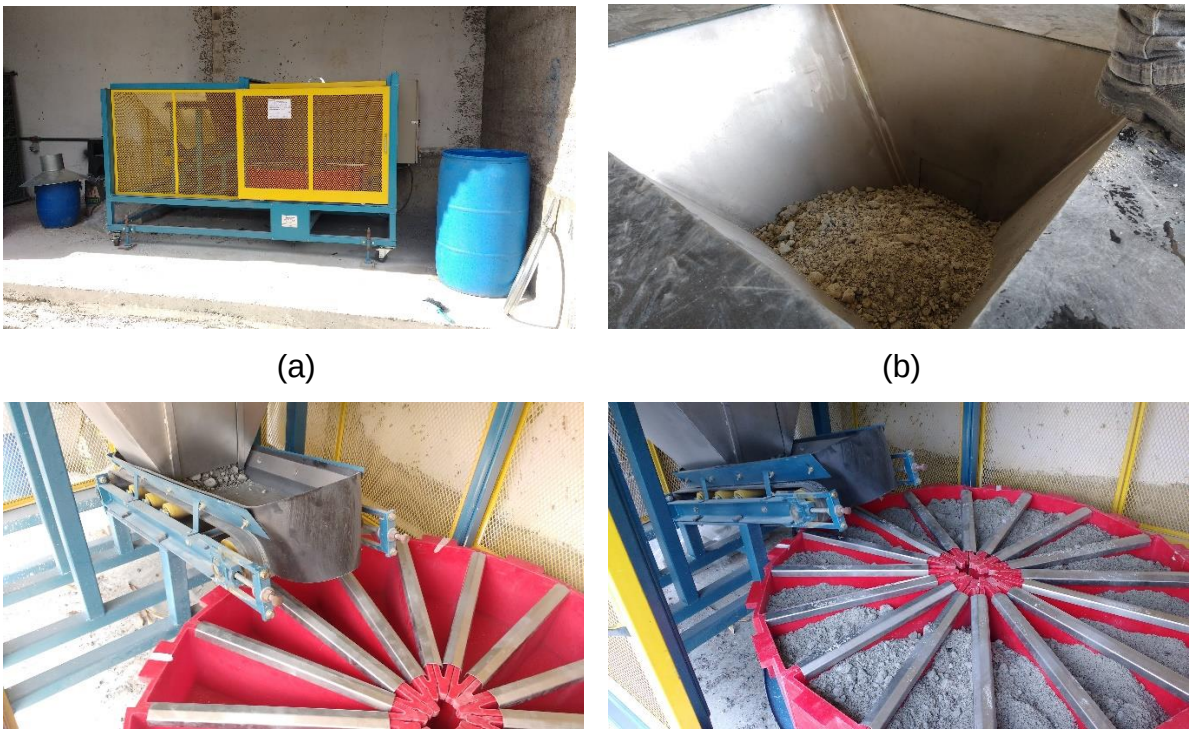

(a) (b)

(c) (d)

Source: Author

Prior to compaction, the particles greater than 19 mm were removed from each of the plastic bags and lightly crushed with a Proctor hammer used for modified energy compaction. The resulting material that was retained at the 12.5 mm sieve was then returned to the plastic bags and the passing material was discarded (JENKINS;

COLLINGS, 2016). This procedure was adopted since there was insufficient material for replacing the 19 mm retained material for equivalent 12.5 mm retained one, as recommended by the South African guidelines (ASPHALT ACADEMY, 2009).

### 4.4.2. Compaction

Afterwards, two samples of each plastic bag of RAP_2F1H and GCS_2F1H were oven dried at 105 ºC (ABNT NBR 6457/16) in order to determine the moisture content prior to compaction. After that, the amount of water necessary to reach the OMC was then added (Figure 46a) and the mixture was revolved until the moisture was homogeneously distributed within the mixture (Figure 46b). A wet towel was left covering the mixture in order to prevent moisture loss (Figure 46c). The preparation process described above was similar for the RAP_2F1H and GCS_2F1H materials.

Figure 46 - (a) Moisture correction, (b) homogenization and (c) covering for moisture loss prevention

(a) (b) (c)

Source: Author

Despite the several types of compaction methods for CRAMs (TEBALDI et al., 2014), the vibratory compaction technique was selected. The vibratory compaction method is recommended since it simulates the particle orientation of the material in field compaction (ASPHALT ACADEMY, 2009). Two specimen geometries were prepared: (i) 100 mm diameter and 200 mm height and (ii) 100 mm diameter and 150 mm height. Both types of specimens were used for moisture loss analysis presented in this

chapter, but only the 200 mm height specimen were used for the filter paper, X-ray microcomputed tomography and triaxial resilient modulus (Tx RM) tests. The 150 mm height specimens were used for dynamic modulus test, presented in Chapter 2.

The equipment used for compaction was a Bosch GSH 11 VC vibratory hammer (Figure 47a) with 1700 W power and approximately 30 kg weight. The base course materials were laid inside the molds (Figure 47b), compacted, extracted (Figure 47c) and stored inside PVC tubes and sealed plastic bags (Figure 47d) in order to maintain the moisture inside.

Figure 47 - Compaction stages using (a) a vibratory hammer: (b) material being laid inside the mold, (c) specimen extraction and (d) storage

(a)   (b)  (c)  (d)

Source: Author

The number of layers and the compacted time per layer (in seconds) is defined according to the specimen size. It is worth noting that the vibratory hammer used in this thesis has small differences in comparison with the recommended South African

one, especially with respect to the power rating specification. Besides, both types of specimen geometry (100 mm x 150 mm and 100 mm x 200 mm) are not specified in the guidelines (ASPHALT ACADEMY, 2009). Therefore, the number of layers and the compacted time were trial and error determined for each type of base course material. Table 13 presents the number of layers, compaction time, dry bulk density achieved, and the degree of compaction (DC).

Table 13 - Assessment of vibratory compaction method

| Material | Specimen height (mm) | Replicate | No. of layers | Compaction time/layer | Dry bulk density | Maximum specific density | DC |
|---|---|---|---|---|---|---|---|
| | | | - | (seconds) | (g/cm³) | (g/cm³) | (%) |
| RAP_2F1H | 150 | 1 | 2 | 5 | 1.981 | 1.914 | 104% |
| | | 2 | | 5 | 1.980 | | 103% |
| | | 3 | | 5 | 1.979 | | 103% |
| | 200 | 1 | | 7 | 1.966 | | 103% |
| | | 2 | | 7 | 1.971 | | 103% |
| | | 3 | | 7 | 1.973 | | 103% |
| | | 4 | | 7 | 1.975 | | 103% |
| | | 5 | | 7 | 1.969 | | 103% |
| GCS_2F1H | 150 | 1 | 2 | 15 | 2.121 | 2.168 | 98% |
| | | 2 | | 15 | 2.161 | | 100% |
| | | 3 | | 15 | 2.168 | | 100% |
| | 200 | 1 | | 20 | 2.064 | | 95% |
| | | 2 | | 20 | 2.159 | | 100% |
| | | 3 | | 20 | 2.139 | | 99% |
| | | 4 | | 20 | 2.147 | | 99% |
| | | 5 | | 20 | 2.146 | | 99% |

### 4.4.3. Curing

Several curing procedures have been adopted for CRAMs, as previously presented. Although Bessa et al. (2016) proposed a curing procedure at 60 ºC for 24h, the authors highlight that at this temperature, asphalt binder redistribution might occur. Conversely, lower temperatures near ambient such as 15 and 25 ºC impairs for laboratory repeatability and reproducibility (FU et al., 2010).

In light of this, the specimens were cured at the intermediate temperature of 40 ºC during seven days in unsealed condition in order to allow water evaporation. During the curing process, the specimens were periodically weighted to evaluate the rate of moisture loss. After that, the specimens were sealed and placed at ambient temperature prior to Tx RM tests. The relative humidity was not controlled during curing.

### 4.4.4. Test methods

In the experimental program, the tests were performed according to different conditions in terms of moisture content. With the purpose of evaluating the moisture influence in the mechanical behavior of the base course materials, different tests were conducted at four conditions, as described below.

- Condition 0 (initial moisture): specimen at the OMC, right after compaction;
- Condition F1 (final no. 1): specimen after the first curing period (seven days at 40 °C);
- Condition I (immersion): specimen after immersion in distilled water during 24 ± 1h at 20 °C, with water levels 50 mm above the top of the specimen;
- Condition F2 (final no. 2): specimen after the second curing period (additional seven days at 40 °C).

Figure 48 shows schematically the tests and conditions performed during the testing programme.

Figure 48 - Schematic representation of the tests performed at different conditions

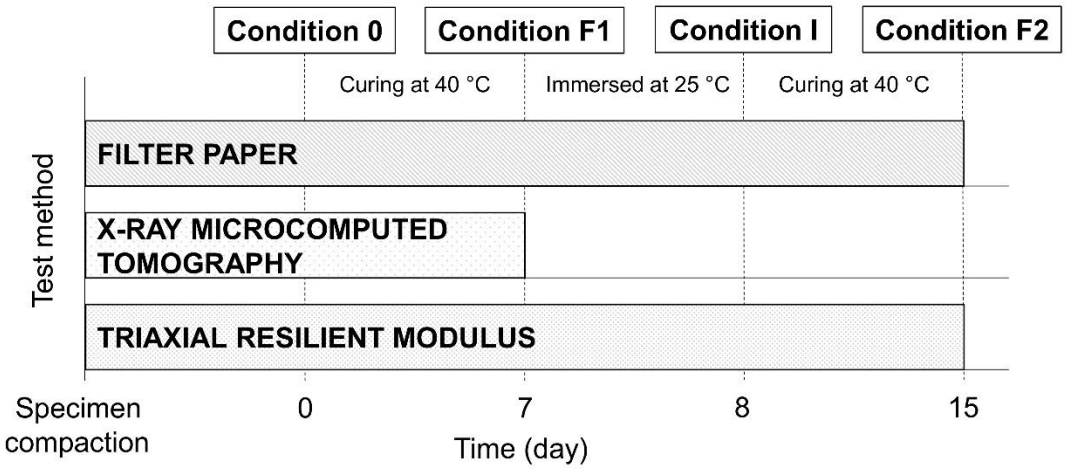


4.4.4.1. Filter paper method

For suction evaluation, the filter paper Whatman Nº 42 was selected for measuring matric suction by means of the contact method. The purpose of this analysis is to provide a physical significance for the curing mechanism, in which stiffness can vary according to the moisture content.

Two filter papers of 70 mm of diameter were placed at the specimens with 100 mm diameter and 200 mm height: one at the bottom (Figure 49a) and one at the top (Figure 49b). The filter papers were not placed at the lateral, since the specimens could be contaminated with vaseline, used to facilitate extraction from the molds. After the filter papers were laid, the specimen was covered with a double layer of plastic film (Figure 49c) followed by a single layer of aluminum paper (Figure 49d) to diminish temperature effects over specimen moisture content. Due to its low cohesion, a PVC tube was placed around the specimen for assisting its manipulation. The whole conjunction was stored inside a Styrofoam box (Figure 49e) for temperature isolation and left for seven days until equilibrium between the moisture value of the filter papers and the specimen was reached. Seven days was assumed as sufficient for filter paper contact method measurements based on literature data (MARINHO, 1994) and is the minimum required by the ASTM standard procedure (ASTM D5298-16). It is important to state

that there is no research regarding the most adequate equilibrium period for foamed asphalt mixtures.

Figure 49 - Placement of the filter paper at the (a) bottom and at the (b) top of the specimen, followed by the (c) plastic film cover, the (d) aluminum paper and (e) storage

(a) (b) (c) (d) (e)

Source: Author

After the seven days, the specimen was uncovered and the filter papers were placed inside airtight sealing plastic bags (10 cm/14 cm) which were previously weighted (Figure 50a). The set (filter paper+plastic bag) was then weighted (Figure 50b) and the humid mass of the filter paper was obtained by subtracting the plastic bag weight. Next, the filter papers were removed from the bags and placed in aluminum capsules for oven drying at 105 ºC (Figure 50c). The filter paper dry mass was then obtained, and the water content was calculated as the difference between the humid and dry masses. All the mass values must be determined to the nearest 0.0001 g. The manipulation of the filter papers was performed with a tweezer, since directly handling may disturb the measurements due to body oils contamination.

Figure 50 - Humid filter paper (a) inside airtight sealing plastic bags, (b) filter paper being weighted and (c) oven dried


(a) (b) (c)

Source: Author

4.4.4.2. X-ray microcomputed tomography and image processing

Microcomputed tomography (microCT) is a non-destructive technique that allows the visualization of reconstructed samples with resolution of the order of micrometers. Evaluating pore structure properties through microCT has received much attention in the last decade. Then a detailed 3D description of pore network can be subsequently used quantitatively to analyze parameters such as total porosity, pores diameters per height, connectivity of pores and pore size distribution, besides providing realistic 3D reconstructions. This technique has already been used to evaluate CRAMs air void distribution (GAO et al., 2015; YU et al., 2018). The microCT evaluation was conducted at the Laboratório de Instrumentação Nuclear at COPPE-UFRJ.

The microCT has been used in different research fields and industry for decades. Recently, since microCT equipment achieved high resolution, many applications are now possible to be evaluated. It is worth noting that the “micro” terminology refers to the image spatial resolution used in this study, which was 59.9 μm, and not to the specimen size. The microCT system used in this work was a V/TOMEX/M (GE). Since the choice of parameters interfere in the generation of the images and the ideal variables depend mainly on the size and composition of the sample, a careful evaluation of different parameters (e.g. voltage, filters, magnification, total images and

X-ray exposure time) is necessary. After that, the data acquisition was performed. The data acquisition time is variable, ranging from minutes to hours, depending on the sample size and parameters chosen. Therefore, the cost-benefit ratio has to be evaluated. The parameters for acquisition of these samples were: voltage 220 kV, current 240 µA, exposure time 250 ms, frame 5, filter of 0.3 mm Cu. A magnification of 3.33, pixel size 59.9 µm and a total of 1800 images for three multi-scan acquisition were necessary. The specimens were kept sealed during the X-ray microCT tests in order to maintain the moisture content constant. Figure 51a presents the test setup during data acquisition and Figure 51b presents the reconstructed specimen after merging the data acquisition from the three multi-scans.

Figure 51 - X-ray computed tomography (a) test setup during data acquisition and (b) 3D reconstructed specimen


(a) (b)

Source: Author

The 3D reconstruction software used was the Phoenix Datos|x, in which adjustments of slice alignment, beam hardening correction, ring artefact reduction, and edge enhancement filter were applied to enhance contrast for air voids. The 3D volume was generated using the software VGStudio max 3.0, where it is possible to visualize the

components of the material and the air voids before and after the curing process for RAP_2F1H and GCS_2F1H mixtures at conditions 0 and F1, respectively.

The CT Analyzer v.1.17.7.2 software was used for the quantification and measurement of air voids in the microtomographic sections. The analyses are performed using the segmentation process directly in greyscale images (Figure 52a). The segmentation in image processing usually means the decomposition of an object into segments, i.e., the identification of a discrete material in the image. In the present study, the adaptive segmentation method ranging from 0 to 255 levels of grey was selected. This method was used to separate the image into two categories (background and object). This separation is accomplished by scanning the image and identifying them as points of the object, or air voids, according to a threshold. After the verification along the sample, the threshold value selected was of 35 grey levels. The analyses were performed in order to calculate the total pore volume and pore size diameter. In the process, the top and the bottom of the sample are determined and a circular region of interest was selected for the boundary conditions of the specimen, where the green region is outside the region of interest, and therefore was not used in the calculations (Figure 52b). The results are the binarized images with the separation of the phases of the material, in which one phase consists of the aggregate skeleton and the asphalt binder (black) and the other phase, that will be quantified, consists of the air voids (white), as shown in Figure 52b.

Figure 52 - Slice reconstructed sample demonstrating the segmentation process: (a) gray scale image and (b) binarized porosity

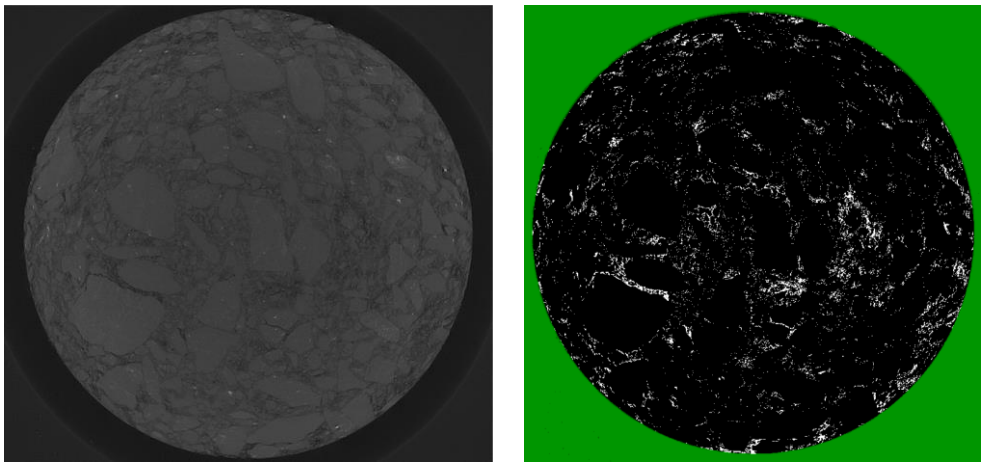

(a) (b)

Source: Author

#### 4.4.4.3. Triaxial resilient modulus test

The Tx RM test was conducted according to the Brazilian standard DNIT ME 134/10, which incorporate a wider range of pressure combinations in comparison with AASHTO T307-99 for base or subbase materials. In this test, a 100 mm diameter and 200 mm height specimen is subjected to cyclic haversine loading, with load period of 0.1 second and rest period of 0.9 second. Different combinations of confining pressure (lateral) and deviator pressure (axial) are used, in order to simulate various stress state conditions. Prior to the test, a conditioning stage is required in order to reduce plastic deformation during the test. All the Tx RM tests were performed at ambient temperature (around 25 °C).

For sample preparation, a thin layer of plaster was used to level the top and bottom of the specimen. It is worth noting that the specimens were very fragile and special care was necessary in order to avoid material loss from the compacted specimen, due to its low cohesion.

With the purpose of evaluating the moisture loss during the curing process, the specimens tested at condition F1 were different from the ones tested at condition 0. After the first curing, both the RAP_2F1H and GCS_2F1H previously cured specimens

were immersed in distilled water and then cured one more time at conditions I and F2, respectively, prior to Tx RM testing. All the Tx RM tests were performed at ambient temperature. Figure 53 presents the specimen during test.

Figure 53 - Specimen during Tx RM test

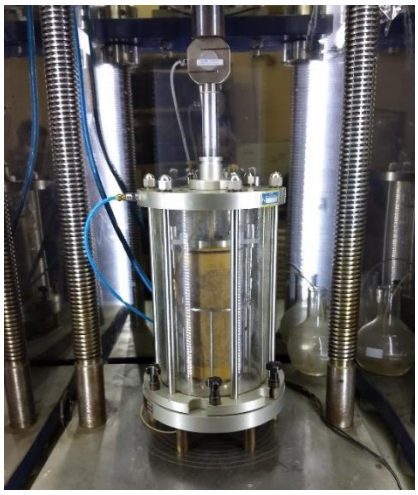

Source: Author

## 4.5. RESULTS AND DISCUSSION

### 4.5.1. Moisture loss evaluation

In order to evaluate moisture loss, both the 150 and 200 mm height specimens were periodically weighted during the curing process (seven days at 40 ºC). The purpose of this analysis is to determine if the type of aggregate or the specimen geometry impart for different moisture loss rates, which may influence the rate of stiffness increase.

For moisture loss modelling, the Michaelis-Menten (MM) model was used. The MM model has been extensively used for biochemistry and biology purposes (RUPPERT; CRESSIE; CARROLL, 1989). McElwain (1978), for example, used the MM model to determine oxygen concentration inside spherical cells by considering external diffusion parameters into the model. In terms of moisture loss evaluation, some studies have also used the MM model to better understand the development of mechanical

properties during curing of CRAMs (GRAZIANI et al., 2016, 2018; GODENZONI; GRAZIANI; BOCCI, 2017).

The MM model, presented in Equation 15, is a time-dependent model described by two regression coefficients $y_A$ and $K_c$ in order to determine the moisture loss (ML) of the compacted specimen.

$$ML = f(t) = \frac{y_A \times t}{K_c + t} \quad (15)$$

Where: ML is the moisture loss (%)
t is time (time unit)
$y_A$ is the asymptotic value (%)
$K_c$ is the Michaelis constant (time unit)

The $y_A$ coefficient is an asymptotic value which represents the ML after long-term curing. At curing time zero, the ML is also zero, but for longer curing periods ($t \rightarrow \infty$) the ML tends to $y_A$. The $K_c$ coefficient corresponds to the time required for ML to reach $y_A/2$. In other words, lower values of $K_c$ indicate higher rates of water evaporation and faster increase of the stiffness of the material (GRAZIANI et al., 2016). Figure 54 presents the moisture evaluation for both 150 mm and 200 mm specimens. The values of $y_A$ and $K_c$ are presented in Table 14.

Figure 54 - Moisture loss evaluation for (a) RAP_2F1H and (b) GCS_2F1H specimens

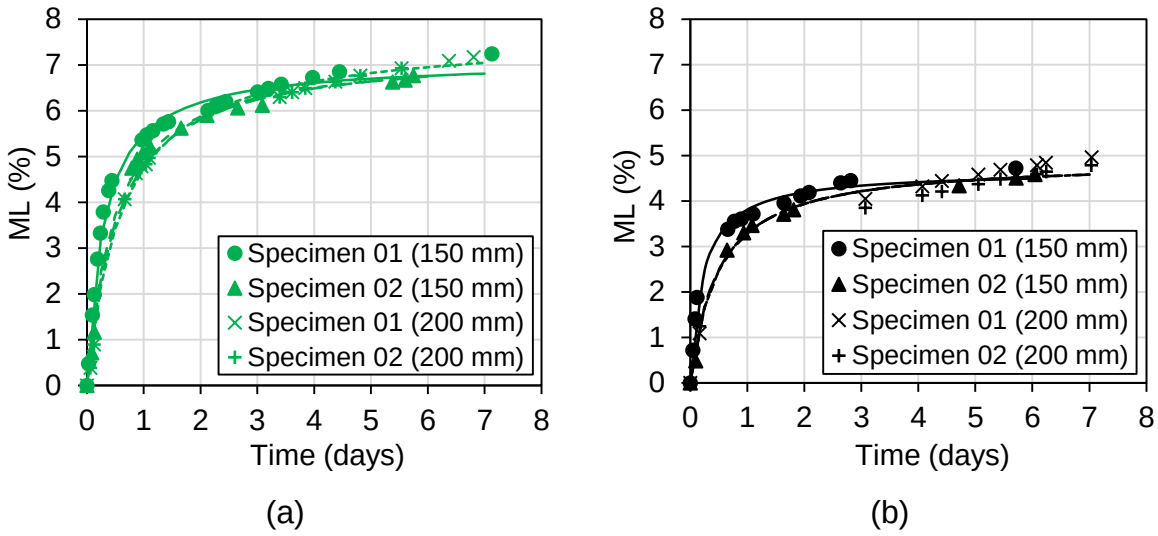


Table 14 - MM model coefficients

| MM model coefficient | Specimen height (mm) | RAP_2F1H | | | GCS_2F1H | | |
|---|---|---|---|---|---|---|---|
| | | Value | Mean | Std. Dev. | Value | Mean | Std. Dev. |
| $y_A$ (%) | 150 | 7.10<br>7.28 | 7.19 | 0.13 | 4.90<br>4.66 | 4.78 | 0.17 |
| | 200 | 7.34<br>7.67 | 7.51 | 0.23 | 4.95<br>5.38 | 5.17 | 0.30 |
| $K_c$ (days) | 150 | 0.30<br>0.48 | 0.39 | 0.13 | 0.49<br>0.22 | 0.36 | 0.19 |
| | 200 | 0.53<br>0.62 | 0.58 | 0.06 | 0.62<br>0.84 | 0.73 | 0.16 |

From Figure 54, it can be seen that the moisture loss still have a slight increase after seven days of curing, which might be attributed to material loss during specimen handling. This happens especially for lower moisture contents, in which the cohesion of the specimen is reduced. It is worth noting that the material loss was not significant during the weighing process.

From Table 14, it can be inferred that the specimen height does not have significant influence in $y_A$ coefficient. It was expected since both 150 and 200 mm specimens presented similar moisture contents and, after seven days of curing, nearly all the water had already evaporated, as illustrated in Figure 54. However, for $K_c$ coefficient, a major

difference between the specimen's sizes was observed. The specimens with 200 mm height presented greater values of $K_c$, indicating a lower moisture loss rate. One possible reason is that the water content within the 200 mm height specimens is greater than the 150 mm ones. Thus, although the exposed surface area of the 200 mm height specimens is greater than the 150 mm ones, from which water can evaporate, the total amount of water available for evaporation is greater, increasing the $K_c$ coefficient. Therefore, adopting a single curing procedure independent of the specimen geometry may lead to distinct residual moisture contents, influencing the mechanical behavior of the materials, especially in the initial curing days. From $K_c$ results, less than 24 hours were necessary to reduce the initial moisture content by half for all the specimens evaluated. This could be related with the specimens' permeability: for higher permeability, lower $K_c$ results might be obtained.

### 4.5.2. Matric suction

Table 15 presents the matric suction results obtained by means of Oliveira's (2004) calibration equation, developed for the same lot of filter papers used in this study, along with the specimen and filter paper moisture contents at the four moisture conditions. Since the other calibration equations (Table 11) resulted in similar matric suction tendencies at different conditions, only Oliveira's equation results were presented for conciseness.

Table 15 - Matric suction results for both S-RAP and S-GCS specimens.

| Mixture | Measurement | Condition | | | |
|---|---|---|---|---|---|
| | | 0 | F1 | I | F2 |
| RAP_2F1H | Specimen moisture (%) | 7.8 | 0.3 | 6.8 | 0.0 |
| | Filter paper moisture (%) | 149.6 | 7.0 | 164.8 | 5.0 |
| | Matric suction (kPa) | 1.8 | 17464.7 | 1.1 | 25958.6 |
| GCS_2F1H | Specimen moisture (%) | 5.3 | 0.2 | 5.8 | 0.0 |
| | Filter paper moisture (%) | 78.2 | 6.5 | 166.9 | 4.5 |
| | Matric suction (kPa) | 23.2 | 19345.4 | 1.0 | 28603.7 |

At lower moisture contents (conditions F1 and F2), it can be seen from Table 15 that the matric suction values increase substantially, as expected. At these conditions, a reduced amount of water is exchanged between the specimen and the filter paper during the equilibrium period. Therefore, the meniscus' radius of curvature decreases, increasing the matric suction within the sample. It is worth noting that the GCS_2F1H present matric suction values slightly higher than the RAP_2F1H ones at most moisture conditions. This might be attributed to the finer gradation of GCS_2F1H in comparison with RAP_2F1H mixture, suggesting that the former has a lower permeability than the latter.

In terms of specimen and filter paper moisture content, it can be seen that the variation of these parameters is equivalent for the GCS_2F1H mixture at different curing conditions. After the immersion stage (condition I), the GCS_2F1H samples presented a moisture content 0.5% higher than at condition 0. The filter paper moisture content was also higher after immersion in comparison with the initial condition. On the other hand, the RAP_2F1H exhibited an opposite trend. At condition I, the specimen moisture content was 1.0% lower than at condition 0, differently from the filter paper moisture content which was higher at condition I than 0. Since the same methodology was used in all filter paper tests, this inverted tendency might be attributed to the equilibrium time adopted. For RAP_2F1H samples, longer periods might be necessary in order to guarantee the equilibrium between the specimen and filter paper.

### 4.5.3. X-ray microCT

In order to evaluate the effects of water evaporation during the first curing, X-ray microCT tests were conducted with RAP_2F1H and GCS_2F1H specimens at conditions 0 and F1. The air void content was then compared at both conditions with the purpose of verifying if the increase of the contact force between the particles, depicted by the matric suction rise, would impart for reduction of the air void content. After curing (Condition F1), the RAP_2F1H and the GCS_2F1H specimens presented an air void reduction from 9.81% to 8.43% and 10.25% to 9.49%, respectively, corresponding to a substantial variation of 14% and 7%. This means that the increase of matric suction changed the internal structure of the specimens.

Figure 55 presents the relationship between the pore size diameter with the total volume of pores at conditions 0 and F1 for the RAP_2F1H (Figure 55a) and GCS_2F1H (Figure 55b) specimens. In other words, it indicates the total volume occupied by a specific pore size diameter within the specimen.

Figure 55 - Pore size diameter distribution per volume occupied for (a) RAP_2F1H and (b) GCS_2F1H

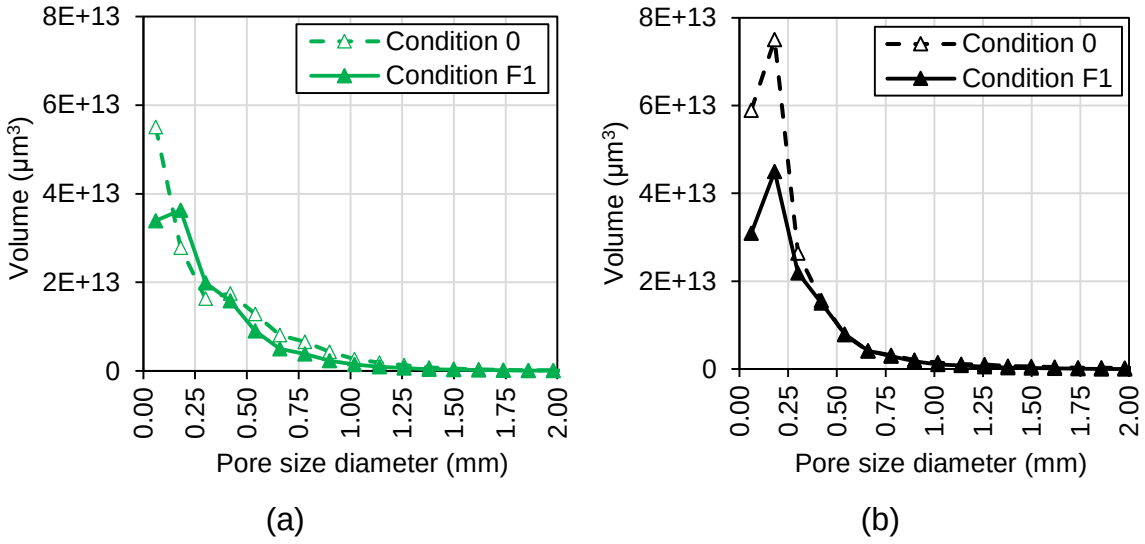


From Figure 55, it can be seen that the major air void volume within the specimen is comprised by pores with small diameter (< 0.5 mm), in which the matric suction is more likely to develop. In addition, the lower pore size diameters occupy a greater volume in the GCS_2F1H than in the RAP_2F1H samples at condition 0, since the former has more fine particles in its composition than the latter. This might be the reason for greater matric suction values obtained for the GCS_2F1H samples. The presence of smaller particles result in a greater volume occupied by the pores with reduced diameter. In consequence, greater suction pressures are generated within the specimen.

Comparing the curves for conditions 0 and F1 a reduction is observed, indicating that the air void total volume reduced due to water evaporation. Since neither the adhesion development, nor the angle of internal friction could induce air void volume reduction,

this result might be attributed to the matric suction increase which enhances the contact forces between the aggregates. In this sense, as moisture content reduces, matric suction rises, increasing the contact forces between the aggregates and, therefore, reducing the air void total volume.

In order to quantitatively evaluate this reduction, the air void total volume can then be calculated as the sum of the volume occupied by each pore size diameter. Figure 56 shows the reduction of the air voids total volume after the curing process for both RAP_2F1H and GCS_2F1H. It can be seen that the GCS_2F1H specimen exhibited a higher air void total volume reduction in comparison with RAP_2F1H. This result suggests that the greater volume occupied by the GCS_2F1H finer particles makes this mixture more susceptible for air void reduction. Considering the lower content of finer particles in the RAP_2F1H mixture, a reduced air void volume is observed.

Figure 56 - Air voids total volume before and after curing

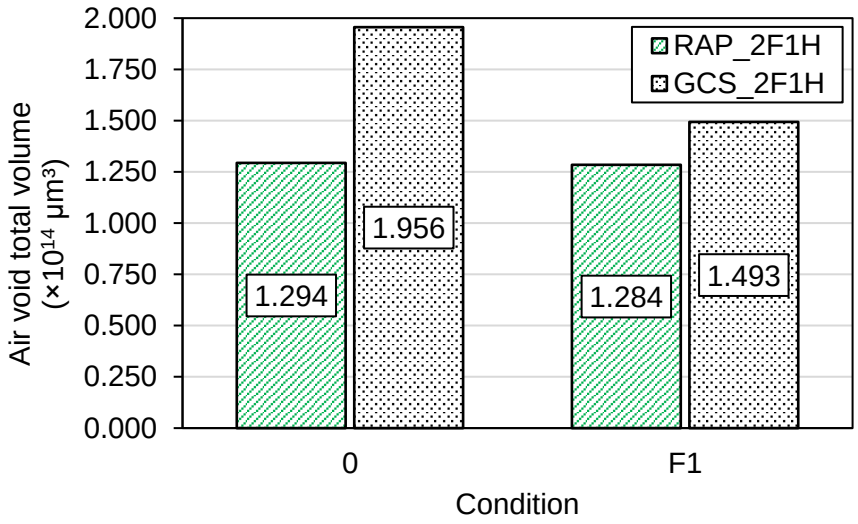


### 4.5.4. Triaxial resilient modulus

The resilient modulus can be expressed in terms of the confining pressure ($\sigma_3$) and two regression coefficients, $k_1$ and $k_2$. The exponential equation that relates these variables is presented in Equation 16. Figure 11a and Figure 11b present the mean

resilient modulus curves of the two tested replicates at the four tested conditions for both RAP_2F1H and GCS_2F1H, respectively. The resilient modulus curves of the replicates are presented in Appendix A.

The resilient modulus (RM) results can be expressed in terms of the confining pressure and two regression coefficients, $k_1$ and $k_2$. The exponential equation that relates these variables is presented in Equation 16.

$$RM = k_1 \sigma_3^{k_2} \tag{16}$$

Figure 57 present the resilient modulus curves for the RAP_2F1H and GCS_2F1H, respectively. Two replicates were tested for each of the curing conditions, 0 and F1.

Figure 57 - Resilient modulus curves for (a) RAP_2F1H and (b) GCS_2F1H

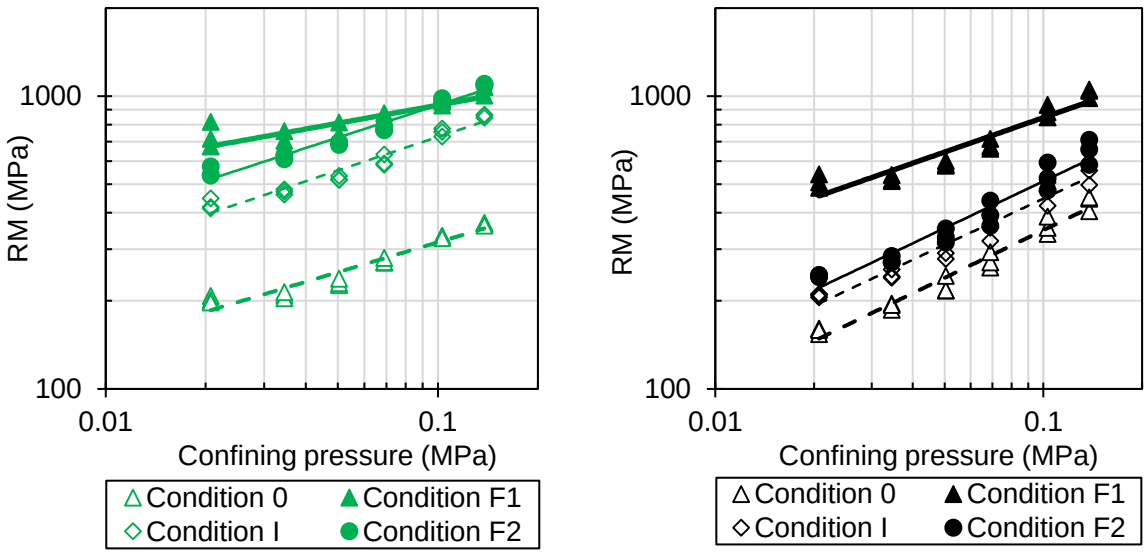


From Figure 57a and Figure 57b, it can be seen that the curing process considerably enhances the base course resilient modulus. At condition 0, the RAP_2F1H resilient

modulus ranged from 140-420 MPa and condition F1 the modulus increased to 620-1020 MPa. The respective values for the GCS_2F1H are 180-350 MPa and 480-1020 MPa. This stiffness increase corresponds to almost three times of its initial value. In general, both of the base course materials exhibited similar resilient modulus values, especially at condition F1, indicating that the use of high RAP content (89%) in the mixture composition resulted in a base course material structurally equivalent to a mixture comprised by virgin aggregates.

In addition, a stress dependency behavior is observed for all the tested conditions, since different resilient modulus values were obtained as the confining pressure varied. Table 16 presents the regression coefficients from Equation 16 along with the coefficients of determination ($R^2$) and the matric suction results. Figure 58 presents the resilient modulus range at each moisture condition (maximum RM at higher confining pressures and minimum RM at lower confining pressures), coupled with the matric suction results for the specimens with greater $R^2$.

Table 16 - Regression coefficients of the RM models

| | | $RM = k_1(\sigma_3)^{k2}$ | | | Matric suction |
|---|---|---|---|---|---|
| Material | Condition | $k_1$ | $k_2$ | $R^2$ | (kPa) |
| | 0 | 692.1 | 0.339 | 0.93 | 1.8 |
| | F1 | 1493.8 | 0.205 | 0.76 | 17464.7 |
| | I | 1740.0 | 0.380 | 0.95 | 1.1 |
| S-RAP | F2 | 2185.0 | 0.370 | 0.97 | 25958.6 |
| | 0 | 1211.8 | 0.541 | 0.97 | 23.2 |
| | F1 | 2077.6 | 0.391 | 0.90 | 19345.4 |
| | I | 1490.8 | 0.524 | 0.95 | 1.0 |
| S-GCS | F2 | 1741.0 | 0.532 | 0.93 | 28603.7 |

Figure 58 - Resilient modulus and matric suction at different moisture conditions

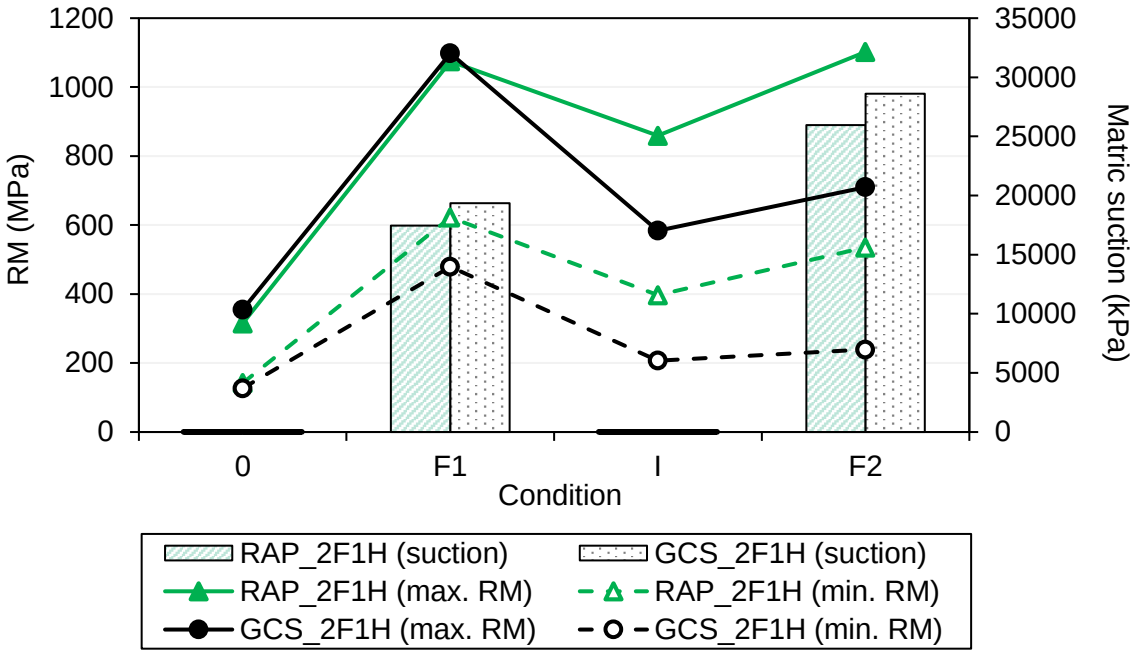


From Figure 58, a correspondence between resilient modulus and matric suction is observed for the RAP_2F1H and GCS_2F1H specimens. The increase of the resilient modulus as a whole might be associated with the increase of the matric suction pressure comparing the results from condition 0 to F1. As the moisture content decreases, the $R_s$ of the meniscus formed by the residual water (contractile skin) reduces, increasing the matric suction and, consequently, the stiffness of the mixtures. For the RAP_2F1H and GCS_2F1H, the matric suction increased from 1.8 to 17464.7 kPa and from 23.2 to 19345.4 kPa, respectively. This justifies the need for adequate field curing prior to the compaction of the asphalt overlay. If insufficient time is available to ensure moisture loss after the base course layer is compacted, the stiffness evolution might be impaired, especially in the initial service life. If the rehabilitated pavement is readily opened to traffic, the stiffness of the foamed mixtures may not be enough to resist traffic loading.

On the other hand, although both the resilient modulus and matric suction decreased at condition I and increased at condition F2, the level of variation between the two tests methods was not the same. After the immersion stage, the RAP_2F1H and GCS_2F1H

exhibit a reduction on the matric suction to values lower than the ones at condition 0, suggesting that the stiffness of the stabilized mixtures would also reduce to lower results in comparison with the initial condition. However, Figure 58 shows that the resilient modulus after the immersion was greater than the ones from condition 0. The same difference was observed after the second curing (condition F2), in which the matric suction results surpassed the ones from condition F1, but it did not result in even higher values of resilient modulus, as depicted in Figure 58. At condition F2, the RAP_2F1H mixture presented lower modulus than at condition F1 for most confining pressures. This difference suggests that, along with the suction of the residual water, other mechanisms might be dominating the loading resistance ability of the foamed mixtures.

From Table 16 it can be observed that, after the first curing period, the $k_2$ values reduced, indicating a lower confining pressure dependency for both RAP_2F1H and GCS_2F1H. This reduction might be related to the bonding development between mastic and aggregate besides the suction increase, as already reported by Fu et al. (2010). At condition 0, the water inside the specimen impairs the adhesion between the mastic and aggregate. In this case, the confining pressure have a greater influence on the specimen mechanical response during the test. After curing (condition F1), the bonds at the mastic-aggregate interface developed and, consequently, contributed for loading resistance. Therefore, the confining pressure will have a lower influence in resilient modulus results and the $k_2$ coefficient reduces. Guatimosim et al. (2018) conducted Tx RM tests for mixtures comprised by RAP with crushed cement treated base material and stabilized with foamed asphalt. The authors also observed a reduction on the resilient modulus curves slope for longer curing periods.

After immersion, $k_2$ values increased for both RAP_2F1H and GCS_2F1H, indicating a higher dependency of the stiffness to the confining pressure. This might be attributed to the loss of adhesion between mastic and aggregates, imparting for a more granular-like mechanical behavior. Moreover, it can be seen that at condition I, the GCS_2F1H specimens exhibited a greater stiffness reduction in comparison with the RAP_2F1H ones. One possible explanation is that the mastic-RAP adhesion is stronger than mastic-virgin aggregates one. Using surface free energy tests for different combinations of asphalt, aggregates and RAP content, Ghabchi, Singh and Zaman

(2014) found that, for higher contents of aged asphalt (RAP > 25%), the work of debonding reduced, indicating a lower debonding potential of the mastic from the aggregate. In other words, the presence of 89% RAP in the RAP_2F1H mixture might have contributed with a better bonding development in comparison with the virgin aggregates of the GCS_2F1H. In addition, although the stiffness reduced after the immersion, the resilient modulus curves did not return to the initial position (condition 0), even though the GCS_2F1H specimens presented greater moisture contents after immersion (6.0%) than at OMC (5.3%). This suggests that the immersion process is not capable of fully damage the mastic-aggregate bonds that developed at condition F1.

After the second curing (condition F2), the $k_2$ coefficient remained constant with water evaporation for both materials, differently from what occurred after the first curing stage, in which the $k_2$ coefficient decreased. This means that after the partial damage of the mastic-aggregate bonds, the adhesion might have been partially recovered after water removal from the interface of mastic with the aggregates. Mehrara and Khodaii (2015) also observed damage recovery of asphalt concrete samples based on normalized dissipated creep strain energy results, but only after the water that induced moisture damage had evaporated. The slight stiffness increase observed at condition F2 could be the result of this partial adhesion recovery, which may not be significant enough to reduce the confining pressure influence, indicated by the reduction of the $k_2$ coefficient.

It is worth noting that the matric suction cannot be effectively separated from the mechanisms of adhesion and frictional sliding of aggregates if only the Tx RM test results are analyzed. Although the hypothesis that additional mechanisms dominating the specimens' loading resistance was confirmed by the different levels of variation of these parameters, it is important to highlight that matric suction and RM exhibited a correspondence at different moisture conditions, especially at 0 and F1. This correspondence could be further investigated with the purpose of predicting the resilient modulus of foamed asphalt stabilized mixtures after the curing process by means of matric suction data. On the other hand, it can be inferred that, at conditions I and F2, although matric suction might influence the stiffness of foamed stabilized mixtures, its effect may be hindered by the adhesion mechanism. In this sense, matric

suction and adhesion mechanisms are occurring simultaneously, but with different levels of variation according to the curing condition. Therefore, the cohesion parameter, frequently adopted by the South African guidelines, might then be described as the sum of matric suction and adhesion components. Additional testing is required in order to evaluate the degree of influence of each of the aforementioned mechanisms separately.

## 4.6. SUMMARY AND FINDINGS

The paper herein evaluates the matric suction role in the stiffness of foamed stabilized mixtures, in conjunction with moisture loss evaluation, X-ray microCT tests and triaxial resilient modulus tests. These mixtures were collected from an experimental test section in which they have been used as base course materials. The following findings can be drawn:

- From the Michaelis-Menten model coefficients, it was found that the specimen geometry influences the specimens' moisture loss rate. Therefore, adopting a single curing procedure independent of the specimen size can lead to different residual moisture contents and, consequently, different mechanical behavior.
- Although the suction approach is commonly used in the unsaturated soil mechanics field, this approach proved to be adequate for better understanding the curing process of foamed stabilized mixtures. The matric suction was found to be significantly influenced by the moisture content of the specimens and provided physical significance to the curing mechanism.
- From X-ray microCT results it was found that the matric suction increase caused a reduction in the air void content and air void total volume within the specimens. This can be attributed to suction mechanism instead of adhesion or changes in angle of internal friction, seeing that only matric suction enhances the contact forces between the particles during the curing process. The increase in the contact forces causes a reduction of the air void content and total volume, which enhances the stiffness of the foamed stabilized mixtures.

- From Tx RM tests, it was observed that the first curing process (F1) is of great importance for stiffness development for both field and laboratory practices. Even after the specimens were immersed, the RM curves did not return to the initial position (condition 0). This means that when foamed stabilized mixtures are used as base course materials, the curing period prior to asphalt overlay must be respected in order to guarantee proper structural performance of the foamed asphalt mixture.
- A correspondence was observed between matric suction and resilient modulus values, since both increased and decreased for the different moisture conditions. However, seeing that the level of variation was not the same, especially for conditions I and F2, it suggests that other mechanisms, such as mastic-aggregate adhesion development, might be occurring at the same time. This indicates that the cohesion parameter could be described as the sum of matric suction and adhesion components.

# 5. THE EFFECT OF NON-LINEAR ELASTIC BEHAVIOR OF FOAMED ASPHALT STABILIZED MIXTURES ON PAVEMENT RESPONSE

## 5.1. INTRODUCTION AND BACKGROUND

The need for sustainable solutions regarding pavement rehabilitation is becoming an increasingly concern. In this sense, the use of cold recycled asphalt mixtures (CRAMs) is a useful alternative to rehabilitate distressed asphalt pavements. CRAMs are comprised by RAP, a bitumen stabilizing agent and an active filler, and do not require heating for mixture and compaction purposes. Therefore, several advantages might be attributed to this type of material, including reduced consumption of raw materials, less emission of pollutants, and lower construction costs (XIAO et al., 2018).

As presented in Chapter 2, the mechanical behavior of CRAMs is strongly influenced by its composition regarding gradation characteristics, the type and content of active filler and bitumen stabilizing agent. Some researchers consider that CRAM resemble a granular material, with stress-state dependency (FU; HARVEY, 2007; GUATIMOSIM, 2015). In contrast, others state that CRAMs are temperature and load frequency dependent, exhibiting viscoelastic properties (DIEFENDERFER et al., 2016; GODENZONI et al., 2017; NIVEDYA et al., 2018). Others researchers even consider that this mixture is influenced by the stress-state, temperature, and load frequency, presenting a visco-elasto-plastic behavior (JENKINS; YU, 2009; COLLINGS; JENKINS, 2011).

In this sense, depending on the assumed mechanical behavior, different pavement responses can be obtained from pavement structural analysis, which is oftentimes used for better understanding the stress-strain distribution within pavement structure. Since Chapter 3 already presented a discussion regarding the influence of CRAMs elastic and viscoelastic properties on pavement structure, this chapter is focused on the analysis of the non-linear elastic behavior of CRAMs, i.e. the stress-state dependency, and its influence on pavement mechanical response.

Some researches have been conducted regarding the non-linear elastic behavior of paving materials. Gómez-Meijide and Pérez (2015) evaluated the mechanical behavior of CRAMs with construction and demolition waste aggregates stabilized with asphalt emulsion. From triaxial resilient modulus tests, the authors observed that the non-linear elastic behavior was evident even at different water contents (9 to 31%), asphalt contents (5 to 7%) and curing stages (before and after curing), since the modulus varied for different stress-state conditions.

Besides the triaxial resilient modulus tests, Ebels (2008) used the regression coefficients of a resilient modulus model as input parameters to simulate the mechanical behavior of a pavement structure with CRAM stabilized with asphalt emulsion as the base course layer. The author observed that considering the CRAM layer as linear elastic, or non-linear elastic substantially affects the stresses and strains within the pavement structure. The linear analysis overestimated the tensile strain at the bottom of the surface layer resulting in a reduction of the fatigue life prediction of three times in comparison with the non-linear analysis, which correspond to a more realistic characterization. Oke (2010) conducted similar analysis and observed that the compressive stresses at the top of the asphalt surface layer increased from 500 to 2000 kPa when CRAMs non-linear properties were not considered.

Other researchers have investigated the stress-state dependency of CRAMs stabilized with foamed asphalt. Loizos, Papavisiliou and Plati (2012) evaluated the influence of FWD load level on non-linear strain measurements at the bottom of the foamed asphalt layer. The authors suggest that the non-linear effect is more pronounced within the foamed asphalt layer at medium temperatures (22-23 °C). Therefore, the viscoelastic properties of the CRAM layer also influence the non-linear response of the mixture. Kuna, Airey and Thom (2018) simulated different pavement structures comprised by a foamed asphalt CRAM base layer with varying contents of RAP and cement. It was concluded that the non-linear analysis resulted in higher strains at the base layer, primarily due to the stress-state dependency of this material.

The aim of this study is to evaluate the impact of the non-linear elastic properties of CRAMs stabilized with foamed asphalt in the mechanical behavior of a pavement structure by means of computational simulation and field instrumentation data. As a

result, using a more realistic material characterization as input data for pavement analysis might provide a better understanding of the CRAMs mechanical behavior and, consequently, contribute with the development of future pavement design considering this type of material.

## 5.2. MATERIALS AND TESTING PROGRAMME

### 5.2.1. Materials and pavement structure

The materials used for this study were collected from the experimental test section in Fernão Dias highway (BR 381), located at Extrema city, in Minas Gerais, Brazil. The test section was constructed in the right lane (heavy traffic lane) of a two-lane segment.

The total length of the experimental test section is 800 m and is comprised by different pavement structures with 100 m length each. The pavement structures differ from each other in terms of the materials used for the base course layer, wearing course layer and layer thickness. For the non-linear elastic analysis, only two of them were selected, namely RAP_2F1H and RAP_3F2C. The proposed rehabilitated structures are presented in Figure 59. It is worth noting that the test section with RAP_2F1H is comprised by a thin layer of gap-graded of only 30 mm in contrast with the 125 mm thickness of the asphalt concrete (AC) layer.

Figure 59 - Pavement structure of the (a) RAP_2F1H and (b) RAP_3F2C test sections

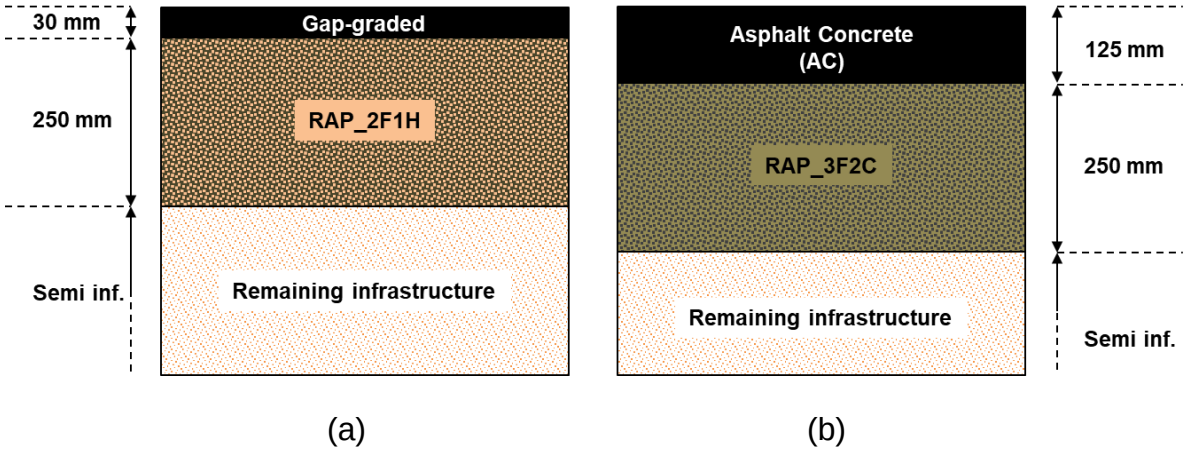


Source: Author

Figure 60 presents the gradation curves and the limits recommended for both RAP_2F1H and RAP_3F2C mixtures. Although the RAP_3F2C gradation curve exceeded the limits recommended by Wirtgen (2012), it was decided to prioritize field representation, and the samples' aggregate composition followed the gradation used in the field. Table 17 presents the gradation composition along with the foamed asphalt content, maximum bulk density and optimum moisture content.

Figure 60 - Gradation cures of the RAP_2F1H and RAP_3F2C mixtures

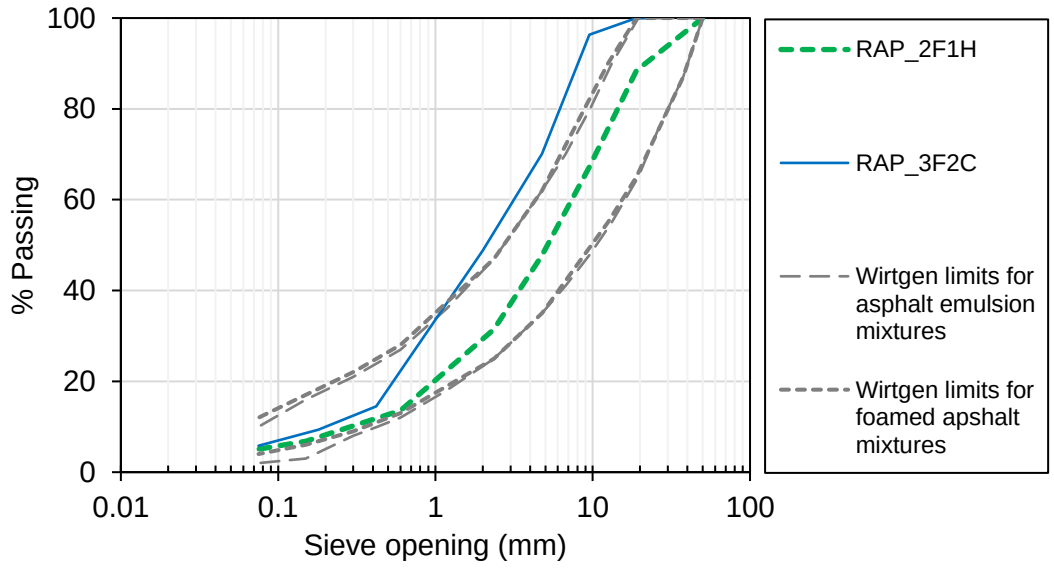

Table 17 - Mixture composition of RAP_2F1H and RAP_3F2C

| Mixture composition | Unit | RAP_2F1H | RAP_3F2C |
|---|---|---|---|
| RAP | % | 89.0 | 68.0 |
| Virgin aggregate | % | 10.0 | 30.0 |
| Active filler | % | 1.0 | 2.0 |
| Asphalt content | % | 2.2 | 3.0 |
| Maximum specific density | g/cm³ | 1.914 | 2.060 |
| OMC | % | 7.8 | 5.3 |

### 5.2.2. Laboratory testing

#### 5.2.2.1. Compaction

The equipment used for compaction was a Bosch GSH 11 VC vibratory hammer with 1700 W power and approximately 30 kg weight. The base course materials were laid inside the molds, compacted, extracted and stored inside PVC tubes and sealed plastic bags in order to maintain the moisture inside. Specimens with 100 mm diameter and 200 mm height were then produced.

The number of layers and the compacted time per layer (seconds) is defined according to the specimen size. It is worth noting that the vibratory hammer used in this thesis has small differences in comparison with the recommended South African one, especially with respect to the power rating specification. Therefore, the number of layers and the compacted time were trial and error determined for each type of base course material. Table 18 presents the number of layers, compaction time, dry bulk density achieved, and the degree of compaction (DC).

Table 18 - Assessment of vibratory compaction method

| Material | Specimen height (mm) | Replicate (-) | No. of layers (-) | Compaction time/layer (s) | Dry bulk density (g/cm³) | Maximum specific density (g/cm³) | DC (%) |
|---|---|---|---|---|---|---|---|
| RAP_2F1H | | 1 | | 7 | 1.973 | | 103 |
| | 200 | 2 | 2 | 7 | 1.975 | 1.914 | 103 |
| RAP_3F2C | | 1 | | 10 | 2.049 | | 99 |
| | 200 | 2 | 2 | 10 | 2.053 | 2.060 | 100 |

#### 5.2.2.2. Curing

Due to cement addition in the RAP_3F2C mixture, a longer curing period was adopted in order to guarantee total hydration of the cement. Cardone et al. (2015) observed increasingly stiffness values for CRAMs cured at 40 ºC during 28 days. Therefore, for the mixtures with cement addition, the same curing procedure was adopted. For the RAP_2F1H mixture, the specimens were cured at 40 ºC for seven days. Thus, the mixtures with either hydrated lime or cement Portland addition were fully cured prior to testing.

#### 5.2.2.3. Trixial resilient modulus test

The Tx RM test was conducted according to the Brazilian standard DNIT ME 134/10, which comprehend a wider range of stress combinations in comparison with AASHTO T307-99 for base or subbase materials. In this test, a 100 mm diameter and 200 mm height specimen is subjected to cyclic haversine loading, with load period of 0.1 second and rest period of 0.9 second. Different combinations of confining and deviator pressure are used, in order to simulate various stress state conditions. Prior to the test, a conditioning stage is required in order to reduce plastic deformation during the test. All the Tx RM tests were performed at ambient temperature (around 25 °C).

Several models have been proposed in order to address the non-linear behavior of granular materials. Attia and Abdelrahman (2011) and Nguyen and Mohajerani (2016) presented a comprehensive review of some of the models commonly used to fit the

resilient modulus data of granular materials. Although the present study is not focused on proposing a non-linear elastic model for the CRAMs, the influence of the resilient modulus model on the pavement mechanical response will be briefly discussed. As presented in Chapter 2, the RAP_3F2C mixture does not exhibit stress-state dependency, since a single modulus was obtained for different confining stresses. Therefore, only the RAP_2F1H was used for the non-linear elastic analysis. Table 19 presents the models used, the regression coefficients and the coefficient of determination ($R^2$) for the calculation of RAP_2F1H resilient modulus (RM).

Table 19 - Resilient modulus model and its regression coefficients for the RAP_2F1H mixture

| Resilient modulus model | Equation | $k_1$ | $k_2$ | $k_3$ | $R^2$ |
|---|---|---|---|---|---|
| Confining pressure | $RM = k_1\sigma_3^{k_2}$ | 1782.1 | 0.277 | - | 0.89 |
| K-θ | $RM = k_1\theta^{k_2}$ | 1099.7 | 0.244 | - | 0.75 |
| Pezo (1993) | $RM = k_1\sigma_3^{k_2}\sigma_d^{k_3}$ | 1852.9 | 0.346 | -0.07 | 0.92 |

From Table 19 it can be seen that the RM can be described as a function of the confining pressure ($\sigma_3$), the first stress invariant ($\theta = \sigma_1+2\sigma_3 = \sigma_d+3\sigma_3$) or the combination of both. According to the $R^2$ results, the K-θ model presented the lowest value. This might be attributed to the fact that the K-θ model accounts for both $\sigma_d$ and $\sigma_3$, not being possible to evaluate the effect of these variables separately. Ebels (2008) states that only an overall stiffening ($k_2 > 0$) or and overall softening ($k_2 < 0$) can be evaluated, but not a stiffening due to the increase of $\sigma_3$ or softening due to the increase of $\sigma_d$ simultaneously. Pezo's model, on the other hand, presented the highest $R^2$ value in comparison with the unidimensional models, mainly due to the addition of a second variable ($\sigma_d$) in the RM model. Lopez, Ekblad and Silfwerbrand (2016) stated that the addition of another variable reduces the error between the predicted and measured values of RM.

### 5.2.3. Experimental test section instrumentation

Prior to sensor installation, a saw machine was used to create three longitudinal cuts at 30 cm distance from each other (Figure 61a). Since the saw was manually operated, some difficulties were found in order to guarantee a smooth surface for the sensor to be in full contact with the cut asphalt. After that, the cuts were cleaned and dried (Figure 61b) to avoid the presence of any debris between the strain gauges and asphalt cuts and an aluminum sheet was used to assist the placement of the sensors at the selected depths (Figure 61c). For the strain measurements in situ, strain gauges from HBM Test and Measurement with nominal resistance of 120 Ω ± 0.35% were installed in the gap-graded and the AC layers at 2 and 11 cm depth, respectively. Since high rates of strain gauge failure with time have already been reported in the literature (AL-QADI et al., 2004), one sensor was installed in each of the three asphalt cuts. Next, a mixture of asphalt binder and fine aggregates was used to fill in the cuts. Figure 61d illustrates a strain gauge installed prior to the filling process.

Figure 61 - Stages of strain gauges installation: (a) cutting asphalt layer, (b) cleaning the cuts, (c) fixing the strain gauges and (d) strain gauge already installed

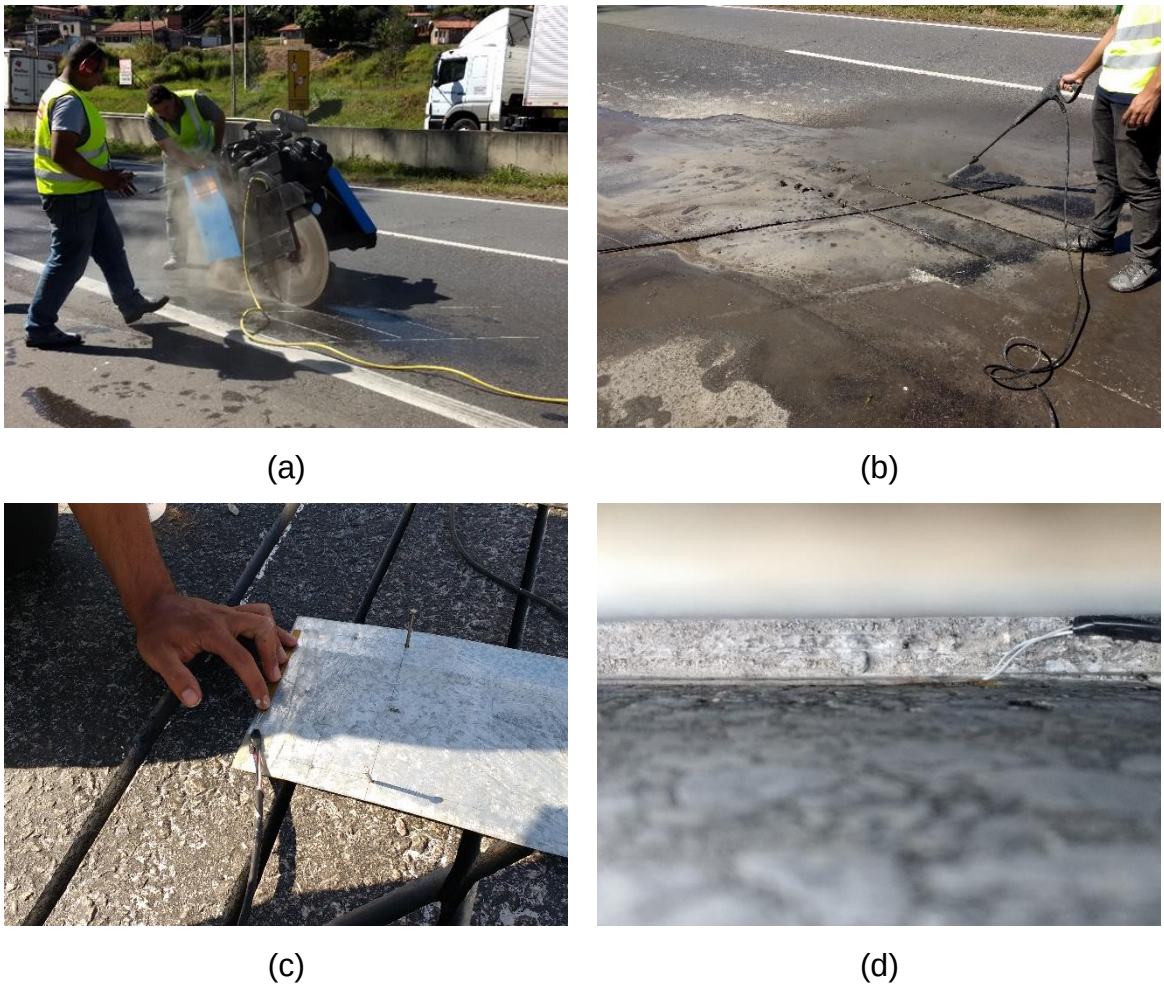

(a) (b)

(c) (d)

Source: Author

For the strain measurements, a QuantumX MX1615B data acquisition module was used. The strain gauge cables were stored inside a concrete box behind the guardrail and a computer was connected to the module for data storage. The setup for the field measurements is illustrated in Figure 62a. After the highway lane was interdicted, the FWD vehicle was aligned with each of the asphalt cuts in order to guarantee that the center of the plate was positioned over the cut (Figure 62b). Since the longitudinal position of the installed strain gauge could not be exactly determined, successive FWD load applications were performed at varying positions along the cut. A 40 kN FWD load was selected and distributed over a circular plate with 15 cm radius. A 50 Hz data acquisition frequency was used to collect the measured strains.

Figure 62 - Setup for field measurement and FWD test being carried out

(a) (b)

Source: Author

### 5.2.4. Pavement analysis

For pavement structural analysis, the multilayer elastic theory (MLET) programs are frequently used due to its lower computational time consumption in comparison with other methods, such as the finite-element method (FEM). Several programs have been developed in order to perform pavement analysis, for instance JULEA, BISAR, MnLayer, KENLAYER, and others. For the purpose of this study, two computer programs were selected for the analysis of CRAM non-linear elastic behavior: the KENLAYER (HUANG, 1993) and the Análise Elástica de Múltiplas Camadas, or AEMC (FRANCO, 2007).

Some researchers have already used the KENLAYER to analyze the non-linear elastic properties of CRAMs (EBELS, 2008; OKE, 2010; KUNA; AIREY; THOM, 2018). To address the material non-linearity, the K-θ model coefficients ($k_1$ and $k_2$) are used as input data and the coefficient of earth pressure at rest ($K_0$) is used to account for the weight of the layered system, which is not accounted for in the AEMC. For the non-linear analysis, although the KENLAYER provides three methods, only the first one was adopted, since it gives better results especially for thick granular layers under thin asphalt ones (HUANG, 2004), which is the case for the RAP_2F1H structure. In this

method, the non-linear layer (i.e. RAP_2F1H) is subdivided into layers of 51 mm maximum thickness and the layers interface can be considered either adhered or non-adhered.

The AEMC have also been used for pavement analysis (BASTOS, 2013; SOUZA JÚNIOR, 2018) and its calculations are based on the JULEA program. The AEMC is part of the calculation routine of the MeDiNa software, currently under evaluation and validation, to be used as the new Brazilian method for asphalt pavement design. For non-linear consideration, other models can also be used as input besides the K-θ model, such as the confining pressure, deviator pressure and Pezo's model, which is not possible to be done in KENLAYER. Additionally, the program subdivides the non-linear layer in three layers, which are considered weightless. The layers interface can also be simulated as adhered or non-adhered.

For load configuration, the FWD load was then simulated. Therefore, a 40 kN load was used with a circular contact area of 15 cm radius and 0.566 MPa of tire inflation pressure. Table 20 presents the input data regarding layer depth, modulus (for linear elastic analysis), Poisson ratio and unit weight for the RAP_2F1H and RAP_3F2C structures. It is worth noting that the asphalt layers and the remaining infrastructure were simulated as linear elastic materials and its modulus were determined from backcalculation of FWD data after 12 months of field curing (ANTT, 2019). The only exception is the gap-graded modulus, which was adopted based on literature data (HUANG et al., 2002; VASCONCELOS et al., 2011; LOSA; LEANDRI; CERCHIAI, 2012), since the BAKFAA software used for backcalculation does not accept layers with less than 5 cm thickness. It is worth noting that, even though the two pavement structures are from the same experimental test section, the variation of backcalculated modulus for the remaining infrastructure can be attributed to structure variability along the length of the experimental test section, due to the lack of additional information regarding the remaining infrastructure.

Table 20 - Input data for pavement analysis

| Pavement structure | Thickness (mm) | Modulus (MPa) | Poisson ratio (-) | Unit weight (g/cm³) |
|---|---|---|---|---|
| Gap-graded | 30 | 2500 | 0.35 | 2.28 |
| RAP_2F1H | 250 | 1033 | 0.45 | 1.97 |
| Remaining infrastructure | -- | 555 | 0.45 | 2.00 |
| AC | 125 | 5136 | 0.35 | 2.46 |
| RAP_3F2C | 250 | 2637 | 0.35 | 2.06 |
| Remaining infrastructure | -- | 382 | 0.45 | 2.00 |

The pavement analysis was conducted at a point located under the FWD plate symmetry axis and at different depths. The analysis can be divided into four stages. In the first one, the base course layers were considered as linear elastic materials and the RAP_2F1H and RAP_3F2C structures were compared in terms of the maximum deflection and the vertical stress at the top of the remaining infrastructure from KENLAYER and AEMC results. In the second stage, the base course layers were simulated as either linear or non-linear elastic materials with adhered or non-adhered layer interface and using both KENLAYER and AEMC programs. Next, the AEMC software was used to evaluate the influence of different resilient modulus model on the pavement response using a non-linear elastic approach. At last, the results from the pavement analysis were compared with strain gauge measurements. In terms of sign convention, the positive and negative values correspond to the tensile and compression strains and stresses, respectively. For the non-linear analysis, the regression coefficients presented in Table 19 were used. Table 21 summarizes the scenarios simulated at each stage.

Table 21 - Summary of the stages of pavement analysis

| Stage | Structure | Base layer behavior | Interface | Software |
|---|---|---|---|---|
| 1 | RAP_2F1H/RAP_3F2C | Linear | Adhered | KENLAYER/AEMC |
| 2 | RAP_2F1H | Linear/Non-linear | Adhered/Non-adhered | KENLAYER/AEMC |
| 3 | RAP_2F1H | Non-linear | Adhered | AEMC |
| 4 | RAP_2F1H/RAP_3F2C | Linear/Non-linear | Adhered/Non-adhered | KENLAYER/AEMC |

## 5.3. RESULTS AND DISCUSSION

### 5.3.1. Effect of pavement structure

In order to evaluate the influence of pavement structure, the maximum deflection ($D_0$) and the vertical stress ($\sigma_v$) at the top of the remaining infrastructure were calculated. The results from both KENLAYER and AEMC linear elastic analysis are presented in Table 22.

Table 22 - Maximum deflection and vertical stress in different pavement structures

| | $D_0$ at surface (0.01 mm) | | $\sigma_v$ at the top of the remaining infrasctructre (kPa) | |
|---|---|---|---|---|
| Material | KENLAYER | AEMC | KENLAYER | AEMC |
| RAP_2F1H | 16.83 | 16.82 | -146.70 | -146.92 |
| RAP_3F2C | 10.11 | 10.11 | -44.58 | -44.55 |

From Table 22 it is evident that the pavement structure plays a significant role on pavement mechanical response. Both $D_0$ and $\sigma_v$ values are lower in the RAP_3F2C structure, which might be attributed primarily to two reasons. Firstly, the presence of cement in RAP_3F2C composition contributes with a stiffness increase, which is not observed in the RAP_2F1H one, since it is comprised by hydrated lime as active filler. Secondly, the AC layer presents a greater stiffness and thickness in contrast with the gap-graded layer. In this sense, with a more robust structure, the segment with RAP_3F2C will contribute more effectively with load dissipation, reducing both $D_0$ and $\sigma_v$ values. No significant difference was observed between the results from KENLAYER and AEMC for the linear elastic analysis.

### 5.3.2. Effect of non-linearity

The effect of the CRAM non-linear elastic behavior on pavement response was also evaluated by means of KENLAYER and AEMC simulations. In this case, only the pavement structure with RAP_2F1H as the base course material was investigated, due

to its non-linear elastic behavior. The horizontal strain, vertical stress, and horizontal stress are presented in Figure 63.

Figure 63 - Stresses and strains distributions from (a, b, c) KENLAYER and (d, e, f) AEMC analysis

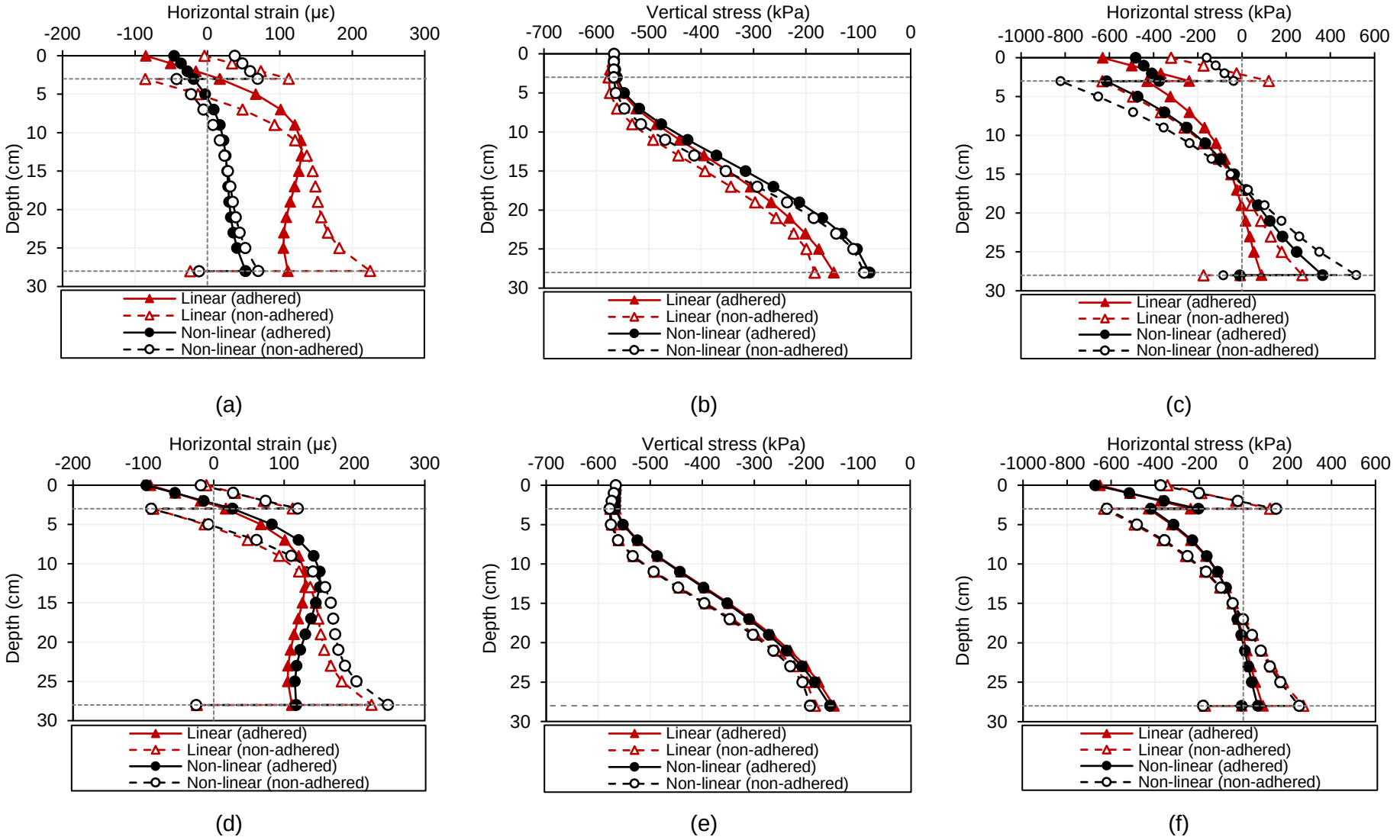

From the KENLAYER analysis (Figure 63a, b and c) a substantial difference is observed between the linear and non-linear elastic results. In terms of horizontal strains, a shift from tensile strain (linear elastic) to compression (non-linear elastic) is observed at the bottom of the gap-graded layer for the adhered case. Thus, not accounting for the stress-state dependency of the RAP_2F1H mixture might suggest that the gap-graded mixture would eventually present fatigue cracking in the future. In addition, the horizontal strains for the non-linear case are much lower in comparison with the linear one, due to the effects of the stress-state within the RAP_2F1H layer. This result indicates that considering the confining pressure effect enhances the bearing capacity of the RAP_2F1H, which will be subjected to greater horizontal stresses in contrast with the linear elastic case, as depicted in Figure 63c. Besides, the vertical stress at the top of the subgrade are considerably lower when the non-linear elastic behavior is considered. Oke (2010) and Kuna, Airey and Thom (2018) also reported different pavement responses when comparing the linear and non-linear results.

The linear elastic results from the AEMC (Figure 63d, e and f) were similar to the KENLAYER, which was already expected, since the same input data is used in both programs. The major differences were observed from the non-linear results. This might be attributed to the fact that the AEMC does not account for the weight of the layered system as KENLAYER does. Besides, there was no relevant distinction between the linear and non-linear elastic results in the AEMC analysis. Further investigations should be conducted regarding the effect of the mathematical calculations used by each of the programs for the non-linear case.

Lastly, the layers interface condition played a significant role in the pavement response for both KENLAYER and AEMC analysis. For the KENLAYER horizontal strains, in particular, the gap-graded layer changed from compression to tensile strains in the non-adhered situation. From Figure 63, it can be observed that, even though the greater tensile strains occur at the bottom of the gap-graded layer, the surface also experiences tensile strains. Although some researchers have already reported tensile strains at the asphalt surface aligned with the outside of tire edges (ALAE et al., 2018),

the occurrence of tensile strain aligned with FWD plate symmetry axis was not expected. According to Franco (2007), analysis points near the surface can generate calculation errors. These errors can be attributed to poor convergence of the infinite integral used for the calculation of the horizontal radial stress. Therefore, the strains results might have the same problem, since they are derived from the stress results (ZHAO et al., 2015).

### 5.3.3. Effect of resilient modulus model

The AEMC program was used to evaluate the influence of different RM models on the RAP_2F1H structure mechanical response. Figure 64 presents the stresses and strains for the K-θ, confining pressure and Pezo's model considering the adhered condition.

Figure 64 - Stresses and strains using different resilient modulus models as input data

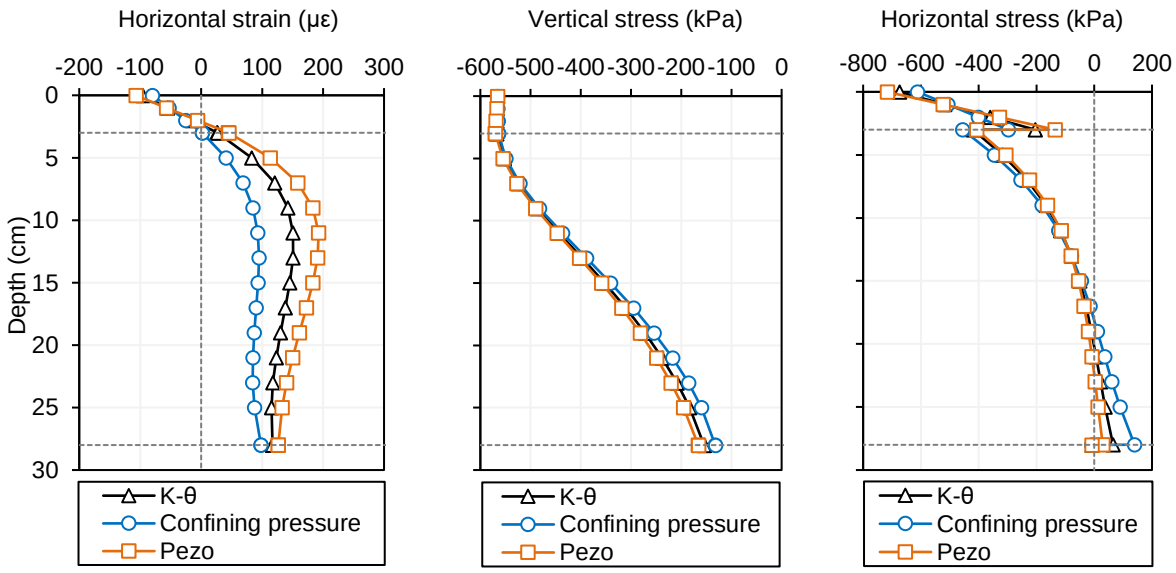


From Figure 64 it can be seen that the RM model have small effects on the vertical and horizontal stresses. The major differences are observed in the horizontal strain. For the confining pressure model, the horizontal strains within the RAP_2F1H were the

lowest, whereas Pezo' model resulted in the highest tensile strains. Comparing the horizontal strains at the bottom of the gap-graded layer (2.99 cm), the tensile strains increase from 1.82 με (confining pressure model) to 44.61 με (Pezo's model), which correspond to a variation of almost 24 times. The strains for the K-θ model, on the other hand, are located right between the other two models results.

Additionally, using the confining pressure model might impart for a higher CRAM stiffness, reducing the horizontal strains and increasing the horizontal stresses. Pezo's model, on the other hand, might consider the CRAM less stiff, increasing the horizontal strains and decreasing the horizontal stresses due to its reduced modulus. Therefore, the confining pressure and Pezo's model might overestimate and underestimate the stiffness of the RAP_2F1H layer, respectively.

It is worth noting that the horizontal strains obtained from KENLAYER and AEMC analysis for the non-linear and adhered scenario are quite distinct. Therefore, besides the differences between the mathematical calculations of each software, the use of different RM models as input data to describe the non-linear elastic properties of CRAMs result in different pavement responses. Since Pezo's model provides a better RM prediction (higher $R^2$), its use might provide a more realistic pavement analysis when considering CRAMs non-linear elastic behavior.

### 5.3.4. Comparison between measured and predicted strains

For strain measurements in situ, successive FWD load applications were necessary since the longitudinal position of the strain gauge inside the asphalt cuts could not be accurately determined. Therefore, the dashed lines in Figure 65 represent each of the strain measurements and the continuous line is the maximum strain obtained from strain gauge data in the RAP_2F1H structure at 2 cm depth of the gap-graded layer. This maximum strain will be used for comparison with KENLAYER and AEMC results for the non-linear elastic simulations, which are presented in Table 23 along with the maximum strain recorded by the strain gauges.

Figure 65 - Strain measurements at the gap-graded layer in the RAP_2F1H structure

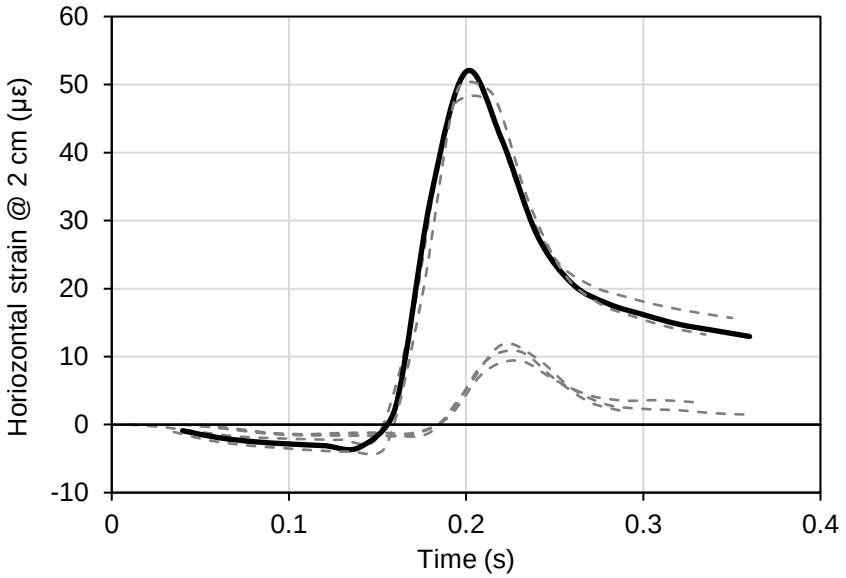


Table 23 - Calculated strain for the RAP_2F1H structure using KENLAYER and AEMC

| | Horizontal strain at 2 cm (με) | | |
|---|---|---|---|
| Interface | KENLAYER | AEMC | Strain gauge |
| Adhered | -27.5 | -14.3 | |
| Non-adhered | 58.9 | 73.7 | 51.9 |

From Figure 65 it can be observed tensile strains in the gap-graded layer at 2 cm depth. The set of curves with lower strain values (approximately 10 με) might have resulted from misalignment between the center of the FWD plate and the strain gauge. Besides, the differences in the measured strains could also be due to temperature variation during FWD testing. As presented in Chapter 3, temperature significantly influences the strain distribution within the asphalt layer and additional analysis should be conducted in order to evaluate the pavement response for different temperatures.

After comparing the measured strains with the calculated ones in Table 23, it can be seen that in the adhered condition the simulation analysis resulted in compression strains, while the strain gauges measured only tensile strains. On the other hand, the non-adhered analysis resulted in higher tensile strains in comparison with the maximum measured result. It suggests that the mechanical behavior of the RAP_2F1H

layer lies between the adhered and non-adhered scenario. Besides, the KENLAYER calculated strain was more similar to the measured one in comparison with AEMC analysis.

Figure 66 presents the strain gauge measurements for the successive FWD load application in the RAP_3F2C structure at 11 cm depth of the AC layer. In the same manner, the measured strains are compared with the calculated ones using both KENLAYER and AEMC for the elastic scenario only. This was done considering that the RAP_3F2C presents a constant modulus for different confining pressures, as already presented in Chapter 2.

Figure 66 - Strain measurements at the gap-graded layer in the RAP_3F2C structure

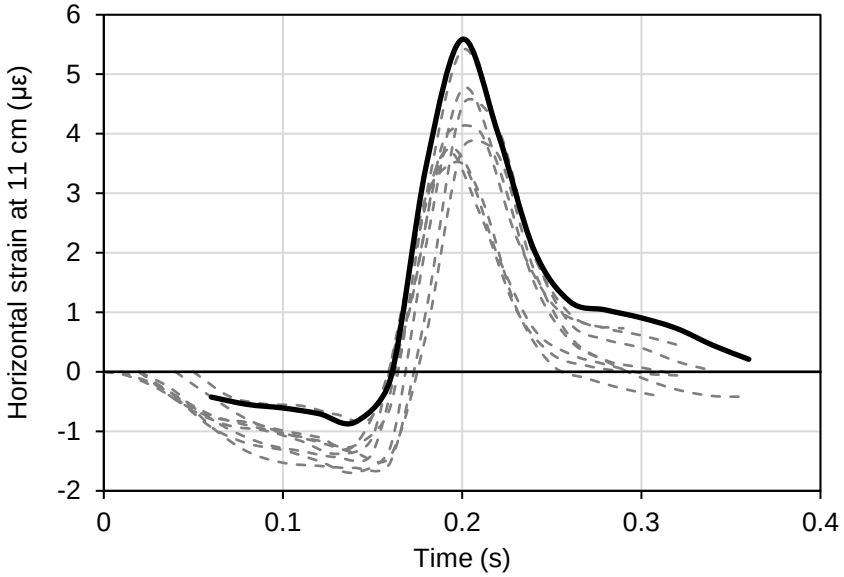


Table 24 - Calculated strain for the RAP_3F2C structure using KENLAYER and AEMC

| | Horizontal strain at 11 cm | | |
|---|---|---|---|
| Interface | KENLAYER | AEMC | Strain gauge |
| Adhered | 27.6 | 27.6 | |
| Non-adhered | 86.0 | 85.9 | 5.59 |

Although KENLAYER and AEMC analysis resulted in tensile strains, as obtained from strain gauge measurements, no correspondence was observed in terms of the magnitude of the deformation for both adhered and non-adhered scenarios. This result indicates that considering the RAP_3F2C layer as a purely linear elastic material, due to its RM independency of the confining pressure, is not totally accurate. Besides, the temperature correction was conducted only for the asphalt concrete layer during the backcalculation process. On the other hand, the RAP_3F2C backcalculated modulus used for the linear elastic analysis was determined without any temperature correction. As presented in Chapter 3, the RAP_3F2C mixture exhibit a viscoelastic behavior which substantially influences the horizontal strains at the AC layer. Therefore, seeing that the viscoelastic analysis is not part of the scope of this study, further analysis should be conducted considering the RAP_3F2C layer as a viscoelastic material in order to properly compare with the strain gauge measurements.

Therefore, although reasonable strain predictions were obtained, especially for the RAP_2F1H structure, some variables were not considered in the simulations. The simplifications and hypothesis that might have contributed for the lack of correspondence in some scenarios are presented next:

- Due to the difficulties of creating a perfectly smooth surface during asphalt cuts, the strain gauge could be imperfectly in contact with the asphalt surface, impairing an accurate data acquisition.
- The FWD plate and the strain gauge might have been imperfectly aligned. If this is the case, lower measured strains are then obtained and the maximum recorded strain can be deceptive.
- The frequency of 50 Hz used for data acquisition might have been too low to precisely measure the strains. Al-Qadi et al. (2004) reported a sampling frequency of 500 Hz for strain measurement in the Virginia Smart Road.
- The viscoelastic properties of the asphalt layers (AC and gap-graded) and the CRAMs (RAP_2F1H and RAP3F2C) were not considered. As already presented in Chapter 3, the stiffness of these materials are affected by temperature and load frequency variation.
- Since the RAP_2F1H is considered a viscoelastic material (temperature and load frequency dependency) and a granular material (with stress-state

dependency), the input parameters used to address this type of mixture in the simulations should consider both behaviors. Assuming the CRAM as a viscoelastic material, the stress dependency is not accounted and vice-versa.

- Dynamic loading should also be simulated instead of static loading as used in most of the linear elastic theory based softwares, such as KENLAYER and AEMC analysis.

## 5.4. SUMMARY AND FINDINGS

The present study is focused on evaluating the influence of the non-linear elastic behavior of CRAMs on pavement response, by means of pavement simulation and instrumentation data collected in situ. Two experimental test section structures were analyzed using both KENLAYER and AEMC softwares, and the following conclusions can be drawn.

- The CRAM composition played a significant role on the pavement response. The RAP_3F2C presented maximum deflections and vertical stress at the top of the remaining infrastructure much lower than the RAP_2F1H. This might be attributed to the presence of cement in RAP_3F2C composition (which hydrates and increase the stiffness of the layer) and the greater thickness of the AC layer in comparison with the gap-graded one.
- Major differences were observed when the RAP_2F1H was considered as either a linear or a non-linear elastic material. For the non-linear case, lower horizontal strains and vertical stresses were observed within pavement structure from KENLAYER analysis. Besides, KENLAYER and AEMC presented different results from the non-linear analysis, which can be attributed to the differences in the algorithm and input data used by each software.
- The resilient modulus model substantially affected the horizontal strains. The confining pressure and Pezo's model presented the lower and higher horizontal strains within the RAP_2F1H layer, respectively, while the K-θ model presented intermediary results. Since Pezo's model provided a better material

characterization, its use is recommended when accounting for CRAMs non-linear elastic behavior.

- After comparing the calculated strains with the collected strain gauge results, it was observed that a partially adhered scenario in the simulations would be more representative of pavement response for the RAP_2F1H structure. The calculated strains on RAP_3F2C structure, on the other hand, were not similar to the measured ones. Other factors, such as temperature influence, data acquisition frequency, and material mechanical behavior should be considered in further analysis.
- A more realistic modeling should be developed to characterize CRAMs, comprising the effects of temperature, load frequency, stress-state and moisture content. With a more realistic material characterization, the stresses and strains within pavement structure could be more accurately predicted in comparison with the measured ones.

# 6. CONCLUSIONS

## 6.1. FINAL CONSIDERATIONS

The CRAMs present several advantages regarding reduction of construction costs, lower emission of pollutant gases, reduced consumption of natural resources, and others. However, its mechanical behavior is not fully understood due to the numerous variables that can influence the stiffness of this material. In order to better understand this material behavior, some of these variables were investigated separately in each chapter.

Chapter 2 presented a study regarding the effect of mixture composition on the mechanical behavior of CRAMs by means of laboratory tests. From triaxial resilient modulus tests, it was observed that mixtures with cement addition (RAP_3E2C and RAP_3F2C) behaved similarly to cementitious materials, which present a constant modulus value for different confining pressures. The other two mixtures, with hydrated lime as active filler (RAP_2F1H and GCS_2F1H), resembled a granular material with stress dependency. From dynamic modulus tests, it was observed that the four CRAMs tested presented viscoelastic behavior, and that the type of binder and form of its distribution during mixing also influenced the CRAMs temperature susceptibility. Therefore, the studied CRAM mixtures held characteristics from both cementitious and viscoelastic materials (RAP_3F2C and RAP_3E2C) or granular and viscoelastic materials (RAP_2F1H and GCS_2F1H), which enhances its mechanical behavior complexity. Assuming just one behavior (granular, or cementitious, or viscoelastic) for further pavement design purposes might inaccurately represent the CRAM.

Thus, different variables were found to affect CRAMs stiffness, such as mixture composition, temperature, load frequency, stress-state, and others. With the purpose of evaluating the influence of temperature and load frequency, Chapter 3 focused on analyzing the pavement response of the RAP_3F2C and RAP_3E2C structures. The 3D Move Analysis software was used to simulate different temperatures obtained from temperature data of the instrumented test sections. It was found that when CRAMs are considered as linear elastic materials, its bearing capacity is underestimated. When its viscoelastic properties are then considered the pavement bearing capacity is increased, reducing the tensile strains at the bottom of the asphalt layer.

For increasing temperatures, it was also observed that the tensile strain at the bottom of the AC layer increased for the RAP_3E2C structure, but decreased for the RAP_3F2C one. This was attributed to the level of temperature susceptibility of the CRAMs, which is higher for the RAP_3E2C in comparison with the RAP_3F2C. The greater temperature susceptibility of the RAP_3E2C imparts for lower stiffness at higher temperatures in comparison with the AC layer, increasing the tensile strains. The RAP_3F2C, on the other hand, is stiffer than the AC layer at higher temperatures, and the surface layer will essentially behave as a load transfer material, reducing the tensile strains. Therefore, Chapter 3 provided several evidences of the CRAMs viscoelastic properties and its significant influence on pavement response.

In order to evaluate the effect of moisture content and stress-state on the curing mechanism, the RAP_2F1H and GCS_2F1H were then investigated in Chapter 4, since the other two mixtures did not exhibit stress dependency. Seeing that few studies have been conducted to evaluate the influence of matric suction pressure on CRAMs stiffness, filter paper and X-ray microCT tests were conducted in conjunction with triaxial resilient modulus tests. Although other mechanisms might dominate the stiffness evolution during the curing process, a correspondence between resilient modulus and matric suction was clearly observed. From the X-ray microCT measurements, this statement was confirmed, since the specimens' air void total volume reduced after the curing process, which could be caused by the increase of matric suction after the reduction of moisture content. In this sense, further analysis should be conducted in order to investigate the possibility of incorporating the matric suction in CRAMs resilient modulus models, which are frequently described as a function of the confining and deviator pressures.

Finally, the non-linear elastic behavior of the RAP_2F1H mixture, depicted by the stress dependency presented in Chapters 2 and 4, was evaluated by means of pavement analysis in both KENLAYER and AEMC software. Different resilient modulus models were used to address RAP_2F1H non-linearity and the stresses and strains were further compared with the linear elastic scenario. It was found that the linear and non-linear analysis provided significantly different results. The KENLAYER simulations, in particular, indicated that when the non-linear behavior of the RAP_2F1H is considered, the horizontal strains within the base course layer decreases in

comparison with the linear elastic case, in which a single modulus is used. Therefore, a linear elastic approach might underestimate the stiffness of the CRAM layer.

Additionally, the calculated strains were compared with the ones collected by the strain gauges from the instrumented test sections during FWD testing. For the RAP_2F1H it was found that a partially adhered scenario would better represent the mechanical behavior of the material observed in situ, since the measured strains lied in between the adhered and non-adhered case for the calculated strain. On the other hand, no significant correspondence was observed for the RAP_3F2C structure regarding calculated and measured strains. Different hypothesis were suggested to explain this discrepancy, such as sensor installation issues, misalignment of the FWD plate and the strain gauge, and no viscoelastic properties consideration.

Therefore, by the end of Chapter 5, it was found that a more realistic material modeling should be formulated in order to properly and accurately predict the pavement response in situ. While Pezo's model describes the CRAMs stiffness for different stress-states, for instance, the sigmoidal model relates the stiffness of this mixture at different temperatures and load frequencies, indicating that these variables are only treated separately. Although some researchers have already proposed models to predict the resilient modulus of foamed mixes addressing both temperature and stress-state (FU; HARVEY, 2007), this approach should be extended to the study of the other types of CRAM, with different active fillers, asphalt binders and aggregate composition.

From this study, it was observed that the complexity of CRAMs mechanical behavior considerably influences the pavement response. Assuming a single behavior for CRAMs can lead to deceptive conclusions regarding stresses and strains calculations, and its mechanical evaluation should be conducted by means of different types of laboratory tests. With the purpose of better representing CRAMs behavior in the future, additional studies should be developed in order to address temperature, load frequency, stress-state and moisture content at the same time. The triaxial dynamic modulus test (ZHAO; TANG; LIU, 2012) would be an alternative for investigating the stiffness of CRAMs, since it allows determining the modulus at different temperatures, load frequencies and stress-states. In this sense, a more realistic material

characterization might lead to the development of more accurate pavement design procedures, encouraging the use of this type of technology.

## 6.2. RECOMMENDATIONS FOR FUTURE WORK

From the findings of the present study, a few recommendations can be made for future works, as follow:

- Determination of the matric suction pressure with different test methods, with a wider range of moisture contents, and with other types of CRAMs like mixtures treated with asphalt emulsion and/or cement as active filler. A more evident relation would be observed between matric suction and resilient modulus, which could provide a clearer perspective of the possibility of incorporating the matric suction result in resilient modulus models.
- Investigate the foamed asphalt mixtures in the asphalt mastic scale and its interaction with finer particles in order to better understand the separate contributions of both adhesion and matric suction in the cohesion parameter.
- Placement of temperature sensors in a wider range of CRAM depths, in order to evaluate the temperature gradient within this type of mixture. Besides, moisture sensors could be used to analyze the moisture content variation in different seasons of the year. This extensive database would be valuable for the development of more adequate equations of temperature and moisture correction during the backcalculation processes.
- Evaluate the CRAMs stiffness by means of the triaxial dynamic modulus test, in which temperature, frequency and stress-state can be addressed simultaneously, with some test adjustments in order to guarantee that the specimen deformation is within the elastic portion. This test configuration would provide a more realistic characterization of the CRAMs that could be further used as input parameters for pavement design procedures.

## 7. REFERENCES

ABDO, A. M. A.; JUNG, S. J. **Effects of Asphalt Mix Design Properties on Pavement Performance: A Mechanistic Approach**. Advances in Civil Engineering, p. 1-7, 2016.

AGÊNCIA NACIONAL DE TRANSPORTES TERRESTRES. **Desenvolvimento do modelo de deterioração de pavimentos asfálticos com uso de instrumentação e sistema weigh-in-motion: fase II.** Autopista Fernão Dias, Centro de Desenvolvimento Tecnológico Arteris, Laboratório de Tecnologia de Pavimentação (USP), Laboratório de Estruturas e Materiais Estruturais (USP), 2019.

ALABASTER, D.; PATRICK, J.; ARAMPAMOORTHY, H.; GONZALEZ, A. **The design of stabilised pavements in New Zealand**. Report No. 498, Wellington, New Zealand: New Zealand Transport Agency, 2013.

ALAE, M.; ZHAO, Y.; ZAREI, S.; FU, G.; CAO, D. **Effects of layer interface conditions on top-down fatigue cracking of asphalt pavements**. International Journal of Pavement Engineering. DOI: 10.1080/10298436.2018.1461870, 2018.

AL-QADI, I. L.; LOULIZI, A.; ELSEIFI, M. A.; LAHOUAR, S. **The Virginia Smart Road: The impact of pavement instrumentation on understanding pavement performance**. Journal of the Association of Asphalt Paving Technologists, v. 73, p. 427-465, 2004.

AMERICAN ASSOCIATION OF STATE HIGHWAY AND TRANSPORTATION OFFICIALS. **T307-99**. Determining the Resilient Modulus of Soils and Aggregate Materials. Washington, D.C., 1999.

_____. **T342-11**. Determining Dynamic Modulus of Hot Mix Asphalt (HMA). Washington, D.C., 2011.

AMERICAN SOCIETY FOR TESTING AND MATERIALS. **D5298 - 16**. Standard test method for measurement of soil potential (suction) using filter paper. West Conshohocken, 2016.

_____. **D5298 - 16**: Standard test method for measurement of soil potential (suction) using filter paper. West Conshohocken, 2016.

_____. **D6307-16**: Standard test method for asphalt content of asphalt mixture by ignition method. West Conshohocken, 2016.

_____. **D7175 - 15**: Standard test method for determining the rheological properties of asphalt binder using a Dynamic Shear Rheometer. West Conshohocken, 2015.

ANDRADE, L. R. **Comparação do comportamento de pavimentos asfálticos com camadas de base granular, tratada com cimento e com estabilizantes asfálticos para tráfego muito pesado**. 2017. 179 p. Master Thesis (Engineering), Escola Politécnica, Universidade de São Paulo, São Paulo, 2017.

ANDRADE, L. R.; VASCONCELOS, K. L.; BERNUCCI, L. L. B. **Avaliação do comportamento estrutural de pavimentos por meio de adoção de parâmetros de bacia deflectométrica**. In: Associação Nacional de Pesquisa e Ensino em Transportes, Rio de Janeiro, Brazil, 2016.

ARANHA, A. L. **Avaliação laboratorial e de campo da tecnologia de reciclagem de base com cimento para a reabilitação de pavimentos**. 2013. 127 p. Master Thesis (Engineering), Escola Politécnica of Universidade de São Paulo, São Paulo, 2013.

ARIAWAN, I. M. A.; SUBAGIO, B. S.; SETIADJI, B. H. **Development of asphalt pavement temperature model for tropical climate conditions in West Bali region**. Procedia Engineering, v. 125, p. 474-480, 2015.

ASAEDA, T.; CA, V. T. **Characteristics of permeable pavement during hot summer weather and impact on the thermal environment**. Building and Environment, v. 35, p. 363-375, 2000.

ASPHALT ACADEMY. **Procedure for Compaction of Test Specimens Using the Vibratory Hammer**. 2009. 7 p.

ASPHALT ACADEMY. **Technical Guideline: Bitumen Stabilised Materials**. Second Edition. Pretoria: Asphalt Academy, 2009. 148 p.

ASPHALT ACADEMY. **The Determination of the Maximum Dry Density and Optimum Moisture Content of Materials Using the Vibratory Hammer Compaction**. 2009. 11 p.

ASPHALT RECYCLING AND RECLAIMING ASSOCIATION. **Recommended Construction Guidelines For Cold Central Plant Recycling (CCPR) Using Bituminous Recycling Agents**. Annapolis: ARRA, 2016. 14 p.

ASPHALT RECYCLING AND RECLAIMING ASSOCIATION. **Recommended Construction Guidelines for Cold In-place Recycling (CIR) Using Bituminous Recycling Agents**. Annapolis: ARRA, 2016. 14 p.

ASSOCIAÇÃO BRASILEIRA DE NORMAS TÉCNICAS. **NBR 14896**: Emulsões asfálticas modificadas por polímero - Determinação do resíduo seco por evaporação, Rio de Janeiro, 2012.

_____. **NBR 6457**: Amostras de solo - Preparação para ensaio de compactação e ensaios de caracterização, Rio de Janeiro, 2016.

ATTIA, M.; ABDELRAHMAN, M. **Effect of state of stress on the resilient modulus of base layer containing reclaimed asphalt pavement**. Road Materials and Pavement Design, v. 12, n. 1, p. 79-97, 2011.

BASTOS, J. B. S. **Influência da variação da umidade no comportamento de pavimentos da região metropolitana de Fortaleza**. 2013. 164 p. Master Thesis (Engineering), Universidade Federal do Ceará, Brazil, 2013.

BESSA, I. S.; ALMEIDA, L. R.; VASCONCELOS, K. L.; BERNUCCI, L. L. B. **Design of cold recycled mixes with asphalt emulsion and Portland cement**. Canadian Journal of Civil Engineering, v. 43, n. 9, p. 773–782, 2016.

BETTI, G.; AIREY, G.; JENKINS, K.; MARRADI, A.; TEBALDI, G. **Active fillers' effect on in situ performances of foam bitumen recycled mixtures**. Road Materials and Pavement Design, v. 18, n. 2, p. 281–296, 2016.

BOCCI, M.; GRILLI, A.; CARDONE, F.; FERROTTI, G. **Full-depth reclamation for the rehabilitation of local roads: A case study**. International Journal of Pavement Engineering, v. 15, n. 3, p. 191–201, 2014.

BONFIM, V. **Fresagem de Pavimentos Asfálticos**. 3rd edition. São Paulo: exceção editorial, 2016. 127 p. ISBN 978-85-60735-00-6.

BOSSO, M. **Uso da tecnologia Weigh-in-Motion para a caracterização do tráfego rodoviário e do excesso de carga em veículos comerciais**. 2018. Masters Thesis (Engineering), Universidade de São Paulo, São Paulo, 2018.

BOZ, I.; CHEN, X.; SOLAIMANIAN, M. **Assessment of emulsified RAP Cold Mixes via Non-Destructive Testing**. International Airfield and Highway Pavements Conference, Philadelphia, p. 107-118, 2017.

BROWN, S. F.; NEEDHAM, D. **A Study of Cement Modified Bitumen Emulsion Mixtures**. Annual Meeting of the Association of Asphalt Paving Technologists, p. 1–22, 2000.

CARDONE, F.; GRILLI, A.; BOCCI, M.; GRAZIANI, A. **Curing And Temperature Sensitivity Of Cement-Bitumen Treated Materials**. International Journal of Pavement Engineering, v. 16, n. 10, p. 868-880, 2015.

CHANDLER, R. J.; CRILLY, M. S.; SMITH, G. M. **A low-cost method of assessing clay desiccation for low-rise buildings**. Proceedings of the Institution of Civil Engineers, v. 92, n. 2, p. 82-89, 1992.

CINCOTTO, M. A. **Cal na Construção Civil**. In: ISAIA, G. C. Materiais de construção civil e princípios de ciências e engenharia de materiais. 2nd edition. São Paulo: IBRACON, 2007. ISBN: 9788598576190.

ČÍŽKOVÁ, Z.; SUDA, J.; VALENTIN, J.; KRPÁLEK, O. **Complex Modulus And Stiffness Modulus Of Cold Recycled Mixes**. International Journal of Advanced Resarch in Science and Engineering. v. 4, n. 2, p. 40–53, 2015.

CNT. Pesquisa CNT de Rodovias: Relatório Gerencial. Brazil: CNT, 403 p., 2017.

COLLINGS, D.; JENKINS, K. **The Long-Term Behavior of Bitumen Stabilized Materials (BSMs)**. 10th Conference On Asphalt Pavement for Southern Africa. 2011.

COPELAND, A. **Reclaimed Asphalt Pavement in Asphalt Mixtures: State of the Practice**. Report No. FHWA-HRT-11-021, Federal Highway Administration, 55 p., 2011.

COPELAND, A.; JONES, C.; BUKOWSKI, J. **A national effort is underway to capitalize on the economic and environmental benefits of recycling asphalt pavements**. Public Roads - Reclaiming Roads. v 73, n. 5, p. 1200, 2010.

CSANYI, L. H. **Foamed Asphalt in Bituminous Paving Mixtures**. Highway Research Board Bulletin. v. 10, n. 160 p. 108–122, 1957.

DAL BEN, M.; JENKINS, K. J. **Road Materials and Pavement Design Performance of cold recycling materials with foamed bitumen and increasing percentage of reclaimed asphalt pavement**. Road Materials and Pavement Design.v. 15, n. 2, p. 348-371, 2014.

DEPARTAMENTO NACIONAL DE ESTRADAS DE RODAGEM. **PRO 199/96**: Redução de amostra de campo de agregados para ensaio de laboratório, 1996.

DEPARTAMENTO NACIONAL DE INFRAESTRUTURA DE TRANSPORTES. DNIT 134/10: Pavimentação - Solos - Determinação do módulo de resiliência - Método de Ensaio. Rio de Janeiro, 2010.

_____. **DNIT 169/14**: Pavimentação - Reciclagem de pavimento em usina com espuma de asfalto - Especificação de Serviço. Rio de Janeiro, 2014.

DIEFENDERFER, B. K.; BOWERS, B. F.; SCHWARTZ, C. W.; FARZANEH, A.; ZHANG, Z. **Dynamic Modulus of Recycled Pavement Mixtures**. Transportation Research Record: Journal of the Transportation Research Board, n. 2575, p. 19–26, 2016.

DONGRÉ, R.; MYERS, L.; D'ANGELO, J. A. **Conversion of Testing Frequency to Loading Time: Impact on Performance Predictions Obtained from the M-E Pavement Design Guide**. In: Transportation Research Board: 85th Annual Meeting, Washington, DC, 2006.

DU, S. **Interaction mechanism of cement and asphalt emulsion in asphalt emulsion mixtures**. Materials and Structures/Materiaux et Constructions, v. 47, n. 7, p. 1149–1159, 2012.

EBELS, L. -J. **Characterisation of Material Properties and Behavior of Cold Bituminous Mixtures for Road Pavements**. 2008. 440 p. Ph.D. Dissertation (Engineering), Stellenbosch University, South Africa, 2008.

EBELS, L. -J.; JENKINS, K. J.; COLLINGS, D; **Cold Mix (Bitumen Stabilisation) Technology in Southern Africa into the 21st Century**. 2005 International Symposium On Pavement Recycling, March, São Paulo, 2005.

EUROPEAN ASPHALT PAVEMENT ASSOCIATION. **Asphalt in Figures 2016**. 2018, 9 p.

FEDERAL HIGHWAY ADMINISTRATION. **Overview of Project Selection Guidelines for Cold In-place and Cold Central Plant Pavement Recycling**. Washington: FHWA, 2017. 13 p.

FRANCO, F. A. C. P. **Método de dimensionamento mecanístico-empírico de pavimentos asfálticos - SISPAV**. 2007. 294 p. Ph.D. Dissertation (Engineering), Universidade Federal do Rio de Janeiro, Brazil, 2007.

FREDLUND, D. G.; RAHARDJO, H. **Soil Mechanics for Unsaturated Soils**. John Wiley & Sons, 1993.

FREDLUND, D. G.; RAHARDJO, H.; FREDLUND, M. D. **Unsaturated Soil Mechanics in Engineering Practice**. New Jersey: John Wiley & Sons, 2012. 909 p.

FU, P.; HARVEY, J. T. **Temperature sensitivity of foamed asphalt mix stiffness: Field and lab study**. International Journal of Pavement Engineering, v. 8, n. 2, p. 137–145, 2007.

FU, P.; JONES, D.; HARVEY, J. T.; BUKHARI, S. A. **Laboratory test methods for foamed asphalt mix resilient modulus**. Road Materials and Pavement Design, v. 10, n. 1, p. 188–212, 2011.

FU, P.; JONES, D.; HARVEY, J. T.; HALLES, F. A. **Investigation of the Curing Mechanism of Foamed Asphalt Mixes Based on Micromechanics Principles**. Journal of Materials in Civil Engineering, v. 22, n. 1, p. 29–38, 2010.

FU, P.; STEVEN, B. D.; JONES, D.; HARVEY, J. T. **Relating laboratory foamed asphalt mix resilient modulus tests to field measurements**. Road Materials and Pavement Design, v. 10, n. 1, p. 155-185, 2009.

GAO, L.; NI, F.; LUO, H.; CHARMOT, S. **Characterization of fair voids in cold in-place recycling mixtures using X-ray computed tomography**. Construction and Building Materials, v. 84, p. 429-436, 2015.

GARCÍA, A.; LURA, P.; PARTL, M. N.; JERJEN, I. **Influence of cement content and environmental humidity on asphalt emulsion and cement composites performance**. Materials and Structures/Materiaux et Constructions, v. 46, n. 8, p. 1275–1289, 2012.

GARILLI, E.; AUTELITANO, F.; GODENZONI, C.; GRAZIANI, A.; GIULIANI, F. **Early age evolution of rheological properties of over-stabilized bitumen emulsion-cement pastes**. Construction and Building Materials, v. 125, p. 352–360, 2016.

GHABCHI, R.; SINGH, D.; ZAMAN, M. **Evaluation of moisture susceptibility of asphalt mixes containing RAP and different types of aggregates and asphalt binders using the surface free energy method**. Construction and Building Materials, v. 73, p. 479-489, 2014.

GIANI, M. I.; DOTELLI, G.; BRANDINI, N.; ZAMPORI, L. **Comparative life cycle assessment of asphalt pavements using reclaimed asphalt , warm mix technology and cold in-place recycling**. Resources, Conservation and Recycling, v. 104, p. 224–238, 2015.

GIULIANI, F.; RASTELLI, S. **An analytical approach to evaluate the performance of cold recycled asphalt mixtures**. In: Proceedings of International RILEM

Conference on the Use of Recycled Materials in Building and Structures, RILEM Publications SARL, 2004, p. 13-22.

GODENZONI, C.; GRAZIANI, A.; BOCCI, M. **Influence of reclaimed asphalt content on the complex modulus of cement bitumen treated materials**. 6th International conference bituminous mixtures and pavements, Thessaloniki (Greece), June, p. 589–596, 2015.

GODENZONI, C.; GRAZIANI, A.; BOCCI, M.; GRILLI, A.; BOCCI, E. **Instrumented test section for analyzing the curing process of cold-recycled mixtures**. November, p. 1275–1282, 2017.

GODENZONI, C.; GRAZIANI, A.; PERRATON, D. **Complex Modulus Characterisation of Cold-Recycled Mixtures With Foamed Bitumen and Different Contents of Reclaimed Asphalt**. Road Materials and Pavement Design, DOI: 10.1080/14680629.2016.1142467, 2016.

GÓMEZ-MEIJIDE, B.; PÉREZ, I. **Nonlinear elastic behavior of bitumen emulsion-stabilized materials with C&D waste aggregates**. Construction and Building Materials, v. 98, p. 853-863, 2015.

GONZÁLEZ, A.; CUBRINOVSKI, M.; ALABASTER, D.; THENOUX, G. **Interpretation of laboratory and full-scale testing of New Zealand foamed bitumen pavements using finite-element modelling**. Road Materials and Pavement Design, v. 13, n. 4, p. 578-598, 2012.

GRAZIANI A; GODENZONI C; CARDONE F; BOCCI M. **Effect of curing on the physical and mechanical properties of cold-recycled bituminous mixtures**. Materials & Design, v. 95, p. 358–369, 2016.

GRAZIANI, A.; IAFELICE, C.; RASCHIA, S.; PERRATON, D.; CARTER, A. **A procedure for characterizing the curing process of cold recycled bitumen emulsion mixtures**. Construction and Building Materials, v. 173, p. 754–762, 2018.

GRILLI, A.; BOCCI, E.; GRAZIANI, A. **Influence of reclaimed asphalt content on the mechanical behavior of cement-treated mixtures**. Road Materials and Pavement Design, v. 14, n. 3, p. 667-678, 2013.

GRILLI, A.; GRAZIANI, A.; BOCCI, M. **Compactability and thermal sensitivity of cement-bitumen-treated materials**. Road Materials and Pavement Design, v. 13, n. 4, p. 599–617, 2012.

GUATIMOSIM, F. V. **Mechanical Behavior and Structural Performance of Recycled Foamed Bitumen**. 2015. 127 p. Master Thesis (Engineering), Escola Politécnica of Universidade de São Paulo, São Paulo, 2015.

GUATIMOSIM, F. V.; VASCONCELOS, K. L.; BERNUCCI, L. L. B.; JENKINS, K. J. **Laboratory and field evaluation of cold recycling mixture with foamed asphalt**. Road Materials and Pavement Design, v. 19, n. 2, p. 385–399, 2018.

GUATIMOSIM, F.; VASCONCELOS, K.; BERNUCCI, L. **Structural evaluation of**

**cold recycling mixture with foamed asphalt**. Bearing Capacity of Roads, Railways and Airfields, p. 1235–1241, 2017.

HAJJ, E. Y.; ULLOA, A.; SIDDHARTHAN, R. V.; SEBAALY, P. E. **Characteristics of the Loading Pulse for the Flow Number Performance Test**. Proceedings of the Association of Asphalt Paving Technologists, Sacramento, CA: Association of Asphalt Paving Technologists (AAPT), 2010, p. 253-294.

HEFER, A. W.; LITTLE, D. N.; LYTTON, R. L. **A Synthesis of Theories and Mechanisms of Bitumen-Aggregate Adhesion Including Recent Advances in Quantifying the Effects of Water**. Journal of the Association of Asphalt Paving Technologists, v. 74, p. 139-196, 2005.

HUANG, B.; MOHAMMAD, L. N.; GRAVES, P. S.; ABADIE, C. **Louisiana experience with crumb rubber-modified hot-mix asphalt pavement**. Transportation Research Record: Journal of the Transportation Research Board, v. 1789, n. 02-2620, 2002.

HUANG, Y. H. **Pavement Analysis and Design**. 1st edition. New Jersey: Prentice Hall, 1993. 805 p.

HUANG, Y. H. **Pavement Analysis and Design**. 2nd edition. New Jersey: Pearson Prentice Hall, 2004. 775 p.

JAMES, A. **Overview of asphalt Emulsion**. In: Transportation Research Board (TRB). Asphalt emulsion technology. Washington: TRB, 2006, p. 7-15.

JENKINS, K. H.; YU, M. **Cold-recycling techniques using bitumen stabilization: Where is this technology going?**. Road Pavement Material Characterization and Rehabilitation: Selected papers from the 2009 GeoHunan International Conference, p. 191-200, 2009.

JENKINS, K. J. **Mix Design Considerations For Cold And Half-Warm Bituminous Mixes With Emphasis On Foamed Bitumen**. 2000. Ph.D. Dissertation (Engineering), Stellenbosch University, South Africa, 2000.

JENKINS, K. J.; COLLINGS, D. C. **Mix design of bitumen-stabilised materials - South Africa and abroad**. Road Materials and Pavement Design, v. 18, n. 2, p. 331-349, 2016.

JENKINS, K. J.; LONG, F. M.; EBELS, L. J. **Foamed bitumen mixes = Shear performance?** International Journal of Pavement Engineering, v. 8, n. 2, p. 85–98, 2007.

JENKINS, K. J.; ROBROCH, S.; HENDERSON, M. G.; WILKINSON, J.; MOLENAAR, A. A. A. **Advanced testing for cold recycling treatment selection on N7 near Cape Town**. In: Proceedings of the 8th Conference on Asphalt Pavements for Southern Africa (CAPSA'04), Sun City, South Africa, 2004.

JOOSTE, F.; LONG, F. **A Knowledge Based Structural Design Method for Pavements Incorporating Bituminous Stabilized Materials**. Technical Memorandum, 2007.

KARLSSON, R.; ISACSSON, U. **Material-Related Aspects of Asphalt Recycling—State-of-the-Art**. Journal of Materials in Civil Engineering, v. 18, n. February, p. 81–92, 2006.

KATICHA, S.; FLINTSCH, G. W.; LOULIZI, A.; WANG, L. **Conversion of testing frequency to loading time applied to the Mechanistic-Empirical pavement design guide**. Transportation Research Record: Journal of the Transportation Research Board, 2087, p. 99-108, 2008.

KHOSRAVIFAR, S.; SCHWARTZ, C. W.; GOULIAS, D. G. **Mechanistic structural properties of foamed asphalt stabilised base materials**. International Journal of Pavement Engineering, v. 16, n. 1, p. 27–38, 2014.

KIM, Y.; IM, S.; LEE, H. T. **Impacts of curing time and moisture content on engineering properties of cold in-place recycling mixtures using foamed or emulsified asphalt**. Journal of Materials in Civil Engineering, v. 23, n. 5, p. 542–553, 2011.

KIM, Y.; LEE, H. “David”; HEITZMAN, M. **Dynamic Modulus and Repeated Load Tests of Cold In-Place Recycling Mixtures Using Foamed Asphalt**. Journal of Materials in Civil Engineering, v. 21, n. 6, p. 279–285, 2009.

KIM, Y.; LEE, H. D.; HEITZMAN, M. **Validation of new mix design procedure for cold in-place recycling with foamed asphalt. Journal of Materials in Civil Engineering**, v. 19, n. 11, p. 1000-1010, 2007.

KRAHN, J.; FREDLUND, D. G. **On total, matric and osmotic suction**. Soil Science, v. 114, n. 5, p. 339–348, 1972.

KUCHIISHI, A. K.; ANDRADE, L. R.; BESSA, I. S.; ESTEVES, S. F.; VASCONCELOS, K. L.; BERNUCCI, L. L. B. **Infuência da granulometria nas propriedades mecânicas de misturas recicladas a frio estabilizadas com emulsão asfáltica e cimento Portland**. Congreso Ibero-Latinoamericano del Asfalto, 12 p., 2017.

KUCHIISHI, A. K.; VASCONCELOS, K. L.; BERNUCCI, L. L. B., **Influence of viscoelastic properties of cold recycled asphalt mixtures on pavement response**. International Society for Asphalt Pavements Conference, 8 p., 2018.

KUNA, K.; AIREY, G.; THOM, N. **Mix design considerations of foamed bitumen mixtures with reclaimed asphalt pavement material**. International Journal of Pavement Engineering, v. 18, n. 10, p. 902–915, 2017.

KUNA, K.; AIREY, G.; THOM, N. **Structural design of pavements incorporating foamed bitumen mixtures**. Proceedings of the Institution of Civil Engineers - Construction Materials, v. 171, n. 1, p. 22-35, 2018.

LEANDRI, P.; LOSA, M.; DI NATALE, A. **Field validation of recycled cold mixes viscoelastic properties**. Construction and Building Materials, v. 75, p. 275–282, 2015.

LEE, N.; CHIA-PEI, C.; KUAN-YU, C. **Benefits in energy savings and CO2 reduction by using reclaimed asphalt pavement**. In: Transportation Research

Board: 91st Annual Meeting, Washington, DC, 2012.

LEONG, E. C.; HE, L.; RAHARDJO, H. **Factors Affection the Filter Paper Method for Total and Matric Suction Measurements**. J. Geotechnical Testing, v. 25, n. 3, 2002.

LI, Y., LIU, L., SUN, L. **Temperature predictions for asphalt pavement with thick asphalt layer** [Special issue]. Construction and Building Materials, v. 160, p. 802-809, 2017.

LI, Z.; HAO, P.; LIU, H.; XU, J.; CHEN, Z. **Investigation of early-stage strength for cold recycled asphalt mixture using foamed asphalt**. Construction and Building Materials, v. 127, p. 410–417, 2016.

LIEBENBERG, J. J. E.; VISSER, A. T. **Stabilization and Structural Design of Marginal Materials for Use in Low-Voume Roads**. Transportation Research Record: Journal of the Transportation Research Board, v. 1819, n. LVR8-1097, 2003.

LIEBENBERG, J. J. E.; VISSER, A. T. **Towards a Mechanistic Structural Design Procedure for Emulsion-Treated Base Layers**. Journal of the South African Institution of Civil Engineering, v. 46, n. 3, p. 2-8, 2004.

LIN, J.; WEI, T.; HONG, J.; ZHAO, Y.; LIU, J. **Research on development mechanism of early-stage strength for cold recycled asphalt mixture using emulsion asphalt**. Construction and Building Materials, v. 99, p. 137–142, 2015.

LOIZOS, A. **In-situ characterization of foamed bitumen treated layer mixes for heavy-duty pavements**. International Journal of Pavement Engineering, v. 8, n. 2, p. 123–135, 2006.

LOIZOS, A.; PAPAVASILIOU, V.; PLATI, C. **Investigating in situ stress-dependent behaviour of foamed asphalt-treated pavement materials**. Road Materials and Pavement Design, v. 13, n. 4, p. 678-690, 2012.

LOPEZ, R. F.; EKBLAD, J.; SILFWERBRAND, J. **Resilient properties of binary granular mixtures: a numerical investigation**. Computers and Geotechnics, v. 76, p. 222-233, 2016.

LOSA, M.; LEANDRI, P.; CERCHIAI, M. **Improvement of pavement sustainability by the use of crumb rubber modified asphalt concrete for wearing courses**. International Journal of Pavement Research and Technology, v. 5, n. 6, p. 395-404, 2012.

LU, N.; LIKOS, W. J. **Unsaturated Soil Mechanics**. New Jersey: John Wiley and Sons, 2004. 569 p.

MARCANDALI DA SILVA, A. H.; VASCONCELOS, K. L.; ARANHA, A. L.; BERNUCCI, L. B.; CHAVES, J. M. **Laboratory and field evaluation of cold-in-place RAP recycling**. In: Transportation Research Board: 92nd Annual Meeting, Washington, DC, 2013.

MARECOS, V.; FONTUL, S.; DE LURDES ANTUNES, M.; SOLLA, M. **Evaluation of a highway pavement using non-destructive tests: Falling Weight Deflectometer and Ground Penetrating Radar**. Construction and Building Materials, v. 154, p. 1164–1172, 2017.

MARINHO, F. A. **Shrinkage behavior of some plastic soils**. 1994. 216 p. Ph.D. Dissertation (Engineering), Imperial College of Science, Technology and Medicine, United Kingdom, 1994.

McELWAIN, D. L. S. **A Re-examination of Oxygen Diffusion in a Spherical Cell with Michaelis-Menten Oxygen Uptake Kinectics**. Journal of Theoretical Biology, v. 71, p. 255-263, 1978.

MEHRARA, A.; KHODAII, A. **Evaluation of moisture conditioning effect on damage recovery of asphalt mixtures during rest time application**. Construction and Building Materials, v. 98, p. 294-304, 2015.

MEJLUN, Ł.; JUDYCKI, J.; DOLZYCKI, B. **Comparison of elastic and viscoelastic analysis of asphalt pavement at high temperature**. Procedia Engineering, v. 172, p. 746-753, 2017.

MEOCCI, M.; GRILLI, A.; LA TORRE, F.; BOCCI, M. **Evaluation of mechanical performance of cement–bitumen-treated materials through laboratory and in-situ testing**. Road Materials and Pavement Design, v. 18, n. 2, p. 376–389, 2016.

MERRILL, D.; NUNN, M.; CARSWELL, I. **A guide to the use and specification of cold recycled materials for the maintenance of road pavements**. Report No. TRL 611, 2004.

MODARRES, A.; RAHIMZADEH, M.; ZARRABI, M. **Field investigation of pavement rehabilitation utilizing cold in-place recycling**. Resources, Conservation and Recycling, v. 83, p. 112–120, 2013.

MOLOTO, P. K. **Accelerated Curing Protocol for Bitumen Stabilized Materials**. 2010. Master Dissertation (Engineering), Stellenbosch University, Sout Africa, 2010.

MONTEPARA, A.; GIULIANI, F. **The Role Of Cement In The Recycling Of Asphalt Pavement Cold-Stabilized With Bituminous Emulsions**. Second International Symposium on Maintenance and Rehabilitation of Pavements and Technological Control, p. 1–13, 2001.

NASIMIFAR, M.; SIDDHARTHAN, R. V.; RADA, G. R.; NAZARIAN, S. **Dynamic analyses of traffic speed deflection devices**. International Journal of Pavement Engineering, v. 18, n. 5, p. 381-390, 2017.

NATIONAL ASPHALT PAVEMENT ASSOCIATION (NAPA). **Designing HMA mixtures with High RAP content: A practical guide**. Maryland: Federal Highway Administration, 2007.

NGUYEN, B. T.; MOHAJERANI, **A. Possible simplified method for the determination of the resilient modulus of unbound granular materials**. Road

Materials and Pavement Design, v. 17, n. 4, p. 841-858, 2016.

NIVEDYA, M. K.; VEERARAGAVAN, A.; KRISHNAN, J. M. **How to characterize the mechanical response of Bitumen Stabilized Material ?** Proceedings of the 4th Chinese-European Workshop on Fuctional Pavement Design. London, UK: CRC Press/Balkema, 2016, p. 355-364.

NIVEDYA, M. K.; VEERARAGAVAN, A.; RAVINDRAN, P.; KRISHNAN, J. M. **Investigation on the influence of air voids and active filler on the mechanical response of bitumen stabilized material**. Journal of Materials in Civil Engineering, v. 30, n. 3, p. 1–13, 2018.

OKE, O. **A study on the development of guidelines for the production of bitumen emulsion stabilised RAPs for roads in the tropics**. 2010. 345 p. Ph.D. Dissertation (Engineering), The University of Nottingham, United Kingdom, 2010.

OLIVEIRA, O. M. **Estudo sobre a resistência ao cisalhamento de um solo residual compactado não saturado**, 2004. Doctoral Dissertation (Engineering), Universidade de São Paulo, São Paulo, 2004.

OLOO, S. **A bearing capacity approach to the design of low-volume traffic roads**, 1994. Ph.D Dissertation (Engineering), Faculty of Graduate Studies and Research, University of Saskatchewan. Saskatoon, Canada, 1994.

PAPAVASILIOU, V.; LOIZOS, A. **Field performance and fatigue characteristics of recycled pavement materials treated with foamed asphalt**. Construction and Building Materials, v. 48, p. 677–684, 2013.

PELLINEN, T. K.; WITCZAK, M. W.; BONAQUIST, R. F. **Asphalt mix master curve construction using sigmoidal fitting function with non-linear least squares optimization**. Proceedings of Pavement Mechanics, Symposium at 15th ASCE Engineering Mechanics Conference (EM2000), New York: Columbia University, 2004.

PÉREZ, I.; MEDINA, L.; ÁNGEL DEL VAL, M. **Mechanical Properties and Behavior of In Situ Materials Which Are Stabilised With Bitumen Emulsion**. Road Materials and Pavement Design. v. 14, n. 2, p. 221-238, 2013.

PEZO, R. F. **A general method of reporting the resilient modulus tests of soils - a pavement engineer's point of view**. In: Transportation Research Board: 72nd Annual Meeting, Washington, DC, 1993.

RAMADHAN, R. H.; WAHHAB, H. I. A. A. **Temperature variation of flexible and rigid pavements in Eastern Saudi Arabia**. Building and Environment, v. 32, n. 4, p. 367-373, 1997.

RASCHIA, S.; PERRATON, D.; CARTER, A.; GRAZIANI, A.; VAILLANCOURT, M. **Effect of Reclaimed Asphalt Gradation on Bitumen Emulsion Mixtures**. 2018.

RUPPERT, D.; CRESSIE, N.; CARROL, R. J. **A Transformation/Weighting Model for Estimating Michaelis-Menten Parameters**. Biometrics, v. 45, n. 2, p. 637-656, 1989.

SAADOON, T.; GARCIA, A.; GÓMEZ-MEIJIDE, B. **Dynamics of water evaporation in cold asphalt mixtures**. Materials and Design, v. 134, p. 196–206, 2017.

SANGIORGI, C.; TATARANNI, P.; SIMONE, A.; VIGNALI, V.; LANTIERI, C.; DONDI, G. **A laboratory and filed evaluation of Cold Recycled Mixture for base layer entirely made with Reclaimed Asphalt Pavement**. Construction and Building Materials, v. 138, p. 232–239, 2017.

SCHWAB, K. **The Global Competitiveness Report The Global Competitiveness Report**. Report. Geneva, 2016.

SCHWARTZ, C. W.; KHOSRAVIFAR, S. **Design and evaluation of foamed asphalt base materials**. Research Report. Maryland Department of Transportation, 86 p., 2013.

SIDDHARTHAN, R. V.; SEBAALY, P. E.; EL-DESOUKY, M.; STRAND, D.; HUFT, D. **Heavy off-road vehicle tire-pavement interactions and response**. Journal of Transportation Engineering, v. 131, n. 3, p. 239-247, 2005.

SIDDHARTHAN, R. V.; YAO, J.; SEBAALY, P. E. **Pavement strain from moving dynamic 3D load distribution**. Journal of Transportation Engineering, v. 124, n. 6, p. 557-566, 1998.

SILVA, A. H. M. **Avaliação do comportamento de pavimentos com camada reciclada de revestimentos asfálticos a frio com emulsão modificada por polímero**. 2011. 143 p. Master Thesis (Engineering), Escola Politécnica of Universidade de São Paulo, São Paulo, 2011.

SMITH, S.; BRAHAM, A. **Comparing layer types for the use of PavementME for asphalt emulsion Full Depth Reclamation design**. Construction and Building Materials, v. 158, p. 481–489, 2017.

SONDAG, M. S.; CHADBOURN, B. A.; DRESCHER, A. **Investigation Of Recycled Asphalt Pavement (RAP) Mixtures**. Report. Minnesota, 2015.

SOUZA JÚNIOR, J. G. **Aplicação do novo método de dimensionamento de pavimentos asfálticos a trechos de uma rodovia federal**. 2018. 218 p. Master Thesis (Engineering), Universidade Federal do Rio de Janeiro, Brazil, 2018.

STIMILLI, A.; FERROTI, G.; GRAZIANI, A.; CANESTRARI, F. **Performance evaluation of a Cold-Recycled Mixture Containing High Percentage of Reclaimed Asphalt**. Road Materials and Pavement Design, v. 14, n. s1, p. 149-161, 2013.

TABAKOVIĆ, A.; MCNALLY, C.; FALLON, E. **Specification development for cold in-situ recycling of asphalt**. Construction and Building Materials, v. 102, p. 318–328, 2016.

TEBALDI, G.; DAVE, E. V.; MARSAC, P.; MURAYA, P.; HUGENER, M.; PASETTO, M.;GRAZIANI, A.; GRILLI, A.; BOCCI, M.; MARRADI, A.; WENDLING, L.; GAUDEFROYC, V.; JENKINS, K. et al. **Synthesis of Standards and Procedures for specimen Preparation and In-field Evaluation of Cold-recycled Asphalt Mixtures**.

Road Materials and Pavement Design, 2014.

TEBALDI, G.; DAVE, E.; MARSAC, P.; MURAYA, P.; HUGENER, M.; PASETTO, M.; GRAZIANI, A.; GRILLI, A.; MARRADI, A.; WENDLING, L.et al. **Classification of recycled asphalt (RA) material**. Second International Symposium on Asphalt Pavement and Environment, 2012, France.

TWAGIRA, E. M. **Influence of Durability Properties on Performance of Bitumen Stabilized Materials**. 2010. 285 p. Ph.D. Dissertation (Engineering), Stellenbosch University, South Africa, 2010.

ULLOA, A.; HAJJ, E. Y.; SIDDHARTHAN, R. V.; SEBAALY, P. E. **Equivalent Loading Frequencies for Dynamic Analysis of Asphalt Pavements**. Journal of Materials in Civil Engineering, v. 25, n. 9, p. 1162-1170, 2013.

VAN GENUCHTEN, M. Th. **A closed-form equation for predicting the hydraulic conductivity of unsaturated soils**. Soil Science Society of America, v. 44, n. 5, p. 892-898, 1980.

VASCONCELOS, K. L.; BERNUCCI, L. L. B.; MOURA, E.; SANSONSUGE, K.; CHAVES, J. M. **Caracterização mecânica de misturas asfálticas contínuas e descontínuas com diferentes ligantes asfálticos**. In: 7o Congresso Brasileiro de Rodovias e Concessões, Foz do Iguaçu, Brazil, 2011.

VOROBEIFF, G. **Design of Foamed Bitumen Layers for Roads**. AustStab Workshop on Road Stabilisation in QLD. Feb 2005.

WALUBITA, L. F.; VAN DE VEM, M. F. C. **Stresses and strains in asphalt-surfacing pavements**. In: 19th Annual South African Transport Conference, Pretoria, South Africa, 2000.

WANG, Y.; LENG, Z.; HU, C. **Cold recycling of reclaimed asphalt pavement towards improved engineering performance**. Journal of Cleaner Production, v. 171, p. 1031-1038, 2018.

WIRTGEN. Wirtgen **Cold Milling Manual: Technology and Application**. Windhagen: Wirtgen GmbH, 2013. 244 p.

WIRTGEN. Wirtgen **Cold Recycling Technology**. First Edition. Windhagen: Wirtgen GmbH, 2012. 370 p.

WU, M.; WEN, H.; MUHUNTHAN, B.; MANAHILOH, K. N. **Influence of Recycled Asphalt Pavement Content on Air Void Distribution, Permeability, and Modulus of Base Layer**. Transportation Research Record: Journal of the Transportation Research Board, v. 2267, p. 65-71, 2012.

XIAO, F.; YAO, S.; WANG, J.; LI, X.; AMIRKHANIAN, S. **A literature review on cold recycling technology of asphalt pavement**. Construction and Building Materials, v. 180, p. 579-604, 2018.

XUAN, D. X.; HOUBEN, L. J. M.; MOLENAAR, A. A. A.; SHUI, Z. H. **Mechanical**

**properties of cement-treated aggregate material - A review**. Materials and Design, v. 33, n. 1, p. 496–502, 2011.

YINFEI, D.; SHENGYUE, W.; JIAN, Z. **Cooling asphalt pavement by a highly oriented heat conduction structure**. Energy and Buildings, v. 102, p. 187-196, 2015.

YU, B.; GU, X.; NI, F.; GAO, L. **Microstructure characterization of cold in-place recycled asphalt mixtures by X-ray computed tomography**. Construction and Building Materials, v. 171, p. 969-976, 2018.

ZAPATA, C. E.; PERERA, Y. Y.; HOUSTON, W. N. **Matric Suction Prediction Model in New AASHTO Mechanistic-Empirical Pavement Design Guide**. Transportation Research Record: Journal of the Transportation Research Board, v. 2101, n. January, p. 53–62, 2009.

ZHAO, Y.; ZHOU, C.; ZENG, W.; NI, Y. **Accurate determination of near-surface responses of asphalt pavements**. Road Materials and Pavement Design, v. 16, n. 1, p. 186-199, 2015.

ZHAO, Y.; TANG, J.; LIU, H. **Construction of triaxial dynamic modulus master curve for asphalt mixtures**. Construction and Building Materials, v. 37, p. 21-26, 2012.

# APPENDIX A - TRIAXIAL RESILIENT MODULUS CURVES

The triaxial resilient modulus curves are presented separately for each type of mixture. The RAP_2F1H and GCS_2F1H resilient modulus curves are presented at the four moisture conditions: 0, F1, I, and F2. The RAP_3E2C and RAP_3F2C resilient modulus curves are presented after being fully cured

Figure 67 - Triaxial resilient modulus curves for the RAP-2F1H mixture

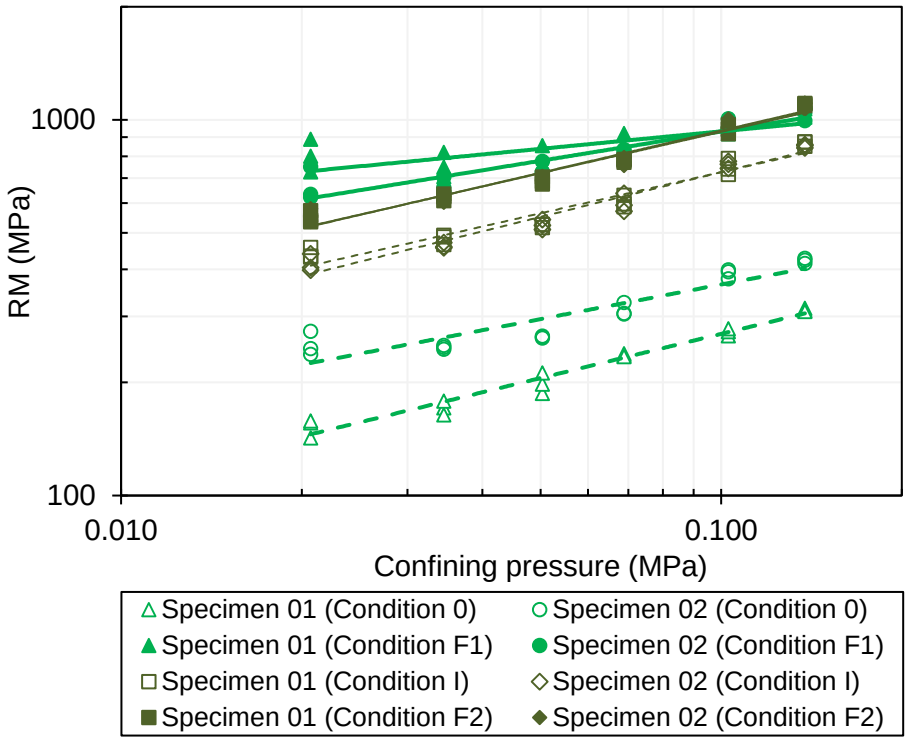

Figure 68 - Triaxial resilient modulus curves for the GCS_2F1H mixture

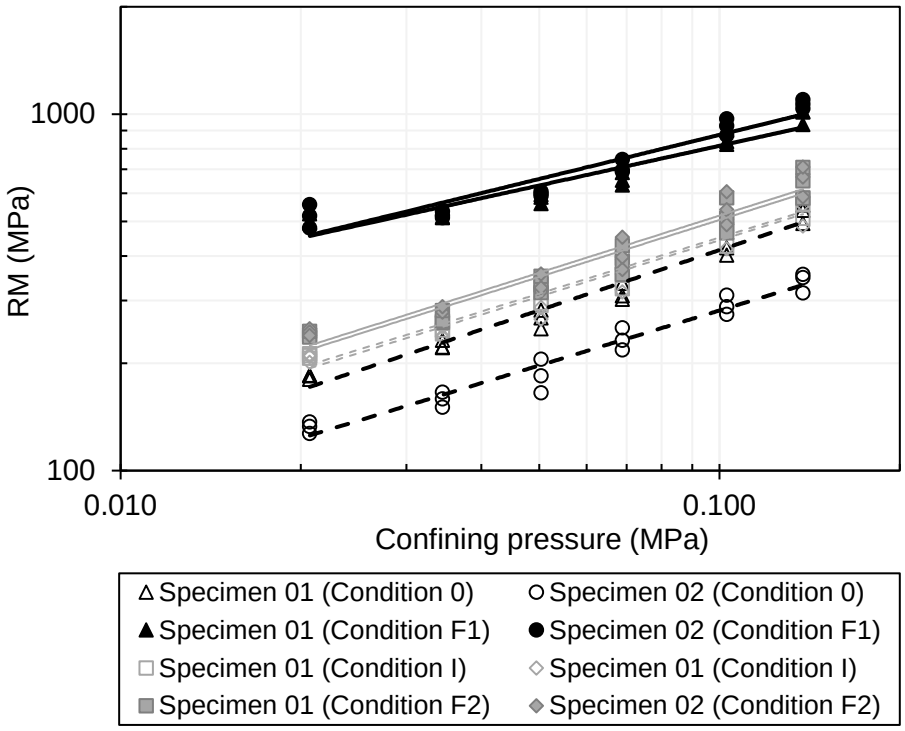


Figure 69 - Triaxial resilient modulus curves for the RAP_3E2C mixture

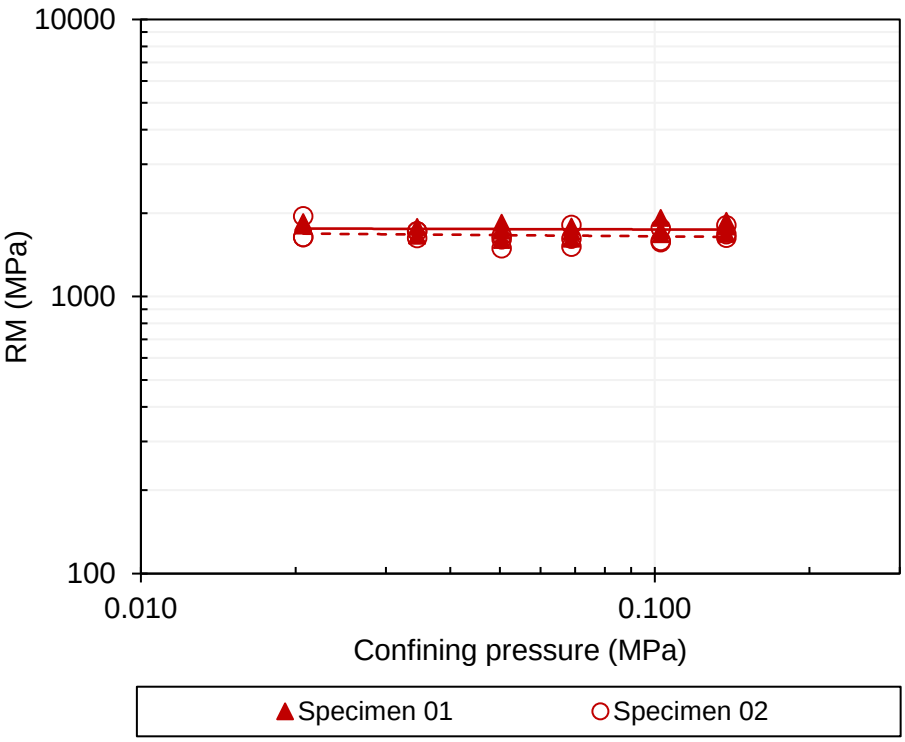

Figure 70 - Triaxial resilient modulus curves for the RAP_3F2C mixture

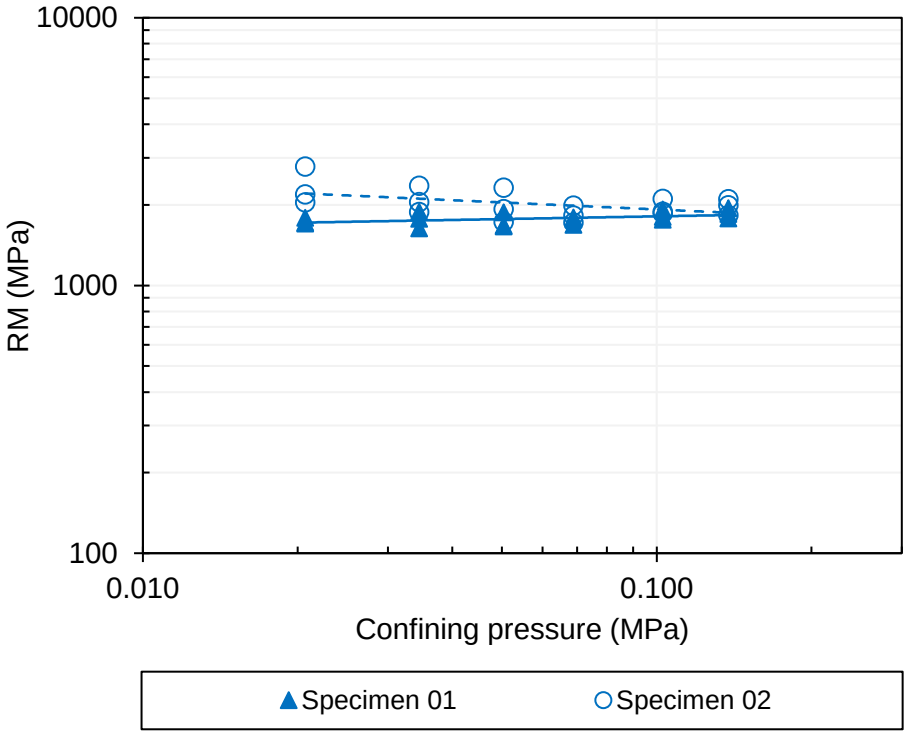

# APPENDIX B - DYNAMIC MODULUS MASTER CURVES

The dynamic shear modulus master curves are presented separately for each type of mixture at the reference temperature of 21.1 ºC.

Figure 71 - |E*| master curves of the gap-graded mixture

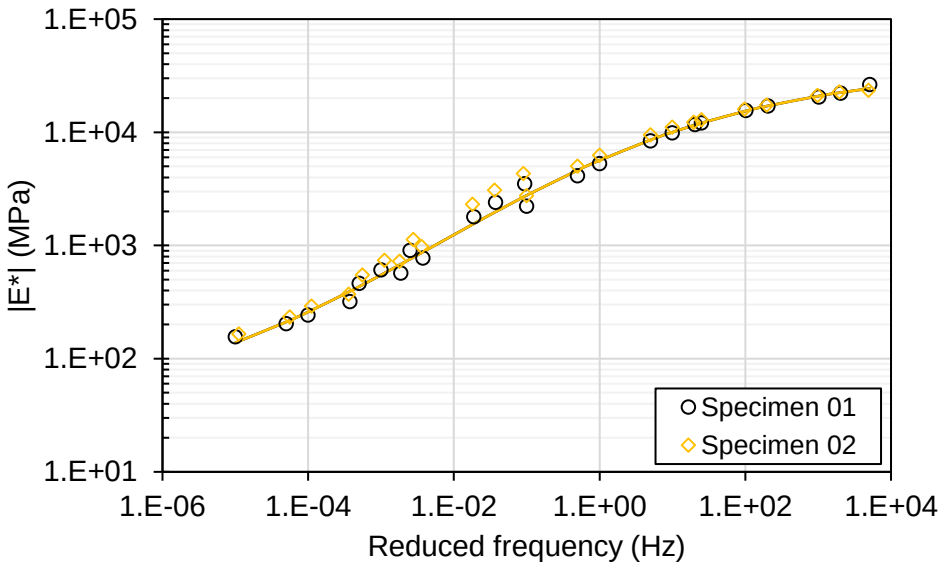

Figure 72 - |E*| master curves of the asphalt concrete mixture

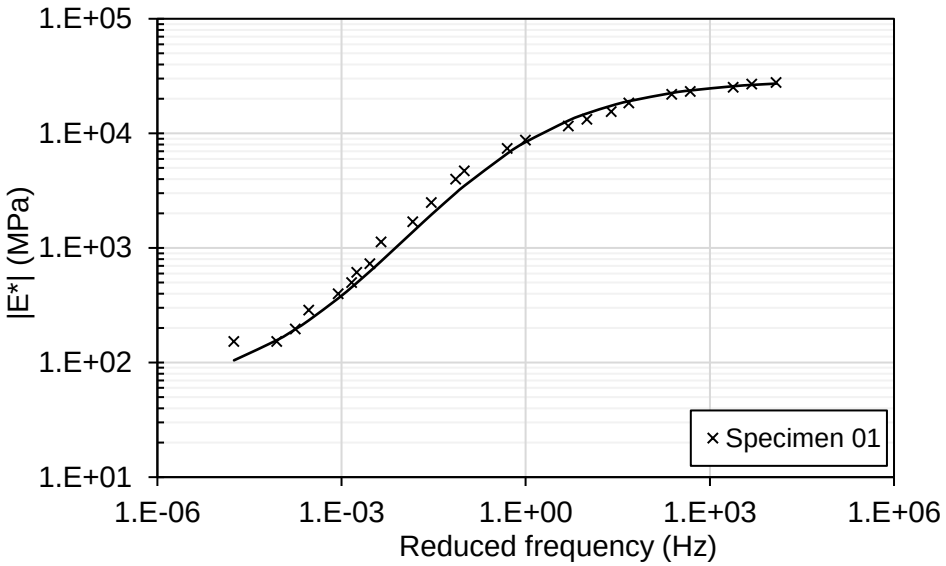


Figure 73 - |E*| master curves of the RAP_2F1H mixture

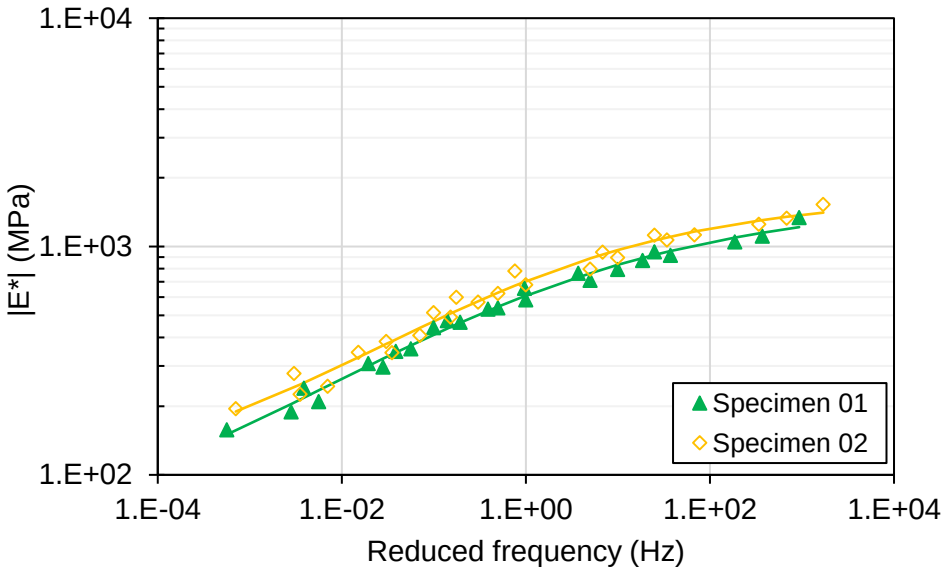

Figure 74 - |E*| master curves of the GCS_2F1H mixture

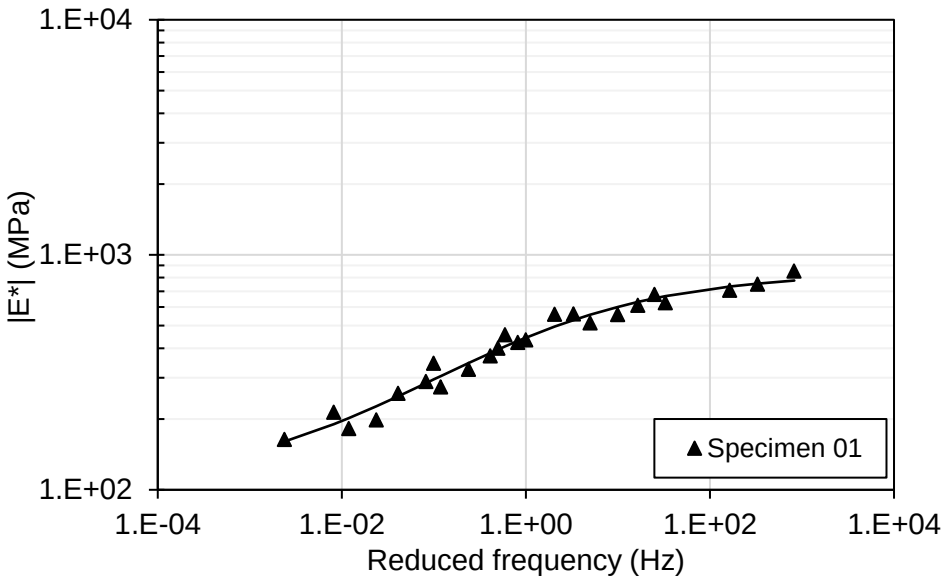


Figure 75 - |E*| master curves of the RAP_3F2C mixture using vibratory compaction

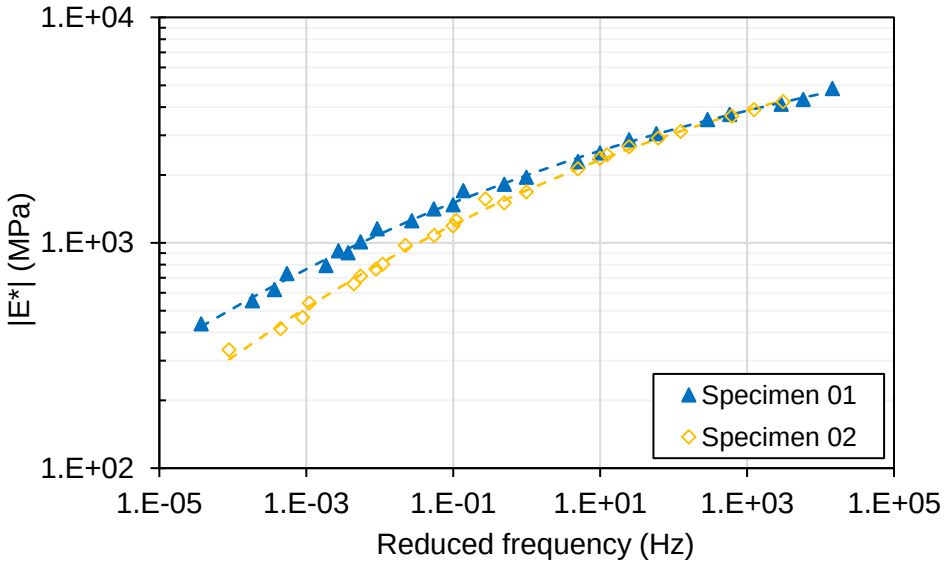

Figure 76 - |E*| master curves of the RAP_3E2C mixture using vibratory compaction

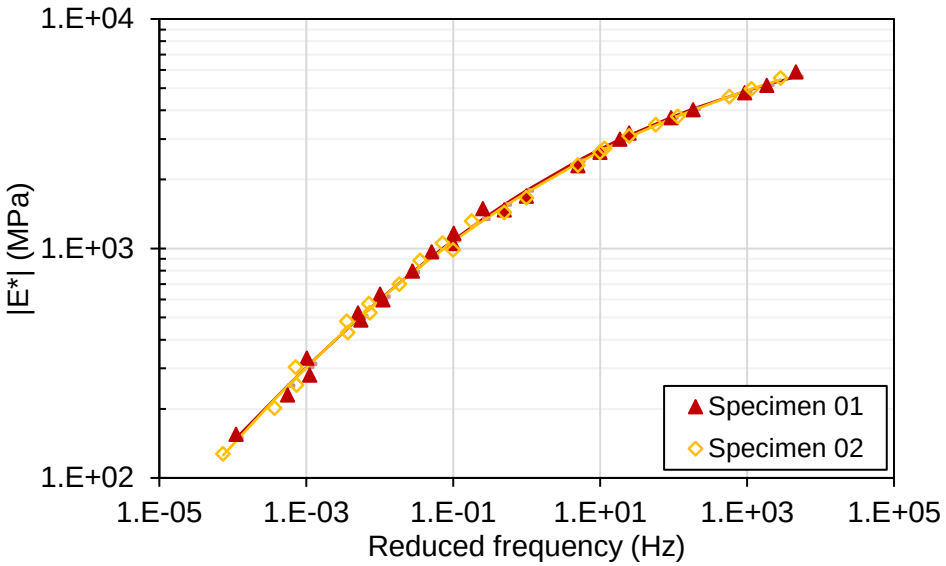


Figure 77 - |E*| master curves of the RAP_3F2C mixture using impulsive compaction (Proctor hammer)

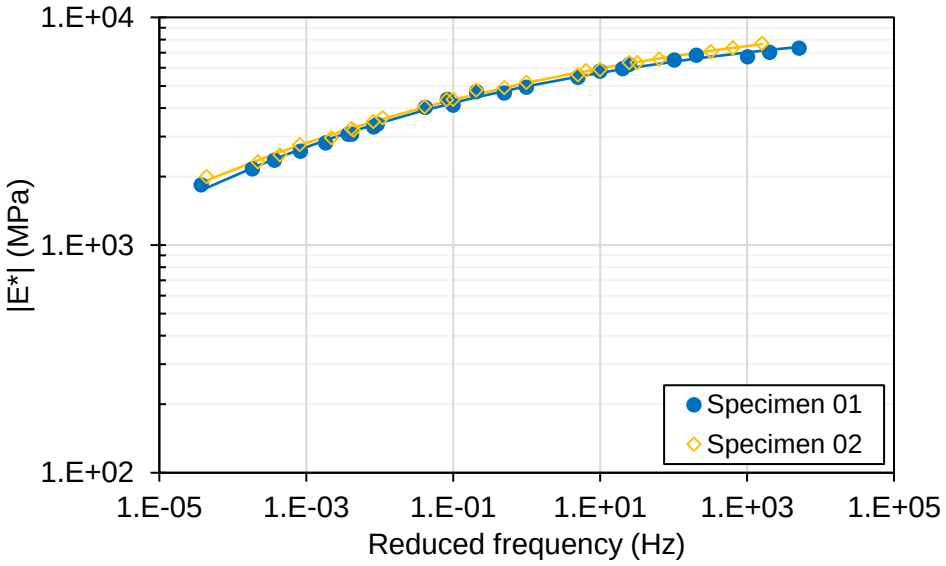

Figure 78 - |E*| master curves of the RAP_3E2C mixture using impulsive compaction (Proctor hammer)

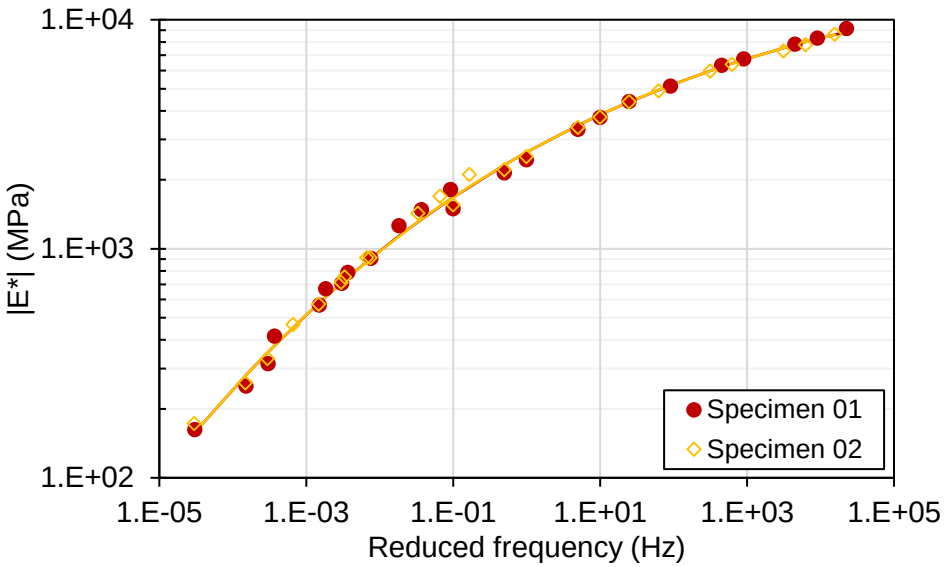

# APPENDIX C - DYNAMIC SHEAR MODULUS MASTER CURVES

The dynamic shear modulus master curves are presented separately for each type of asphalt binder at the reference temperature of 40 ºC.

Figure 79 - |G*| master curves of the asphalt concrete binder

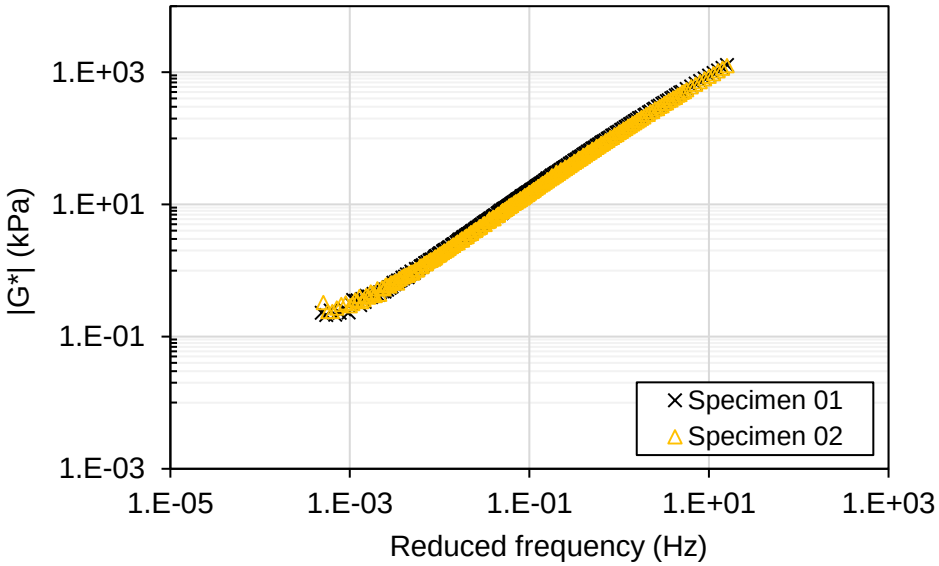

Figure 80 - |G*| master curves of the RAP_3F2C binder

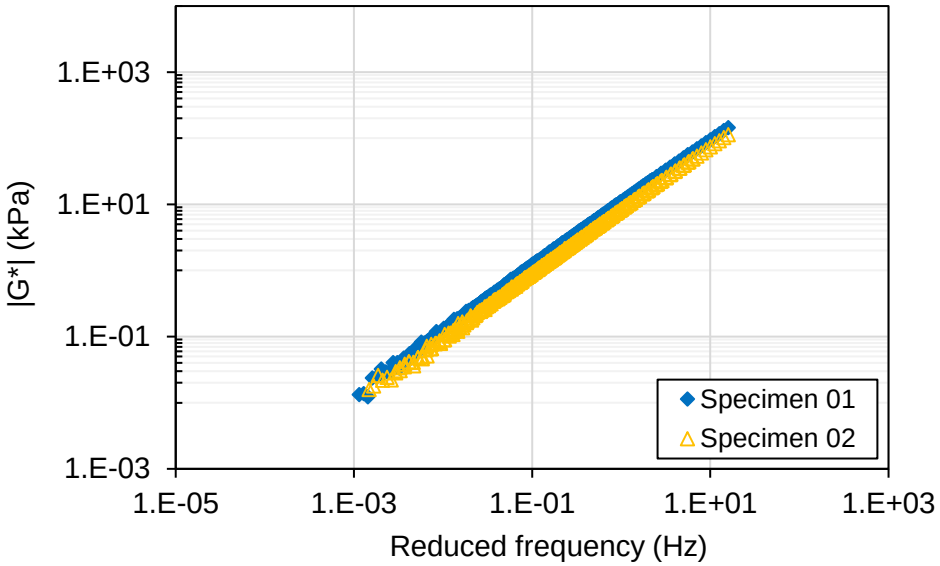


Figure 81 - |G*| master curves of the RAP_3E2C binder